

**Zwitterionic Microscale Hydrogels for Protein Delivery,
Stabilization, and Immobilization**

By

Amir Erfani

Bachelor of Science in Chemical Engineering
Semnan University
Semnan, Iran
2013

Master of Science in Chemical Engineering
Semnan University
Semnan, Iran
2015

Submitted to the Faculty of the
Graduate College of the
Oklahoma State University
in partial fulfillment of
the requirements for
the degree of
DOCTOR OF PHILOSOPHY
May, 2021

Zwitterionic Microscale Hydrogels for Protein Delivery, Stabilization, and Immobilization

Dissertation Approved:

Dr. Clint P. Aichele

Dissertation Adviser

Dr. Joshua D. Ramsey

Dissertation Co-Adviser

Dr. Jeffery L. White

Dr. Steve D. Hartson

ACKNOWLEDGEMENTS

I would like to thank everyone who helped me and gave me the opportunity to do the work described here. First, I would like to thank, Dr. Jeffery White, for serving on my committee and for providing funding through my PhD. I would like to thank Dr. Steve Hartson for serving on my committee. I would also like to thank my friends and labmates, Dr Nicholas Flynn, Dr. Payam Zarrintaj, Josh Seaberg, Abanoub Hanna, and Saeed Manoochehri for their support. I would like to thank Dr. Katie Weigandt at NIST for her help on Neutron Scattering. Most importantly, I would like to thank my advisors, Dr. Clint Aichele and Dr. Joshua Ramsey, for all of their guidance and support ever since the beginning of my time here. I would like to thank the School of Chemical Engineering at Oklahoma State University for all of the great opportunities provided to me.

Acknowledgments reflect the views of the author and are not endorsed by committee members or Oklahoma State University

Name: Amir Erfani

Date of Degree: May 2021

Title of Study: Zwitterionic Microscale Hydrogels for Protein Delivery, Stabilization, and Immobilization

Major Field: Chemical Engineering

Abstract

Proteins are incredibly useful in medicine and industrial chemistry. Many of the most recent breakthroughs in cancer therapy are based on monoclonal antibody treatments. Yet, there are major difficulties that can act as deterrents in developments of such therapies. Sustained subcutaneous, oral or pulmonary deliveries of such therapeutics are limited by the poor stability, short half-life, and non-specific interactions between the therapeutic biomolecules (e.g. antibody) and the delivery vehicle. Similarly, usage of proteins as enzymes in processes is limited by poor stability, short half-life, and difficulties with reusability. With growing usage of proteins as pharmaceuticals and biocatalysts, and apparent shortcomings in both fields, there is a growing need to design materials that are protein compatible and can improve protein stability. The key to successfully utilizing proteins as therapeutics, biocatalysts or biosensors is to maintain their conformation and function. There is emerging evidence that biomimetic, biocompatible zwitterionic polymers can prevent non-specific interactions within protein systems and increase protein stability. In this work, zwitterionic microscale hydrogels of two different zwitterionic moieties (carboxybetaine and sulfobetaine), were synthesized. For the purpose of protein delivery, a biodegradable zwitterionic poly(carboxybetaine), pCB, based microscale hydrogel (microgel) covalently crosslinked with tetra(ethylene glycol) diacrylate was synthesized for antibody encapsulation. The resulting microgels were characterized via FTIR, diffusion NMR, SANS, and cell culture studies. The microgels were found to contain up to 97.5% water content and showed excellent degradability that can be tuned with crosslinking density. Cell compatibility of the microgel was studied by assessing the toxicity and immunogenicity *in vitro*. Cells exposed to the microgel showed complete viability and no pro-inflammatory secretion of interleukin 6 (IL6) or tumor necrosis factor-alpha (TNF α). The microgel was loaded with Immunoglobulin G (as a model antibody), using a post-fabrication loading technique, and antibody sustained release from microgels of varying crosslinking densities was studied. The released antibodies (especially from the high crosslinked microgels) proved to be completely active and able to bind with antibody receptors. Furthermore, for the purpose of protein immobilization, a reaction scheme was developed and studied for covalent immobilization of the protein (α -chymotrypsin) (ChT) within the zwitterionic microscale hydrogels. Confocal laser microscopy studies showed that immobilized ChT (i-ChT) was distributed within the hydrogel. The enzyme-immobilized microgels showed excellent reusability (72% of its initial activity after 10 uses) and could undergo several freezing/drying/rehydration cycles while retaining enzymatic activity. The i-ChT activity, half-life, and conformational stability were studied at varying pH and temperatures with results compared to free ChT in buffer. ChT immobilized within pCB hydrogel showed increased enzymatic stability as observed by a 13 °C increase in the temperature at which i-ChT loses activity compared to free ChT. Furthermore, enzyme half-life increased up to seven-fold for the pCB immobilized ChT, and the increased stability resulted in higher activity at elevated pH. The i-ChT was most active at pH of 8.5 and was partially active up to the pH of 10.2. This research paves the way for designing protein delivery vectors as well as fabrication of enzyme immobilized materials with extended enzyme lifetime and activity.

TABLE OF CONTENTS

Chapter	Page
I. Introduction	1
1.1 Introduction.....	2
1.2 Aims and Scopes.....	2
1.3 Dissertation Organization	3
II. Interactions between Biomolecules and Zwitterionic Moieties	8
2.1 Introduction.....	9
2.2 Zwitterionic Materials: Polymers, Hydrogels, and Nanoparticles.....	9
2.3 Dynamics and Solution Behavior of Zwitterions and Zwitterionic Polymers.....	15
2.4 Zwitterionic Strategies in Therapeutics	21
2.5 Summary and Future Perspective	37
III. Encapsulation and Delivery of Model Protein (Albumin) from within Poly(Sulfobetaine) Microgel	40
3.1 Introduction.....	41
3.2 Materials and Methods.....	43
3.3 Results.....	49
3.3.1 Zwitterionic pSB Hydrogel Beads	49
3.3.2 Thermophysical Properties	50
3.3.3 Post-fabrication Protein Loading	54
3.3.4 Protein Release and Released Protein Bioactivity	56
3.3.5 Protein Stability	58
3.3.6 Cytotoxicity.....	59
3.4. Conclusions.....	60
IV. Biodegradable Zwitterionic Poly(Carboxybetaine) Microgel for Sustained Delivery of Antibodies with Extended Stability and Preserved Function	62
4.1 Introduction.....	64
4.2 Materials and Methods.....	66
4.3 Results.....	72
4.3.1 Biodegradable pCB Microgels.....	72
4.3.2 Degradation of the Microgels	72
4.3.3 <i>In vitro</i> Cytotoxicity and Immunogenicity of the Microgel.....	80

Chapter	Page
4.3.4 Antibody Loading and Release	82
4.4. Conclusions	83
V. Zwitterionic Poly(carboxybetaine) Microgels for Enzyme (Chymotrypsin) Covalent Immobilization	89
5.1 Introduction	91
5.2. Materials and Methods	96
5.3 Results	101
5.3.1 Poly(carboxy betaine) Microgel	101
5.3.2 Enzyme-immobilized Zwitterionic pCB Microgel	103
5.3.3 Enzymatic Activity of Immobilized ChT	109
5.3.4 ChT Deactivation and Half-life	111
5.5 Conclusions	114
 VI. Conclusions and Future Directions	 115
References	120
 Appendices	
A. Effect of Zwitterionic Betaine Surfactant on Interfacial Behavior of Bovine Serum Albumin (BSA)	140
B. Vita	164

LIST OF TABLES

Table	Page
Table 2.1. Most widely studied zwitterionic building blocks	10
Table 2.2. Recent drug delivery strategies utilizing zwitterionic moieties.....	29
Table 3.1. Measured solvent diffusion coefficients in different studied hydrogels.....	53
Table 5.1. Half-life of chymotrypsin at pH of 8 and different temperatures	112
Table 5.2. Half-life of chymotrypsin in different pHs at T=40 °C	113

LIST OF FIGURES

Figure	Page
Figure 1.1. Different architectures in which zwitterionic moieties have been applied in biologically relevant systems.....	4
Figure 1.2. Biodegradable zwitterionic poly(carboxybetaine) microgel for sustained delivery of antibodies	5
Figure 1.3. Zwitterionic poly(carboxybetaine) microgels for enzyme covalent immobilization	6
Figure 2.1. Common zwitterionic polymers	11
Figure 2.2. Different architectures for zwitterionic moieties.....	12
Figure 2.3. Proposed schematic of zwitterion dipole moment and hydration	16
Figure 2.4. Anti-polyelectrolyte effect on the zwitterionic polymers.....	19
Figure 3.1. Schematics for the fabrication of pSB hydrogel beads	44
Figure 3.2. SEM of the freeze-dried hydrogels.....	49
Figure 3.3. Equilibrium water content of the zwitterionic hydrogels.....	50
Figure 3.4. Effects of temperature on water content of zwitterionic pSB hydrogels...	51
Figure 3.5. Ionresponsivity of the zwitterionic poly(sulfobetaine) hydrogels.....	52
Figure 3.6. ¹ H NMR spectra of zwitterionic hydrogel.....	54
Figure 3.7. Confocal microscopy of the hydrogels with FITC-BSA	55
Figure 3.8. Confocal microscopy of averaged projection of hydrogels.....	55
Figure 3.9. The amount of protein loaded inside hydrogels	56
Figure 3.10. BSA release plots from the zwitterionic pSB hydrogels	57
Figure 3.11. The enzymatic activities of the released proteins.....	58
Figure 3.12. BSA aggregation and released BSA enzymatic activity.....	59
Figure 3.13. Fibroblast cells treated with different amounts of hydrogel beads	60
Figure 4.1. Schematics for the fabrication and loading of microgels.....	73
Figure 4.2. SEM of the freeze-dried zwitterionic pCB microgels formed with different crosslinking densities.....	75
Figure 4.3. Characterization of the synthesized zwitterionic poly(carboxybetaine) microgel crosslinked with tetra (ethylene glycol) diacrylate.....	77
Figure 4.4. Small-angle neutron scattering (SANS) of the zwitterionic poly (carboxybetaine) microgels crosslinked with TTEGDA.....	79
Figure 4.5. Microgel degradation.....	80
Figure 4.6. Biodegradability of the microgels (microscale hydrogels)	

in PBS observed in SEM micrographs.....	81
Figure 4.7. Cytotoxicity and immunogenicity of biodegradable zwitterionic pCB microgels.	83
Figure 4.8. Immunoglobulin G (IgG) loaded zwitterionic microgels.	84
Figure 4.9. Antibody (Ab) release from zwitterionic microgels and activity of released Ab activity evaluated using human IgG ELISA.	85
Figure 5.1. Molecular structure of α -chymotrypsin.....	94
Figure 5.2. Monomer synthesis reaction scheme and the molecular structures of N-(3-(Dimethylamino)propyl) methacrylamide (reactant) and the synthesized monomer carboxybetaine methyl methacrylate (CBMA).	97
Figure 5.3. ^1H NMR spectra of the and the zwitterionic polymerizable carboxybetaine monomer.....	97
Figure 5.4. Schematics for the fabrication of poly(carboxybetaine) microgel	102
Figure 5.5. SEM micrograph of the lyophilized (freeze-dried) blank microgel (no enzyme)	103
Figure 5.6. Reaction scheme for protein immobilization.	104
Figure 5.7. SEM of the lyophilized (freeze-dried) microscale hydrogel beads	105
Figure 5.8 Confocal microscopy of the fluorescently labeled enzyme (chymotrypsin) immobilized microgel (microscale hydrogel).	106
Figure 5.9. A schematic representation of the chymotrypsin immobilized poly(carboxybetaine) zwitterionic hydrogel.....	106
Figure 5.10. Characterization of the synthesized zwitterionic microgel.	108
Figure 5.11. Reusability of chymotrypsin (ChT) immobilized within poly(carboxybetaine).	109
Figure 5.12. The esterase enzymatic activity of chymotrypsin immobilized within pCB microgel at different conditions compared with free chymotrypsin in solution.	111

CHAPTER I

Introduction

1.1 Introduction

A zwitterion (or inner salt, formerly dipolar ion) is a small molecule containing an identical number of cationic and anionic functional groups. The ability of some zwitterionic molecules to improve protein stability was discovered in the early 1980s, when glycine betaine and proline were found to improve solvation of protein molecules [1, 2]. The first attempt to understand the thermodynamic effects of zwitterionic cosolutes on water-protein interactions was carried out in 1996 by observing protein-water interactions in the presence of glycine betaine [3]. Glycine betaine displayed a negative preferential interaction with the model protein, resulting in exclusion of the zwitterion from the protein surface and improvement in protein solvation [3]. Developments in the field of zwitterionic polymers (charge neutral polymers consisting of zwitterionic monomers) greatly advanced the understanding of zwitterionic moieties throughout the 1990s and early 2000s. By 2008 zwitterionic polymers (or polyzwitterions) had been shown to resist non-specific biomolecule (e.g., protein) adsorption [4-8]. Not until 2012, however, did *in vivo* results from zwitterionic polymer-conjugated proteins attract broader attention from the scientific community [9, 10]. Researchers have been working to synthesize zwitterionic materials for diverse biomedical applications such as drug delivery, protein stabilization, and surface modification of implantable materials. These zwitterionic materials have been used in assorted architectures including protein conjugates, surface coatings, nanoparticles, hydrogels, and liposomes.

1.2 Aims and Scopes

While emerging evidence indicates that the zwitterionized polymers in the form of protein conjugates have biocompatibility properties that can have applications in intravenous protein delivery [11], there is little empirical information on the use of such materials for protein sustained delivery,

stabilization, and immobilization. *The overall objective of this work is to synthesize and evaluate zwitterionic microscale hydrogels that can improve protein stability/delivery and protein immobilization properties.* Our **central hypothesis** is that a network of super-hydrophilic polyzwitterions can prevent protein aggregation and denaturation and maintain protein activity. This scientific research tries to address unmet proteins formulation, delivery, and reusability needs with the help of zwitterionic motifs.

Research Aim 1: Evaluate the effectiveness of zwitterionic hydrogels for encapsulation and delivery of proteins and antibodies

For this purpose, biodegradable zwitterionic microgels were synthesized to enable cell-compatible and non-immunogenic antibody delivery.

Research Aim 2. Characterize the effectiveness of zwitterionic hydrogels for enzyme immobilization

We immobilized proteins (enzymes) in these zwitterionic microgel networks and studied the enzymatic activity of the enzyme.

1.3 Dissertation Organization

In Chapter 2 (see Figure 1.1), I review the current literature on the interactions between zwitterionic moieties and biomacromolecules.

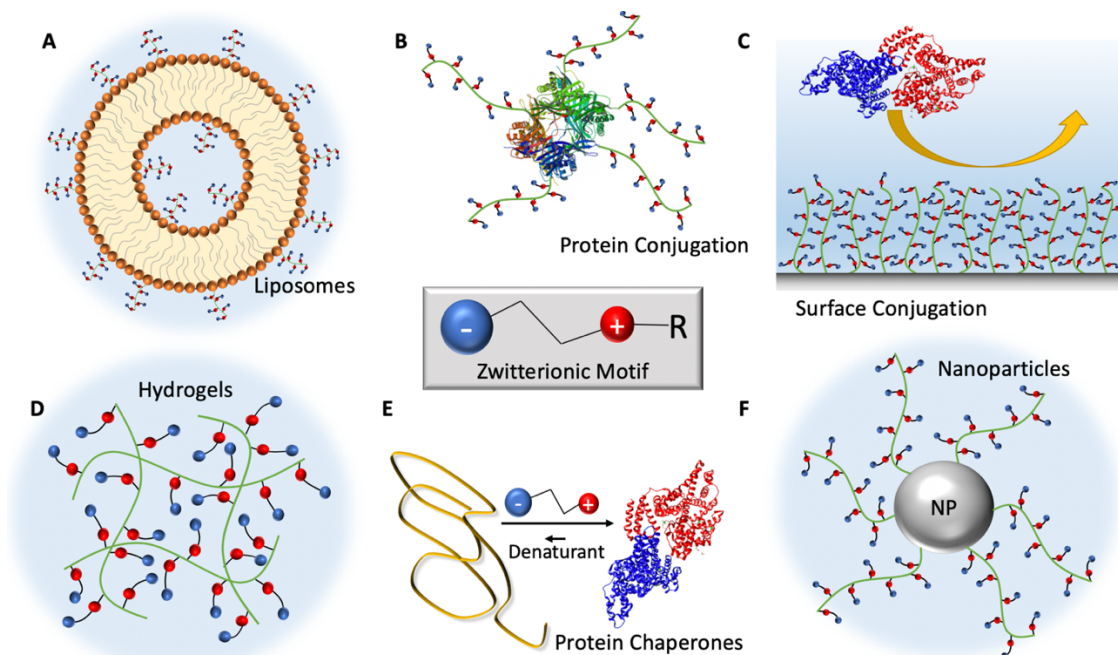


Figure 1.1. Different architectures in which zwitterionic moieties have been applied in biologically relevant systems and are reviewed in chapter 2 of this dissertation.

In Chapter 3, I explore zwitterionic microscale hydrogels based on poly sulfobetaine polymers (pSB). I investigate loading/release of a model protein (bovine serum albumin) from the microgels. This chapter is a proof of concept for the more specific use of the microgels. In Chapter 4, I report synthesis and use of biodegradable zwitterionic microgels for encapsulation and release of antibodies (see Figure 1.2). Carboxybetaine, a natural osmolyte, was used as the repeating unit of the polymer crosslinked with a degradable crosslinker. I investigated how a post-fabrication loading of a model antibody (IgG) can result in release of active antibody.

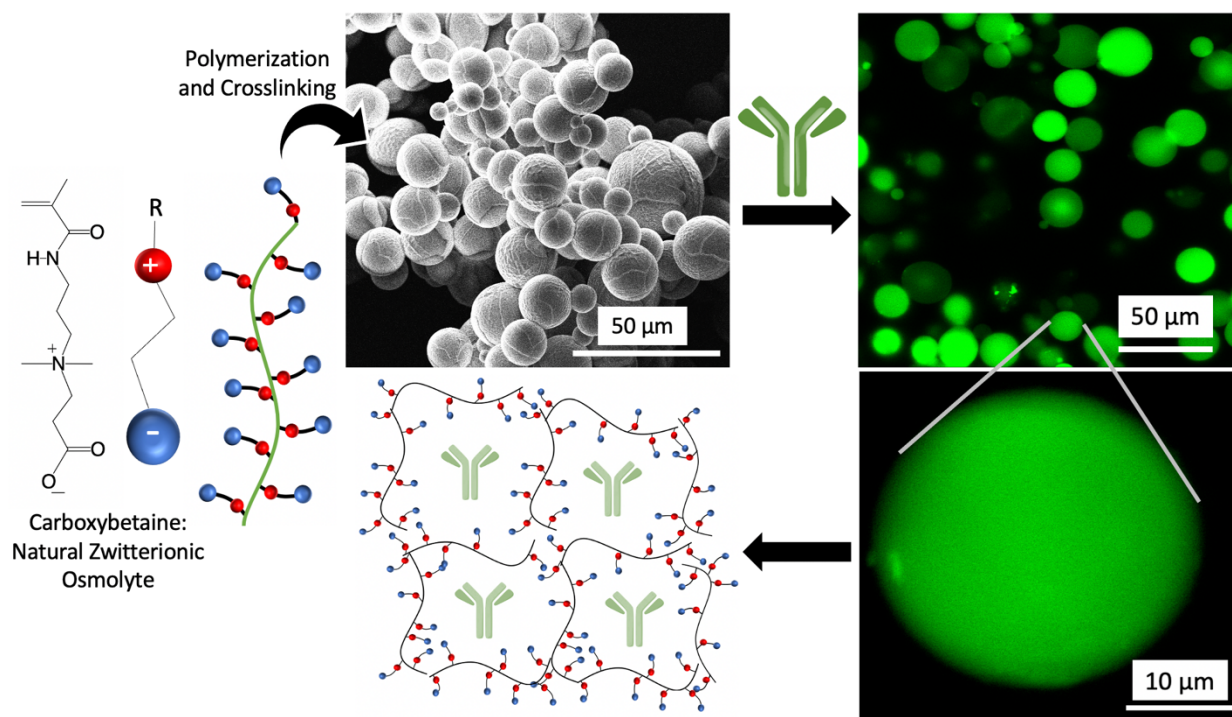


Figure 1.2. Biodegradable zwitterionic poly(carboxybetaine) microgel for sustained delivery of antibodies explored in the Chapter 4 of this dissertation.

In Chapter 5, I explore zwitterionic microscale hydrogels for enzyme immobilization. Zwitterionic poly carboxy betaine (pCB) microgels were synthesized using inverse emulsion polymerization. A multi-point covalent immobilization scheme was studied to chemically immobilize ChT within the microgel. I investigated how a post-fabrication loading/immobilization procedure can result in immobilization of bioactive proteins within the microgel and compared the enzymatic activity of free and immobilized enzyme at different pHs and temperatures. I also investigated how immobilization within a super-hydrophilic network of polyzwitterions can affect the stability and half-life of the enzyme.

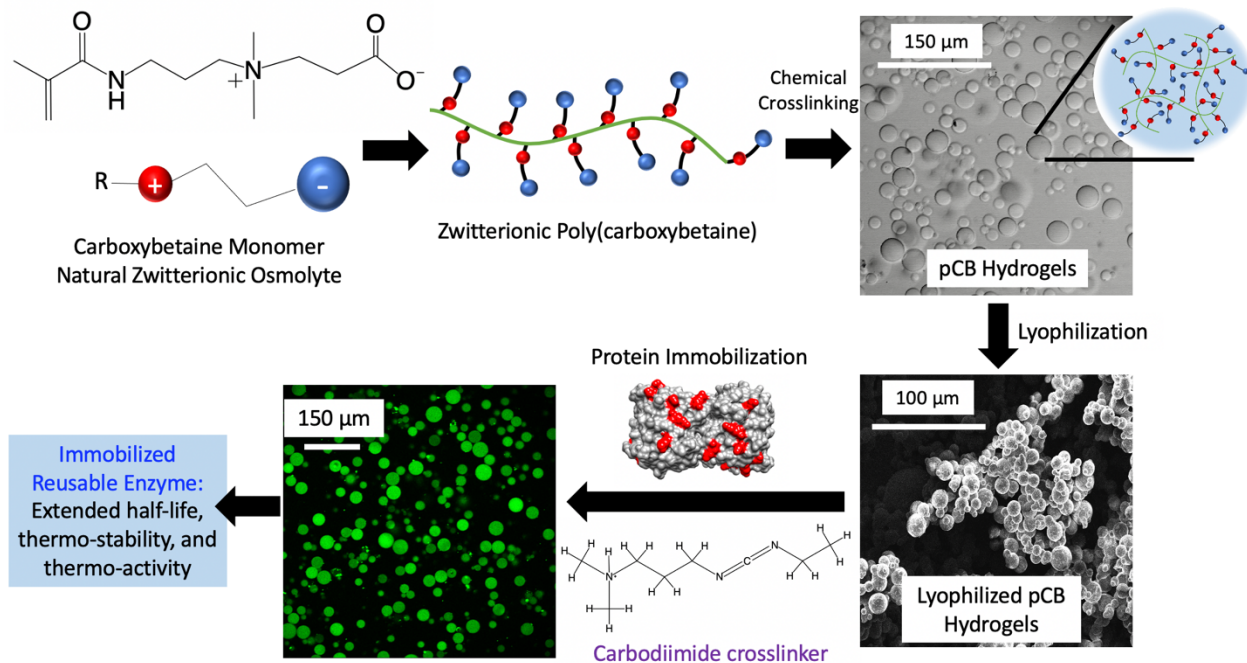


Figure 1.3. Zwitterionic poly(carboxybetaine) microgels for enzyme (chymotrypsin) covalent immobilization explored in Chapter 5 of this dissertation.

CHAPTER II

Interactions between Biomolecules and Zwitterionic Moieties

Chapter Overview

Throughout the last decade, zwitterionic moieties have gained attention as constituents of biocompatible materials for exhibiting super-hydrophilic properties that prevent non-specific protein adsorption. In this chapter, I summarize recent advancements that further our understanding of interactions between biomolecules and zwitterionic moieties. I focus on the solution behavior of zwitterions and zwitterionic polymers and the molecular interactions between these molecules and biomolecules as determined by both experimental and theoretical studies. Further, I discuss the implications of using such interactions *in vivo* and how zwitterionic moieties may be incorporated to facilitate targeted delivery of proteins, genes, or small molecules. Finally, I discuss current knowledge gaps that need to be addressed to advance the field.

2.1 Introduction

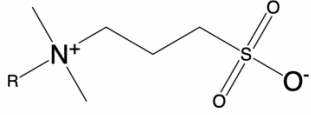
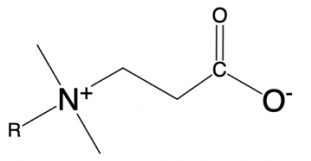
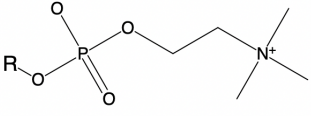
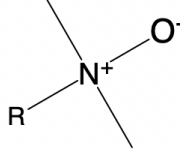
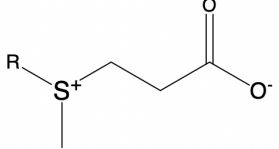
While reviews exist on synthesis of zwitterionic polymers [12], zwitterionic polymer-conjugated surfaces [13], and zwitterionic membrane coatings [14], a compilation of the interactions between zwitterionic moieties and biomolecules is not present in the literature. Additionally, this review does not address polyampholytes, which may carry opposing charges on separate monomers [15]. Instead the review focuses on interactions between biomolecules and zwitterionic moieties, zwitterionic polymers and zwitterionic polypeptides and their application of zwitterionic strategies for drug delivery.

2.2 Zwitterionic Polymers, Hydrogels, and Nanoparticles

2.2.1 Zwitterionic building blocks

Zwitterionic molecules are found in numerous biological systems and perform functions ranging from regulation of osmotic pressure [16] to modification of cell surface properties [17]. Zwitterions found in nature have frequently become building blocks for synthetic zwitterionic polymers (Table 2.1). The three most commonly utilized zwitterionic building blocks each include a different anion: sulfobetaines (SBs) contain a sulfite anion, whereas carboxybetaines (CBs) have a carboxylate anion, and phosphorylcholines (PCs) have a phosphate anion. These zwitterionic building blocks with polymerizable functional R groups can be subsequently polymerized to zwitterionic polymers. Monomers of CB, SB, dimethylamine oxide (DMAO) and dimethylsulfonio propionate (DMSP) carry the anion farthest from the R-group, whereas the anion in PC is adjacent to the R-group. As positive surface charges display favorable interactions with anionic cell membranes, PC is the only zwitterionic moiety known to enhance zwitterionic cellular uptake [18, 19]. Figure 2.1 displays the most common zwitterionic building blocks in polymerized form.

Table 2.1: Most widely studied zwitterionic building blocks molecular structure and their natural occurrence.

Building block	Molecular structure	Natural occurrence	Synthetic macromolecules
Sulfobetaine (SB) (also known as choline sulfate)		Salt tolerance mechanism in saline soil herbs[16]	[6, 20-27]
Carboxybetaine (CB)		Osmolyte in plants such as sugar beets[28]	[29-39]
Phosphorylcholine (PC)		Mammalian plasma membrane[17]	[40-46]
Dimethylamine oxide (DMAO)		Organic osmolyte present in saltwater fishes[47]	[47-49]
Dimethyl sulfoniopropionate (DMSP)		Protein stabilizer in marine algae[50, 51]	[52]

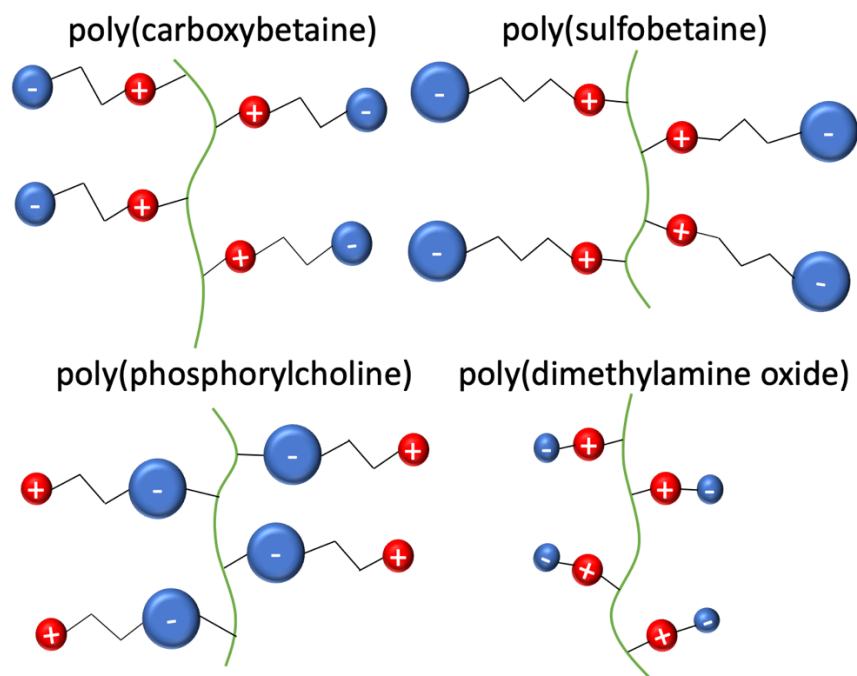


Figure 2.1: Common zwitterionic polymers constructed from the zwitterionic building blocks (Table 2.1). Poly(carboxybetaine), poly(sulfobetaines), and poly(dimethylamine oxide) carry the anion distal to the polymer backbone, whereas poly(phosphorylcholine) carries the anion proximal to the backbone. Poly(carboxybetaine) contains a carboxylate anion and commonly two carbon atoms between charges [29, 34, 35], whereas poly(sulfobetaine) contains the larger sulfite ion and a longer three-carbon linkage [26, 53]. Poly(phosphorylcholine) includes a phosphate ion separated from its cation by two carbons [54], while poly(dimethylamine oxide) has no carbon atoms between its O^- anion and the cation.

2.2.2 Zwitterionic materials in different architectures

Zwitterions have been utilized in a variety of architectures designed for biological applications (Figure 2.2). These architectures include zwitterionic inner salts as protein chaperones and stabilizers [25, 55], zwitterionic polymer-protein conjugates [11, 56], zwitterion-conjugated surfaces [7, 57, 58], zwitterionic nanoparticles [18], hydrogels [34, 59-61], and liposomes [62].

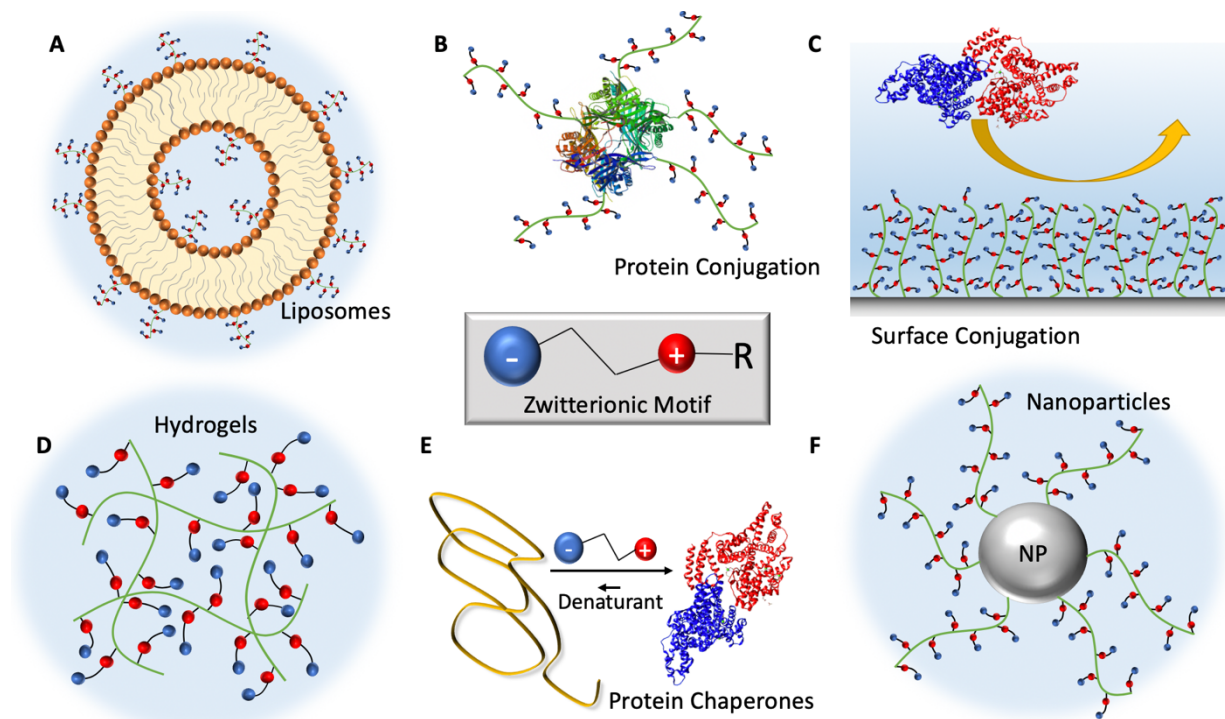


Figure 2.2: Illustration of different architectures in which zwitterionic moieties have been applied in biological systems. These include liposomes (A), zwitterionic polymers-protein conjugates [63, 64] (B), zwitterion-conjugated surfaces [64, 65] (C), hydrogels (D), zwitterionic inner salts as protein chaperones [64, 65] and stabilizers (E), and zwitterionic nanoparticles (F).

Protein-zwitterion interactions have been exploited in several architectures. Zwitterions have been found to enhance the hydrophobic effects that drive protein folding and can, therefore, expand the temperature range over which proteins are stable [66, 67]. Similarly, various zwitterionic moieties (Figure 2.2E) have shown ability to renature proteins from a denatured state [68, 69]. Other studies have conjugated zwitterionic polymers directly to proteins (Figure 2.2B) with the result of reduced immune clearance and increased protein efficacy [11, 70]. Zwitterions are unique in their ability to serve simultaneously as enhancers of protein function while extending circulation time and improving protein stability [10].

Zwitterionic surface coatings (Figure 2.2C) are capable of conveying stealth properties to a polymer substrate to avoid the body's fibrotic and immune responses, and these properties are widely recognized for drug delivery applications [9, 71]. Recently, Chen et al. showed that the hydrophilic properties of a zwitterionic polymer may be transferred to the exterior of a polymer substrate, allowing for enhanced penetration of water into the pores of the structure [72]. Additionally, zwitterionic polymer surface coatings have been used in anti-icing applications by reducing the freezing point of surface-adjacent solutions [73]. Further applications of zwitterionic polymer-based surface coatings include bioseparations and functionalization of nanoparticles onto porous structures for liquid chromatography [6, 74].

Nanoparticles (NPs), Figure 2.2F, are widely utilized in medicine as protein blockers, biocatalysts, imaging agents, and drug carriers [75]. When unmodified, NPs are prone to aggregation and removal from the body, but conjugation with zwitterionic polymers has been shown to overcome these challenges [18, 76, 77]. The anti-aggregation effects exhibited by zwitterionic polymers are comparable to those displayed by poly(ethylene glycol) (PEG) [78]. The concurrent anionic and cationic properties of zwitterionic molecules can reduce NP aggregation by reducing the effective NP surface energy while also simultaneously increasing NP circulation time and cellular uptake *in vivo* [18, 76, 77]. These effects can be enhanced with the use of pH-sensitive zwitterionic moieties capable of adjusting the NP ζ -potential in response to the surrounding microenvironment [18].

Hydrogels (Figure 2.2D) and zwitterions have also been used in conjunction to create crosslinked, hydrated, solid-phase polymers with high hydrophilicity and strong anti-fouling properties [30]. Hydrogels are widely utilized as drug carriers capable of adsorbing drugs, transporting them through the body, and releasing them at a desired location [79]. With the

addition of zwitterionic moieties, hydrogel structures have exhibited enhanced mechanical properties and reduced non-specific protein adsorption [29], adjusted drug loading capacity, and altered diffusion rates [79]. Recently, it has been shown that poly(carboxybetaine) (pCB) and poly(sulfobetaine) (pSB) hydrogels display anti-biofouling effects along with tunable hydrogel functionalization and physicochemical properties [53]. Wu et al. found that the drug loading capacity and diffusion rate from a hydrogel are dependent on the anti-biofouling molecules composing the hydrogel, with different combinations of PEG and pSB showing variations in diffusion rates and drug loading capacity *in vitro* [79]. For most zwitterionic hydrogels, the mechanical benefits of enhanced crosslinking must be balanced against reduced anti-biofouling properties resulting from crosslink disruption of the main polymer hydration shell [29]. This challenge has been addressed by Carr et al. who designed a CB-based crosslink for a CB-based hydrogel that increased the strength of the hydrogel with negligible impact on its anti-biofouling capabilities [29]. As such, zwitterions have shown promise to enhance the utility and biocompatibility of hydrogel structures.

Liposomes (Figure 2.2A), bilayered spheres formed from amphiphilic molecules, have also been shown to display enhanced properties when modified with zwitterionic moieties. Liposomes have been used as drug delivery vehicles as they shield entrapped liquid from the surrounding environment [62]. pCB has been shown to stabilize liposome structure and increase circulation time *in vivo* through increased hydrophilicity and anti-biofouling [62]. As with NPs and hydrogels, this increased liposome retention time is due to a reduction in adsorbed protein molecules, which decreases the liposome removal rate through the reticuloendothelial system [62].

2.3 Dynamics and Solution Behavior of Zwitterions and Zwitterionic Polymers

Zwitterionic polymer hydration, along with inter- and intramolecular interactions of zwitterionic polymers in solution, is foundational to understanding zwitterionic polymer functionality in conjunction with biomolecules. Zwitterionic polymers are well soluble in aqueous solutions, can be hydrated with water molecules and show anti-polyelectrolyte effect in solution [80, 81]. These solution behaviors are a result of ionic interactions, hydrophobic and hydrophilic interactions, and other weak interactions or self-associations observed in zwitterionic polymers systems [39, 42, 53, 82-84].

2.3.1 Hydration of zwitterionic polymers

The hydration of a molecule describes the interactions between the molecule and the surrounding aqueous solvent [85]. The hydration shell surrounding zwitterionic molecules has been hypothesized to be the basis of their anti-biofouling properties [42, 86]. Water molecules have been shown to form a cage structure around zwitterionic polymers, similar to the molecular organization of ice [42]. Water molecules are attracted to the charged functional groups of the zwitterion through ionic solvation, which forms an energy barrier that biomolecules must surmount to contact the zwitterion [86]. This energy barrier is greater than that associated with a poly(ethylene glycol) hydration shell, which is formed through hydrogen bonding rather than ionic solvation [86]. The degree of hydration is dependent on a number of factors, such as molecular weight, surface chemistry, density, chain conformation, and presence and concentration of salt [86, 87].

Zwitterionic properties can vary widely based on anion and cation composition and the length of the carbon chain separating them. The strength and orientation of the zwitterionic

dipole moment, itself a function of the constituent ions and their orientation (Figure 2.3), plays a major role in explaining the behavior of zwitterions in solution [88]. In addition, Niu et al. reported that the strength of a zwitterion dipole moment can be tuned by adjusting the length of the carbon chain between the anion and cation [89]. Furthermore, for zwitterionic polymer the orientation of the dipole moment can influence the tendency for self-aggregation [88]. Orientation of the dipole towards the polymer backbone, as with polyphosphorylcholine (pMPC), has been shown to increase aggregation in comparison to dipole moment orientation away from the polymer backbone [88].

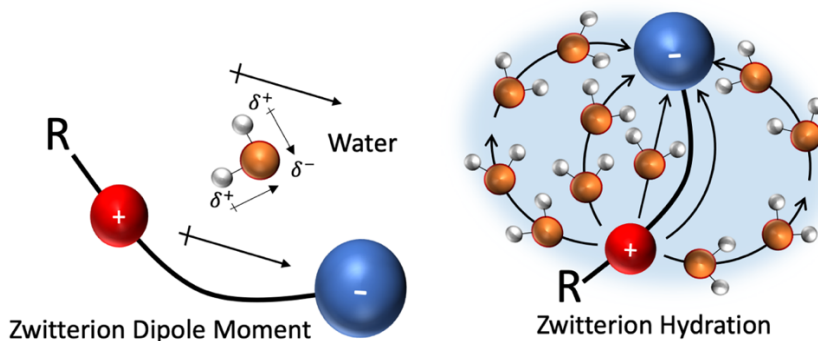


Figure 2.3: Proposed schematic of zwitterion dipole moment and hydration. Left: the negative and positive charges generate a dipole moment that is controlled by their effective distance [88, 90]. Water molecules can align themselves with the zwitterionic molecule dipole moment [57, 91].

2.3.2. Zwitterionic polymers and cosolvents

In general, the solubility of a zwitterionic polymer depends on its molecular weight, concentration, and the salt composition of the solution [92]. Though hydrophilic, zwitterionic polymers can be insoluble in pure water because the electrostatic attractions between the charged functional groups cause the zwitterionic polymers to take a collapsed-coil form [93]. The solubility of zwitterionic polymers increases with the addition of salt, which obstruct the electrostatic attractions between zwitterions, allowing the zwitterionic polymers to dissolve and

take on chain-like conformations [92-95]. Changes in salt concentration do not affect different zwitterions equally. For example, pSB is more affected by salt variations than pCB, for which pSB has been termed an “electrolyte sensitive zwitterion”[94].

Zwitterionic electrolyte sensitivity can be explained by the “like-dissolves-like” concept proposed by Collins [96]. This concept describes how anions and cations preferentially associate with opposing ions of similar strength (ions of equal water affinity) [96-98]. Accordingly, CB associates with strong ions better than SB, and SB better associates with weak ions [97]. The strength of the ions composing a zwitterion will also impact its solubility in different solvent types, with CB showing greater solubility in polar solvents than SB due to its stronger carboxylic acid moiety [93, 99]. Similarly, variation in zwitterionic polymer and ionic cosolvents can cause changes in the organization of the surrounding water [97]. Finally, zwitterionic polymer conformation (and thus solubility) becomes independent of salt concentration once a critical threshold has been reached [100].

The Hofmeister salt series can be used to understand the effects that various ions have on zwitterionic polymers [100-103]. The Hofmeister series classifies ions based on their kosmotropic (water ordering) or chaotropic (water disturbing) behaviors [102] as determined by the solvation energy between the ions and the surrounding water [104, 105]. Based on this effect, zwitterionic pair self-association can be interrupted by ions of similar Hofmeister behavior. The Hofmeister series also explains how adjacent anions and cations can increase interactions between hydrophilic moieties within a solution and how ion specific interactions affect the structure of the water in hydration shell.

The Hofmeister series can also be used to explain how zwitterionic polymers can affect protein conformational stability. As the chemical groups present within each zwitterionic monomer are the ions that increase the hydrophobic effect, the Hofmeister theory predicts that the presence of zwitterionic polymers will enhance the hydrophobic effect that drive protein folding in solution, resulting in greater protein stability [10].

The Hofmeister salt theory can also clarify why zwitterionic polymers display properties that differ from PEG [10]. Unlike zwitterionic polymers, PEG does not increase the strength of interactions between hydrophobic groups in solution and thus should not affect protein conformational stability. Moreover, PEG can weaken the hydrophobic pocket necessary for the formation of some protein-substrate complexes, which reduces protein-substrate binding affinity [106]. In contrast, zwitterionic polymers enhance the stability of the hydrophobic pocket in these complexes [106].

In the case of surface-grafted zwitterions, salt-dependency is affected by an asymmetric hydration state (Figure 2.2C). Sakamaki, et al. found that the anion of surface-conjugated pSB demonstrated a hydration dependency on the presence of a salt, whereas the cation did not [87]. The impact of salt concentration on zwitterionic polymer conformation has also been shown to affect the polymer surface grafting thickness [94]. This can be a useful control method for synthesizing zwitterionic polymer surface conjugates, as the thickness of the final layer may be adjusted by varying the concentration of salt present during grafting [94].

The changes caused by varying salt concentrations in zwitterionic polymer solutions are examples of the anti-polyelectrolyte effect, as illustrated in Figure 2.4. The anti-polyelectrolyte effect is the expansion of a polymer chain in the presence of a salt [100, 107]. This has been

widely observed in zwitterionic hydrogels, which swell in the presence of salt [107-110]. The anti-polyelectrolyte effect is also dependent on the properties of the zwitterionic polymer sidechains. The presence of hydrophobic sidechains reduces the anti-polyelectrolyte effect since salt ions fail to disrupt hydrophobic self-associations as they do electrostatic self-associations [81]. Nevertheless, there is still debate on the extent to which the anti-polyelectrolyte effect occurs due to an incomplete understanding of the dynamics of salt interactions with zwitterionic polymer chains and the impact that electrostatic interactions have on chain conformation [100].

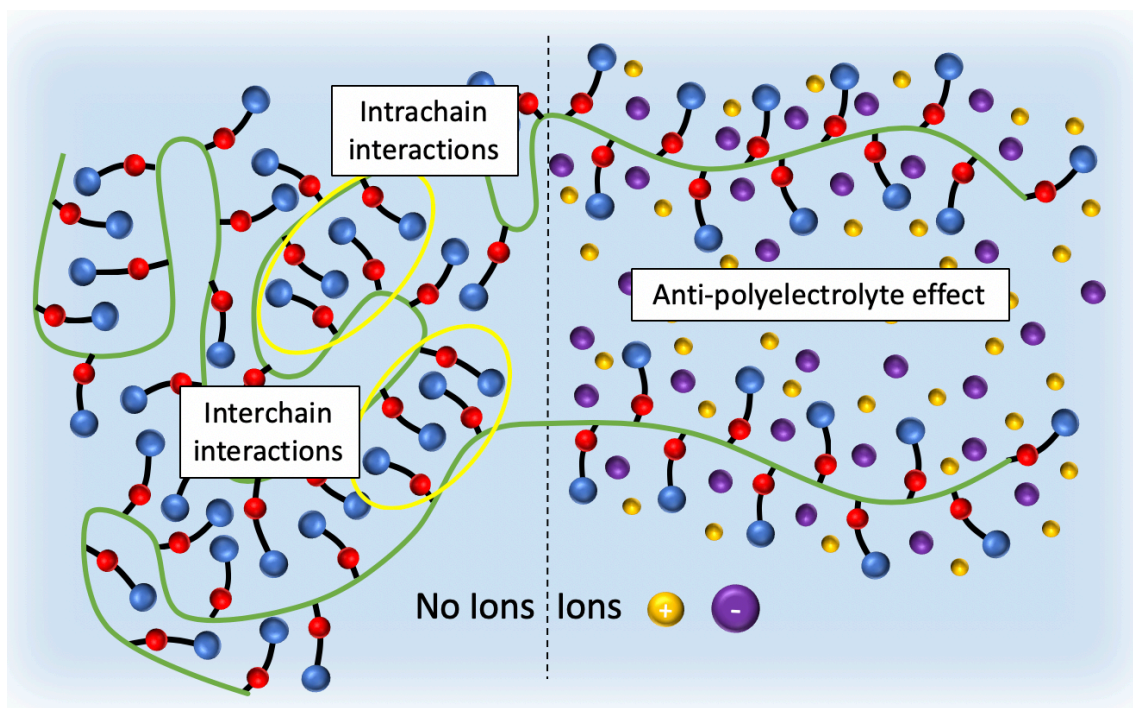


Figure 2.3: Illustration of the anti-polyelectrolyte effect on the zwitterionic polymers (polyzwitterions) interchain and intrachain interactions [80, 95, 111]. Left: The dipole-dipole interactions in zwitterionic polymers result in interchain and intrachain associations [95]. Right: dipole-dipole interactions can be weakened by ionic co-solutes and are explained by the Hofmeister salt behavior [81, 95].

2.3.3. Zwitterionic polymers solubility with temperature variation

The solubility of a polymer in a specific solvent is commonly temperature dependent, with some polymers having an upper critical solubility temperature (UCST), some polymers having a

lower critical solubility temperature (LCST), and some polymers having both an UCST and an LCST. The UCST of a solution is the temperature above which the constituents are completely soluble, whereas the LCST is the upper bound for complete solubility [53, 112, 113]. These critical solubility temperatures have been exploited to great effect for drug delivery applications employing polymers or copolymers as vectors. For example, pNIPAM-based drug delivery systems have an LCST, below which the polymer and drug are completely soluble in one another [114]. Once the delivery system is administered *in vivo* and the system temperature increases above the LCST, phase separation takes place, and sustained drug delivery is achieved as the drug diffuses out of the concentrated polymer system. In contrast to polymers such as pNIPAM, zwitterionic polymers typically display UCST (but not an LCST) behavior [92, 113]. The UCST of the polymer can be used to release the drug only within in areas that temperature exceeds the UCST [115]. The UCST is commonly manipulated by altering polymer molecular weight, which may be necessary for tuning drug encapsulation and release [84]. For zwitterionic polymers, addition of a hydrophobic pendant group to the polymer chain increases the UCST, whereas addition of electrolytes decreases the UCST [53]. Moreover, the UCST can be manipulated by polyionic cosolutes. With pSB for instance, addition of polyanions have shown to decrease the UCST while addition of polycations have increased the UCST [92]. Through these techniques, the UCST can be manipulated to create a polymer suitable for a specific application.

2.3.4. Zwitterionic moieties in amphiphilic molecules

Amphiphilic molecules contain both hydrophilic and hydrophobic groups and can take a variety of forms, including small-molecule surfactants and macromolecular copolymers. The super-hydrophilicity of zwitterions makes them useful as building blocks for amphiphilic molecules. Such zwitterionic surfactants have been reported to interact synergistically with ionic

surfactants to reduce the solution surface tension below the sum of the individual surfactants [116]. SB-containing surfactants have also been shown to stabilize protein structures while preventing thermal and shear aggregation [117].

For amphiphilic zwitterionic copolymers, hydrophobic interactions play a major role in the shape of polymer micelles and aggregates [83]. Headgroup polarity causes zwitterionic polymers to typically take an antiparallel formation between polymer chains, resulting in disk-like, tube-like, or string-like geometries rather than spherical [83]. Amphiphilic block copolymers consisting of zwitterions and hydrophobic moieties have been investigated for their ability to disperse small hydrophobic drugs in water [118]. Star-shaped, amphiphilic copolymers containing zwitterionic blocks were found to be more capable of forming micelles than their linear counterparts, and the micelles formed were smaller than those formed by linear copolymers [119]. Finally, the shape of micelles formed from these amphiphilic, zwitterionic copolymers is a function of solution pH and the strength of the dipole between the charged moieties in the zwitterionic polymer headgroup [120, 121].

2.4 Zwitterionic Strategies in Therapeutics

Zwitterionic moieties possess properties uniquely suited for a variety of applications in the field of therapeutics and biotechnology. In the following section, I discuss strategies employed to take advantage of the properties of zwitterionic materials in conjunction with proteins, genes, and small-molecule drugs.

2.4.1. Zwitterions and therapeutics

Reduction of biofouling

As resistance to protein adsorption is a key in determining the biocompatibility of a material, zwitterionic moieties have been recognized for their potential as biocompatible, anti-biofouling surface materials [122]. Zwitterionic polymers have been studied for use in both implanted medical devices [123, 124] and for wound healing applications [26]. Chou et al. showed that pCB may be incorporated into a hydrogel to prevent protein binding and developed a hydrogel coating that exhibited biofouling of less than 5 ng/cm² [123]. Zhang et al. furthered this understanding by showing that pCB-based hydrogels resisted collagen capsule formation for at least three months when implanted in a mouse model, whereas non-zwitterionic hydrogels showed complete collagen encapsulation within 4 weeks [124]. This study also reported that the zwitterionic hydrogels promoted angiogenesis in the surrounding tissue. Similarly, pSB hydrogels have been shown to enhance wound regeneration. In a mouse study conducted by Wu, et al., pSB hydrogels reduced inflammation, enhanced angiogenesis, and managed macrophage polarization to promote full-thickness wound healing [26]. The study also found in an *in vivo* study that pSB hydrogels outperformed PEG-based hydrogels for wound healing applications [26]. As such, zwitterions show potential for use as surface coatings in medical devices in extended contact with static tissues [124].

Anti-biofouling surface properties have a profound effect on nano-scale components. For example, the surface properties of a NP directly influence its protein corona and biological fate [125]. While PEG has been shown to reduce but not eliminate the development of a protein corona [125-127], NPs conjugated with pPC and pCB have been shown to produce only a soft, reversible protein corona while pSB has been shown to eliminate the protein corona entirely

[128]. Consequently, researchers have applied zwitterionic motifs to NP surfaces for reduced protein adsorption and enhanced retention *in vivo*. Walker, et al. developed zwitterionic (glutamic acid – lysine)_x (E_kx) peptides with surface attachment and antibody-binding terminals to create a bio-functional surface coating for an organosilica NP [129]. The organosilica NPs were used to capture dengue NS1 antigen at concentrations down to 10 ng/mL in both serum and PBS, suggesting the peptide effectively prevented non-specific protein adsorption and maintained antibody efficacy *in vitro* [129]. Yet this enhanced protection and maintenance of protein activity is not limited to biomedical applications; in a comparison between hydrophilic polymers encapsulating horseradish peroxidase for wastewater treatment, pCB exhibited enhanced enzymatic performance and protein stability over several other hydrophilic polymers including pNIPAM [130].

Extension of circulation half-life and maintenance of bioactivity

The increased hydrophilicity conferred to surfaces with zwitterionic moieties makes the development of zwitterionic polymer-based protein delivery promising. Many therapeutics are quickly recognized and removed from circulation by the immune system and thus have been modified with, incorporated into, or encapsulated in hydrophilic and biocompatible coatings. While PEG has been ubiquitous to this point in the drug delivery field, as discussed earlier, its use may decrease the bioactivity or efficacy of the loaded therapeutic [10]. Furthermore, continued administration of PEGylated proteins and NPs has been shown to induce anti-PEG antibody production [131, 132]. In 2015, one Phase III clinical trial of a PEGylated RNA aptamer was discontinued due to anaphylactic reactions against the PEG, with some reactions leading to death [133]. With these issues confronting PEG, alternative biocompatible coatings are needed. The hydrophilic properties of zwitterions have been shown to extend the circulation

half-life of nano- and micro-scale complexes *in vivo* as well as maintaining the bioactivity [134, 135], enhancing therapeutic efficacy [136], and preventing antibody formation against either the therapeutic or zwitterionic macromolecule [70].

Proteins

Multiple studies have utilized uricase, a highly immunogenic protein, as a model therapeutic to determine how pCB affects the induced immune response [10, 11, 135]. pCB has been shown to overcome the challenges posed by anti-PEG antibody generation *in vivo*. Liu and Jiang compared uricase PEGylation with pCB conjugation and found that pCB maintained enzyme stability and activity and showed reduced antibody response in comparison to PEG [11]. Li et al. supported this finding when they encapsulated uricase in a pCB nanocage and reported no recognizable immune response while maintaining uricase therapeutic efficacy in a gouty rat model [135]. Finally, Zhang et al. developed a pCB gel network encapsulating uricase that effectively prevented anti-uricase and anti-pCB antibody formation for 21 days in a rat model [70]. Through these studies, it may be concluded that pCB can mask immunogenic proteins from the immune system, leading to reduced antibody incitation and response.

pCB has also been shown to overcome the challenge of reduced bioactivity in encapsulated or modified protein therapeutics. In a 2012 study, Keefe and Jiang showed that pCB conjugation to a model protein maintained protein stability similar to PEGylation but enhanced enzymatic binding affinity over that of PEGylation through improved protein-substrate hydrophobic interactions [10]. Xie et al. reported that conjugation of pCB to insulin did not result in a significant reduction of *in vitro* bioactivity, while pCB-conjugated insulin displayed a 24% increase in pharmacological activity over the native protein *in vivo* [136]. Extended circulation

time has also been conferred to proteins through direct conjugation with zwitterionic peptides [134]. Banskota et al. reported that fusion of a zwitterionic polypeptide to glucagon-like peptide-1 (GLP-1) extended the circulation time of the protein and showed improvement over the free protein in treatment of type-2 diabetes in mouse models [134].

Genes

Substantial resources have been invested into developing gene therapy technologies, which treat disease through transferring genetic material to the patient through viral vectors, polymers, or lipids [137, 138]. The challenges facing gene therapy are myriad, including extra- and intracellular barriers, gene packaging, stability in serum, cell targeting, endosomal escape, cytoplasm transport, nuclear localization, and unpacking of the genetic material [138]. Technologies incorporating the zwitterionic materials have been shown to potentially overcome many of these challenges through improved nucleic acid packaging, enhanced cell transfection, and environmentally responsive gene release [139-143].

Zwitterionic complexes with nucleic acids avoid clearance from the circulatory system. Such complexes are also non-immunogenic and enhance cellular uptake over similar PEGylated complexes [19]. Li et al. designed pCB lipoplexes (cationic liposomes) that exhibited pH-sensitive properties to deliver siRNA. These hybrid cationic/zwitterionic lipoplexes avoided protein adsorption better than PEGylated lipoplexes, showed accumulation within the tumor microenvironment, and displayed strong endosomal escape properties [19]. In another set of studies, polyethyleneimine (PEI) was grafted with PC- and SB-based polymers to create NPs containing enhanced green fluorescent protein [142, 144]. These complexes were then compared to PEI NPs for their ability to provide stability in serum, transfect cells, and limit cytotoxicity

[142, 144]. In each case, the zwitterionic grafting showed decreased protein adsorption and cytotoxicity as well as increased cell transfection in comparison to PEI, which suggests that zwitterions could replace PEG in gene delivery applications [142, 144].

Stimulus-responsive therapeutic delivery

Stimulus-responsive zwitterionic drug delivery strategies frequently employ release triggers including pH [143], temperature [84], presence of reactive oxygen species (ROS) [140], or redox potential [145]. Tumors are a frequent target of stimulus-responsive systems. The simplest cancer targeting strategy relies on the enhanced permeability and retention (EPR) effect, in which leaky tumor vasculature promotes a passive buildup of nano-scale particles within the tumor environment [146, 147]. Several delivery strategies utilize the EPR effect to passively target tumors with zwitterionic drug carriers before reduced pH or elevated reduction potential triggers drug release [60, 129, 140, 143, 145, 148-151].

While chemical modification can confer pH-responsive properties to zwitterionic building blocks [53], some zwitterions display pH-sensitivity based on the pKa of their constituent ions [39]. The charge of SB is not pH-dependent, but the charge of CB can be either neutral or positive depending on the pH of the solution [100]. Enhanced therapeutic efficacy in a tumor environment can be achieved utilizing a pH-triggered mechanism to induce a change in ζ -potential from negative to positive, which enhances cellular uptake by improving binding efficacy to negatively charged cellular membranes [143, 150]. One such system was developed with PC-based micelles that demonstrated an increase in cellular uptake in an acidic environment prompted through a change in the surface charge [150]. In another recent study, a zwitterionic polymer micelle was shown to be capable of self-assembly at pH 7.4 but displayed aggregate formation, increased ζ -potential, cellular uptake, and drug release at pH 6.5 [148].

Using pH-sensitive hydrozone linkages is another method used to selectively release a therapeutic. Chen et al. incorporated hydrozone linkages when developing zwitterionic pMPC-doxorubicin (DOX) chemotherapy prodrugs. DOX release increased in acidic conditions, with the half-life values of released DOX ranging from 2 to 40 hours at pH 5 [151]. Additionally, cell-culture studies showed that a maximum tolerated DOX dose (MTD) was 3 to 5 times greater than the MTD of free DOX [149, 151]. Shortly afterward, another zwitterionic-DOX delivery strategy was published that utilized a pMPC-based copolymer [60]. As with the prior study, release of DOX increased at reduced pH, achieving 45% release over 75 hours at pH 5.0 compared to 30% release over 75 hours at pH 7.4 [60]. An alternative pH-induced DOX-release system has been developed in which DOX was incorporated into a zwitterionic arginyl-glycyl-aspartic acid (RGD)-conjugated polypeptide [152]. At pH 7.4, the total DOX released was 20% over 24 hours in comparison to 60% DOX released at pH 5.0 [152]. *In vivo* studies showed that the RGD-DOX polypeptide exhibited the EPR effect and reduced systemic toxicity, lending it potential for clinical use [152].

ROS-responsive gene delivery systems have been designed to exhibit a change in ζ -potential in the presence of a peroxide. Recently, Li, et al. developed an ROS-responsive zwitterionic dendrimer that exhibited a ζ -potential shift from 12.3 mV to -5.0 mV when exposed to 80 mM H₂O₂ for 320 minutes [140]. One novelty of this approach is that the zwitterionic moiety was formed in response to peroxide, which resulted in transfection efficiency 4.5 times higher than PEI and greater than 90% cell viability in HeLa cells [140]. In another study, redox-sensitive blocks and pSB blocks were self-assembled through electrostatic interactions to create a gene carrier system [145]. The zwitterions conferred excellent stability, low cytotoxicity, and high serum tolerance to the system, while disulfide reduction led to efficient gene delivery in

upregulated redox environments [145]. When tasked with delivering the anticancer p53 gene to MCF-7 cells, the gene carrier induced over 50% cell death and apoptosis in comparison to 3% for the untreated control and 15% for PEI [145].

Zwitterionic moieties may be utilized in NP drug delivery systems without interfering with other functionalities. A pMPC copolymer prodrug nanocarrier has been developed that contained the hydrophobic photosensitizer drug chlorin e6 (Ce6) connected by redox-responsive disulfides [153]. The zwitterions conferred aqueous solubility to Ce6 while the disulfide bonds allowed targeted drug release in the presence of upregulated glutathione, making it available for ROS generation with light irradiation [153]. Table 2.2 highlights some recent studies utilizing zwitterionic materials to address the challenges of delivering proteins, genes, and small molecule therapeutics safely and effectively throughout the body.

Table 2.1. Recent drug delivery strategies utilizing different zwitterionic moieties. These zwitterionic moieties include poly(sulfobetaine)(pSB), polycarboxybetaine (pCB), polyphosphorylcholine (pMPC), poly(dimethylammonium oxide) (pDMAO) and other zwitterionic moieties

Drug Category	Therapeutic Delivered	Stimulus Sensitivity	Zwitterion	Biological Effect	Advantages	Disa
Small molecule drugs	DOX	pH	pMPC	<i>In vitro</i> study showed strong DOX release and cellular uptake	Increased DOX release in acidic environments	Ree viabilit con
	DOX	pH	pMPC	Achieved high intracellular concentrations and maximum tolerated dose	Increased DOX release in acidic environments	Low DOX 15% I
	DOX	pH	pMPC	Extended circulation time and increased tumor accumulation	Increased DOX release in acidic environments	Show lung accum PEGy
	DOX	pH	pMPC	High accumulation and internalization in HeLa	Increased DOX release in acidic	Ove requi

				cells	environments	DOX
DOX	pH	pCB	Enhanced endosomal escape resulted in increased anti-tumor efficacy <i>in vitro</i> and <i>in vivo</i>	Zwitterionic coating lost at pH 6.8	High kidney	
DOX	pH	pCB	Excellent stability in serum and reduced toxicity	Increased DOX release in acidic environments	Only release a	
DOX	pH	pCB	<i>in vitro</i> and <i>in vivo</i> studies showed high anticancer efficiency and reduced side effects	Increased DOX release in acidic environments	Small DOX	
DOX	pH	CPMA	Empty micelles showed low cytotoxicity, but DOX loading showed strong anti-tumor effects	Increased DOX release in acidic environments	Charge differ cop differ viabil DOX con	
DOX	pH	pSB	Reduced cytotoxicity through shielding of copolymer charge	Increased DOX release in acidic environments	No diff viabil DOX con	
DOX	N/A	pSB	Induced apoptosis and inhibited tumor growth	Cellular uptake mechanism varies with tunable size and surface charge	High p charge ag	
DOX	pH	pSB	Resisted non-specific protein absorption and showed low cytotoxicity	Increased DOX release in acidic environments	Incr releas comp	
DOX	redox potential	pSB	No immunogenic response in BALB/c mice	Increased DOX release in reductive environments	High li accumu	
chlorin e6	redox potential	pMPC	Prodrug inhibited cancer growth upon irradiation	Carries and releases photosensitive drug that produces ROS	15% of wit	

					upon irradiation	
	Curcumin	N/A	pCB	Enhanced suppression of A β fibrillogenesis and reduced cytotoxicity	Increased drug efficacy	No se
Gene Delivery	DNA	pH	pSB	Reduced cytotoxicity	Increased transfection in acidic environments	May sh
	DNA	pH, temperature	carbobenzoxy-l-lysine (A-Lys(Cbz)-OH)	Complexed with DNA	ζ -potential and diameter varied with temperature and pH	DNA l size an
	DNA	temperature	pDMAO	DNA capture corresponded to protonation/deprotonation of zwitterion	Thermo-reversible capture and release of DNA	Micel hinde cha
	DNA	ROS	poly(amido amine)-N-(4-boronobenzyl)-N,N-diethyl-2-(propionyloxy)ethan-1-aminium	Higher gene transfection and lower cytotoxicity than PEI	ζ -potential shift in the presence of peroxide	Zwitter respo
	DNA	redox potential	pMPC	Excellent transfection efficiency and low cytotoxicity	Increased cell death in MCF-7 cells	High I for re
	DNA	N/A	pMPC	Reduced protein adsorption and cytotoxicity	Enhanced cell transfection	Tra efficien less presen
	DNA	N/A	pSB	Reduced protein adsorption and cytotoxicity	Increased cell transfection	Var polyple low g
	DNA	N/A	pMPC	Reduced cytotoxicity in comparison to Lipofectamine®	Maintained transfection with reduced cytotoxicity	Cel decr incre
	DNA	N/A	pSB	Enabled permanent DNA editing and resulted in high protein expression <i>in vitro</i> and <i>in vivo</i>	Protection for CRISPR/Cas9 gene editing	Cel decr incre

	RNA	N/A	pCB	Gene delivery efficiency increased in serum-containing medium	Increased gene expression and uptake	Reduced efficiency
	RNA	pH	pCB	Extended circulation time and increased tumor accumulation <i>in vivo</i>	Enhanced endosomal escape	Enhanced clearance
	RNA	Magnetic field	pMPC	Excellent anti-fouling in solutions of 31 iabil serum albumin and fetal bovine serum	Increased siRNA release with oscillating magnetic field	Minimized aggregation
Protein and peptide delivery	Insulin	Oral	pMPC	Showed affinity for epithelial cells and improved cellular uptake	Passed mucus barrier for oral drug delivery	Oral delivery required
	Insulin	N/A	pCB, pMPC	Enhanced <i>in vivo</i> protein delivery in comparison to PEGylated complexes	Increased blood sugar control in mice	Some studies show
	Insulin	N/A	pCB	pCB-insulin complex showed improved performance <i>in vivo</i> over insulin alone	Increased protein activity <i>in vivo</i>	Increased complex insulin
	Uricase	N/A	pCB	Maintained enzyme activity and induced no antibody production	Improved therapeutic properties over PEGylated complexes	May show similar
	Uricase	N/A	pCB	Showed no immune response against either the protein or the polymer	Maintained enzyme activity	ζ-polymer neutralized
	Horseradish Peroxidase	N/A	pCB	Increased enzymatic activity and protein stability	Stabilized protein for an industrial process	Decreased activity
	GLP1	N/A	(Val-Pro-Lys-Glu-Gly) _n	Enhanced treatment of type-2 diabetes in a mouse model	Increased circulation time	Opposite amino acid show

2.4.2. Zwitterions and stabilization of drugs and biological complexes

Protein refolding and stabilization

Protein folding and conformation is driven by the hydrophobic effects. As discussed earlier, super-hydrophilic properties of zwitterions enhance interactions between hydrophobic moieties in the surroundings. While driven by hydrophobic effects, protein folding can be affected by various molecular chaperones that navigate the protein structure to the final folded form [68]. Zwitterions can act as molecular chaperones to assist in protein folding and refolding. Non-detergent sulfobetaines (NDSBs) have been shown to enhance refolding of lysozyme up to 12-fold through adjustment of the balance between protein aggregation and folding [69]. Expert-Bezançon et al. built upon these findings by analyzing the effect that NDSBs have on the refolding of four different proteins and designing new SBs to optimize the chaperone characteristics [170]. These modified NDSBs achieved 97% and 100% refolding yield in the tryptophan synthase β 2 subunit [170].

Protein renaturation is influenced by zwitterionic molecules in a variety of ways. One early study showed that NDSB 256 enhanced refolding of the tryptophan synthase β 2 subunit by preventing aggregation within the first 2.5 seconds of dilution in refolding buffer [24]. By preventing this aggregation, the renatured protein yield increased from less than 10% with no zwitterions to 100% with the addition of 1.8 M NDSB [24]. More recently, NDSB 201 has been shown to inhibit aggregation of the extracellular domain of type II TGF- β receptor (TBR II-ECD) through binding to a phenylalanine pocket on the TBR II-ECD and stabilizing the folded state by decreasing the entropy of the unfolded conformation [25]. NDSBs are not the only zwitterions known to serve as molecular chaperones; both zwitterionic polymers and detergent

SBs may assist protein refolding and enhance solubility through non-specific association with hydrophobic domains [55, 171]. Zwitterionic monomers lacking the ability to self-assemble have not been shown to operate in this manner [55, 171].

Zwitterionic stabilization of proteins may expand the temperature range at which proteins are stable. Zwitterionic encapsulation can protect proteins from the effect of heat-induced denaturation [172]. Furthermore, zwitterionic-polymer-based core-shell nanogels have been shown to prevent aggregation and loss of lysozyme function when heated by acting as molecular chaperones to stabilize 2nd, 3rd, and 4th order structures [66]. Zwitterions can also extend the time that a protein is enzymatically active in solution. Sakaki et al. developed a poly(MPC)-poly(styrene) copolymer that acts as an effective stabilizer of an antibody-enzyme conjugate for use with enzyme-linked immunosorbent assay (ELISA) [67]. In the study, 1 wt. % poly(MPC)-poly(styrene) retained up to 92% of protein-antibody activity after 37 days in comparison to 10% retention with no stabilizer and 29% retention with a 1 wt. % casein solution [67]. As such, protein stabilization with zwitterionic moieties shows potential for diverse areas beyond protein refolding.

Nucleic acid binding and packaging

The presence of zwitterions has been shown to affect the binding, winding, and packaging of DNA for gene therapy purposes [173, 174]. Interactions between nucleic acids and zwitterions are a function of the structure and concentration of the nucleic acids, zwitterions, and ions in the localized environment. The association between nucleic acids and PC zwitterionic lipid monolayer is driven by hydrophobic interactions between the nucleic acid backbones and exposed lipids rather than with the zwitterionic moieties [173]. With the addition of divalent cations, however, a study by Mengistu et al. found that DNA interactions with zwitterionic PC

lipids were enhanced and a theoretical model was developed to describe zwitterionic DNA complex formation with divalent cation mediation [174]. This model predicted that the presence of cations increases the favorability of the adsorption free energy of DNA on a theoretical zwitterionic surface, which encourages the formation of DNA/zwitterionic complexes [174].

Nucleic acid conjugation with zwitterions can either enhance or diminish gene expression.[175, 176] One study used 2'-O-aminopropyl (AP)-RNA modification to convert a standard RNA strand into a zwitterionic polymer that showed the highest nuclease resistance of any phosphodiester analog [175]. Structural models suggested that the AP modification interfered with the exonuclease metal ion binding site, inhibited RNA enzymatic breakdown, and increased gene expression [175]. In another study, a photoreactive pMPC-based polymer was developed to inhibit the unwinding of DNA when exposed to UV radiation [175]. The phosphorylcholine moieties conveyed water solubility, low cytotoxicity, and high membrane permeability to the polymer, while application of UV light induced a conformation change in the polymer that wrapped it around a DNA strand and inhibited transcription and replication [176]. These findings suggest that zwitterionic moieties can reduce nucleic acid expression in response to an external stimulus as well as increase expression through nuclease inhibition.

Drug solubilization

Zwitterionic moieties have found use as small molecule drug solubilizers. Zwitterionic copolymers enhance drug solubility and absorption, which makes them intriguing prospects as solvent additives for insoluble drugs [177]. Paclitaxel (PTX), which is sparingly soluble in aqueous solutions, showed enhanced solubility in solution with a pMPC-based amphiphilic copolymer, with the PTX-copolymer interaction resulting in slow PTX release [178]. Zwitterions have also shown efficacy in solubility enhancement through covalent attachment to the active

drug. In a study conducted by Zhao et al. curcumin was conjugated to pCB and the highly hydrated zwitterions conferred enhanced drug solubility and efficacy over free curcumin [37]. Accordingly, both covalent and/or non-covalent associations of zwitterionic copolymers may enhance solubility and overall efficacy of small molecule drugs [37, 160, 177, 178].

2.5 Concluding Remarks and Future Perspective

Our collective understanding of interactions between zwitterionic moieties and water, salts, and biomolecules has expanded greatly within the past decade. Researchers have utilized the unique properties of zwitterionic monomers, polymers, and amphiphilic molecules to great effect with applications ranging from protein stabilization to stimulus-responsive drug delivery systems. Despite these advances, however, there remain gaps in the literature that must be addressed to further our understanding of this class of molecules and their interactions with biomolecules.

Although the association of zwitterionic moieties with ions has been studied, these studies do not provide a complete mechanistic view of zwitterionic polymer dynamics and structure in solution, let alone in conjunction with higher order biomolecules [97]. Studies have not yet fully revealed ion-specific interactions on water structure and subsequently the hydration of zwitterionic polymers. Furthermore, there is a discontinuity between understanding zwitterions as natural protein osmolytes and understanding zwitterionic polymers as protein stabilizers; while each has been studied, there is a dearth of information on how polymerization of these natural osmolytes affects their function with respect to hydration. Though some have investigated the effect of zwitterionic polymers on the molecular ordering of water, the effect zwitterionic polymers have on protein hydration is yet unknown. Furthermore, most of the studies on zwitterionic polymer dynamics have focused on zwitterionic monomers with the anion

as the distal charge (pCB and pSB), and it is still to be determined if these findings apply to zwitterions with reversed dipole orientation such as pMPC. The structure of the zwitterionic moieties and polymer packing is very important and there is a clear in knowledge gap in this regard. Similarly, the chaperone effect exhibited by zwitterions on proteins is poorly understood and would likely benefit from simulation studies on the energy of refolding in the presence of different zwitterionic chaperones. Additionally, though it has been reported that protein structure and function are not inhibited by the presence of zwitterions, there have been few investigations into enzyme-substrate reaction kinetics in the presence of zwitterionic polymers. This information would allow for direct comparison with PEG to determine how hydrophilic polymers affect cooperativity in enzymatic activity.

Though these limitations in understanding currently exist, application of zwitterionic technology is promising. I expect these materials to find applications in biosensors, protein separation, protein immobilization techniques, cryoprotectants, and biopharmaceuticals. I further expect to see growing interest from biopharmaceutical and biotech companies in the commercialization of such technologies.

Acknowledgements

This chapter was previously published as: Erfani, Amir, Joshua Seaberg, Clint Philip Aichele, and Joshua D. Ramsey. "Interactions between biomolecules and zwitterionic moieties: a review." *Biomacromolecules* (2020).

CHAPTER III

Encapsulation and Delivery of Protein from within Poly(Sulfobetaine)

Hydrogel Beads

Chapter Overview

In this chapter, I present the experimental results on synthesis of zwitterionic poly(sulfobetaine methyl methacrylate) based zwitterionic hydrogel beads. Our study revealed that the pSB hydrogels are non-toxic, ionresponsive, and their swelling is temperature dependent. The zwitterionic hydrogel beads were capable of undergoing lyophilization without aggregation. Hydrogel beads were loaded with a model protein, bovine serum albumin (BSA), using a post-fabrication loading technique. The protein loading was studied using confocal laser microscopy, indicating homogenous protein dispersion of up to 40 μg BSA/mg hydrogel within the beads. Furthermore, the release rate of the protein from the synthesized hydrogel was studied at different crosslinker to monomer ratios. The protein encapsulated within the zwitterionic hydrogel had slower rates of thermal aggregation compared to non-encapsulated protein in solution. Furthermore, the protein loaded inside the zwitterionic hydrogel better maintained its bioactivity.

3.1 Introduction

Emerging evidence shows that zwitterionic polymers can enhance the efficacy of therapeutic proteins and zwitterionic conjugates promote protein stability [179, 180]. Because of the antifouling properties of zwitterionic polymers, there have been attempts to form zwitterionic hydrogels by crosslinking these polymers to develop anti-biofouling coatings [181-186].

Utilization of hydrogels for biomedical [182, 187-189], agriculture [190], and food industry applications [191] has gained increasing attention for the last two decades. In the case of biomedical applications, hydrogels have potential for use for delivering both small molecules (i.e., localized chemotherapy) and macromolecular (i.e., antibodies and hormones) pharmaceuticals. Hydrogels beads have been investigated for peroral [187], subcutaneous [192] and intramuscular drug administrations.

When administering macromolecular drugs (i.e. proteins), problems such as protein solubility, stability at physiological conditions, efficacy, and immunogenicity can be challenging to address [193]. Undesired interactions between protein and the polymeric networks can result in unfolding and deactivation of the protein [194-196]. Clearly, there is a need for more compatible hydrogels. At 37 °C, many of therapeutic proteins such as antibodies are highly prone to aggregation [197, 198]. For sustained delivery of such proteins, a major challenge arises from the fact that many materials, such as silicon and other hydrophobic coatings, are inherently incompatible with proteins and lead to protein binding and aggregation. Protein conformational changes and aggregation during protein encapsulation and release is considered one of the most important problems for sustained protein delivery [194]. For instance, protein aggregation, structural changes, and denaturing have hindered the development of PLGA microsphere technology for protein encapsulation [199]. Additionally, protein structure and function have a

significant impact on its immunogenicity [200]. For protein therapies, denaturation and aggregation of the protein can result in unwanted immunogenicity followed by clearance of the therapeutic from the body [194, 200]. Similarly, the aggregation and denaturing of vaccine protein can prevent the desired immune responses required for the vaccine to function.

Protein adsorption is a key factor in determining the biocompatibility of a polymer or a surface. Chou et al. showed that zwitterions may be incorporated into coatings to prevent protein binding by incorporating a non-fouling, poly carboxybetaine (pCB) zwitterionic hydrogel coating, exhibiting extremely low fouling [123]. The anti-biofouling and anti-inflammatory characteristics of zwitterionic hydrogels have been exploited for wound healing applications [26]. These non-fouling surface properties [201] have a profound effect on nano-scale components, such as the surface properties of a nanoparticle (NP) [125]. As such, super-hydrophilic zwitterions on the NP surface can resist protein adsorption and enhance its retention within the body [202].

To our knowledge, there is no published reports studying the encapsulation of proteins inside zwitterionic polymer networks (hydrogel beads). Furthermore, post-fabrication loading of proteins inside these hydrogels has also not been previously investigated. Our hypothesis was that a network of super-hydrophilic polyzwitterions can outperform other materials in preventing the protein denaturation during encapsulation within the hydrogel.

Here we have synthesized pSB zwitterionic hydrogel beads and studied their physicochemical properties. We investigated how a post-fabrication loading procedure can result in loading of bioactive proteins within the hydrogels. We have studied the release rate and the activity of the released protein. We also investigated how a super-hydrophilic network of poly

zwitterions can affect the thermal stability of a model protein loaded inside the hydrogel. Additionally, the *in vitro* cytotoxicity of the pSB hydrogel beads was studied.

3.2. Experimental section

3.2.1 Chemicals

Bovine serum albumin (BSA), FITC-albumin conjugate, (2-(Methacryloyloxy) ethyl) dimethyl-(3-sulfopropyl) ammonium hydroxide (SBMA) and p-nitro phenyl caprylate were purchased from Sigma Aldrich. N, N'-Methylenebisacrylamide, tetra methyl ethylene diamine (TEMED), span 80, cyclohexane, and ammonium persulfate (APS) were purchased from Fisher Scientific. All chemicals used were of analytical grade and used without any further purification.

3.2.2 Zwitterionic hydrogel preparation

Inverse emulsion free radical polymerization technique was used for preparation of the hydrogel beads. Monomer (SBMA), the crosslinker N, N'-Methylenebisacrylamide (bisacrylamide), and the initiator, APS, were dissolved in PBS to constitute the aqueous phase. The concentration of APS in aqueous phase was set to 2 wt%. The crosslinker: monomer ratio was varied between 1:50 to 1:5. The monomer concentration in the aqueous phase was varied for different samples prepared for different experiments. For the water content studies, the monomer concentration was set to 20 wt%. For the hydrogel diffusometry and protein loading/release samples the monomer concentration was set to 25, 24, 20, 18, 16, and 10 wt%, for the different crosslinker: monomer ratios of 1:5, 1:10, 1:15, 1:20, 1:30, and 1:50 respectively. The oil phase consisted of 5 wt% span 80 in cyclohexane. Span 80 is oil soluble which facilitated the formation of a water-in-oil emulsion. The aqueous phase was added drop-wise to the oil phase. A vortex mixer was used to generate the emulsion. The ratio of oil to aqueous phase was fixed at 9:1 (v/v) to prevent phase inversion and coalescence of dispersed phase. After emulsion formation, the

catalyst, TEMED, was added to the emulsion (0.4 vol%). After 30 seconds of mixing, the samples were placed on a shaker table to prevent settling of the hydrogel beads before the reaction is finished. The reaction was allowed to proceed for two hours. All the reaction steps were carried out at 25 °C. The process for fabrication of hydrogel is summarized in Figure 3.1.

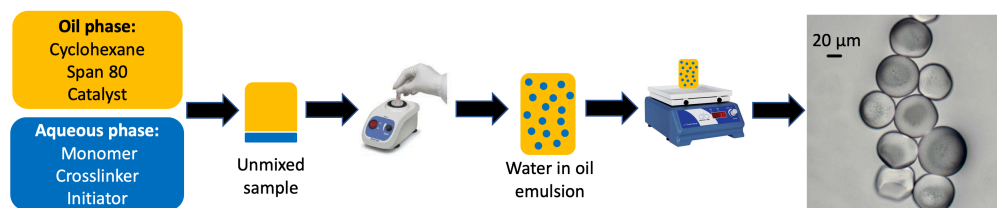


Figure 3.1. Schematics for the fabrication of hydrogel beads

3.2.3 Protein loading

Here a post-fabrication protein loading strategy was utilized. The hydrogel beads were washed with DI water and frozen at -80 °C then placed in a freeze dryer. The dried beads were subsequently suspended in a concentrated protein solution (40 mg/ml BSA) for an extended period of time (3 to 5 days) at the 25 °C temperature.

3.2.4 Hydrogel properties

Equilibrium water content

To determine the water content, hydrogels were equilibrated in PBS or Deionized water for an extended amount of time (3 to 5 days) until their mass equilibrate at 25 °C. Later the swollen hydrogels were weighed, freeze dried and weighed again. For weighing the samples, water (or PBS) was poured out of the tube and the hydrogels were moved to a plastic weighing boat and the excess water (or PBS) was removed using delicate task wipers. The equilibrium water content (EWC) was calculated as follows:

$$\text{EWC} = \frac{\text{mass of water}}{\text{total mass}}$$

Confocal microscopy

Confocal microscopy was used for investigating the protein loading inside the gel beads. For this purpose, a confocal laser microscope (Leica DM E14) was used with 60 × magnification lens. The fluorescently labeled albumin (FITC-albumin conjugate, Sigma) was excited at 488 nm. The hydrogel beads were observed at multiple planes (30 planes) and the intensity of the fluorescent light emitted from each section was compared for evaluating the protein loading.

NMR diffusometry

The diffusive properties of the gels were investigated using pulsed field gradient NMR diffusometry [203, 204]. A 400 MHz Bruker NMR spectroscope equipped with a gradient probe was used. The diffusion tests were carried out using stimulated echo sequence [205] with 100 ms diffusion times. For this purpose, the hydrogel was prepared using the bulk polymerization technique. Hydrogels with different (crosslinker: monomer) ratios were prepared at their equilibrium water contents (previously measured) inside 5 mm NMR tubes. The solvent was prepared as a 9:1 H₂O/D₂O mixture. The self-diffusion of H₂O molecules was measured at 25 °C. The reduced diffusivity of each hydrogel formulation was calculated as:

$$D_{reduced} = \frac{D_{eff}}{D_0}$$

In which $D_{reduced}$ is the reduced diffusivity, D_{eff} is the measured, effective diffusivity in the hydrogel and D_0 is the diffusivity of the free H₂O/D₂O mixture. Furthermore, the tortuosity (τ) and reduced diffusivity are related as follows [206]:

$$D_{reduced} = \frac{1}{\tau}$$

3.2.5 Protein release and bioactivity of the released proteins

Measurement of protein release

The hydrogel beads were loaded with fluorescently labelled BSA at 25 °C. Later the hydrogels were immersed in PBS solution and the amount of protein released from the gel was determined using fluorescence spectroscopy. The volume ratio of the PBS buffer to the hydrogel beads was set to 30. Also, the PBS was periodically replaced with fresh buffer every 24 hrs to preserve the sink conditions. The excitation and emission wavelengths were set to 485 and 535 nm respectively. Solutions with different known concentrations of fluorescently labelled BSA in buffer were prepared and the fluorescence intensity of each sample was measured to prepare a standard plot. Later, this standard plot was used to estimate the concentration of BSA in the buffer during the release experiments. For this purpose, the fluorescence intensity of the release samples was linearly correlated with the known concentration data points.

Bioactivity of released proteins

The purpose of the activity test was to investigate if the proteins released from the hydrogels retain their native conformation and enzymatic activity. For this purpose, the BSA esterolytic activity was measured using a p-nitro phenyl caprylate activity assay [207]. Samples of fresh BSA and BSA released from the hydrogels were prepared at 0.250 mg/ml concentration. The bicinchoninic acid assay (BCA) was used to measure the released BSA concentration, completing the assay according to the manufacturer's protocol. Later 3.63 µl of 6 mM solution of caprylate is added to 100 µl of BSA sample. The samples were then stored at 37 °C for 4 hours. The absorbance of the samples was measured at 410 nm using a Packard SpectraCount plate reader. Furthermore, the protein activity was normalized by the protein concentration. The experiments were carried out in triplicate.

3.2.6 Protein stability

For temperature stability tests, the samples (protein solutions and protein-loaded hydrogels) were incubated at 70° C for different durations to measure protein susceptibility to aggregation. After incubation, the protein from the hydrogels were released into PBS buffer. The samples of released protein were analyzed using native poly acrylamide gel electrophoresis (N-PAGE) to compare the amount of protein monomer lost due to aggregation. Direct comparison was carried out for protein in solution and protein inside the hydrogel at equivalent protein concentrations. Samples were loaded onto 8 wt% polyacrylamide gels and were run at 200 V similar to the work of Flynn et al. [208]. A Bio-Rad Tetra Cell mini gel electrophoresis apparatus was utilized for this purpose. Gels were stained with Coomassie G-250 before imaging. The relative band intensities were compared to determine the amount of protein monomer present in each sample using UVP imaging system software. Furthermore, the BSA esterolytic enzymatic activity of the thermal stability samples was also measured. Experiments were carried out in triplicates.

3.2.7 *In vitro* cell viability assay

For this purpose, at first, zwitterionic polymer pSB was synthesized using free radical polymerization. The reaction was carried out at 25 °C in a buffered solution with pH of 7.6 (PBS). The SBMA monomer was dissolved in PBS at 200 mg/ml concentration. A 10 vol% of APS solution (10 wt% APS in PBS) and 0.4 vol% TEMED was used as the initiator and catalyst respectively. The reaction proceeded for 4 hours on a shaker. The pSB was then purified using a 3.5 kDa dialysis membrane. The ¹H NMR was used to confirm the reaction and to evaluate the average molecular weight. This was achieved by the end group analysis, in which the end groups and the repeating monomer groups were identified and accurate integration lead to evaluation of

the average molecular weight. It is noteworthy that the evaluation of the molecular weight using ^1H NMR was only used for the polymer in solution and not the crosslinked hydrogel beads.

To determine if pSB and hydrogels are cytotoxic, a cell viability assay was used to measure pSB and hydrogel cytotoxicity *in vitro*. Mice fibroblast cells (NIH 3T3) were seeded at 2×10^5 cells/well in DMEM supplemented with 10 vol% calf serum approximately 24 hours before beginning the cell viability assay. Varying concentrations of pSB (0-3 mg/ml) were added to the wells and treated for 24 hours. The Cell Titer Blue cell viability assay (Promega) was performed to evaluate the cell viability by measuring fluorescence intensity. In the case of gel beads, hydrogels were added to the wells at different weight to volume concentrations to the point that a layer of hydrogel beads covered the seeded cells. After treatment for 24-hours, the hydrogel beads were removed, by rinsing the cells with PBS and aspirating. Cell viability was measured for 5 replicates for each sample using the Cell Titer Blue cell viability assay. The cell viability was calculated using:

$$\text{Cell Viability} = \frac{I_s - I_{IPA}}{I_0 - I_{IPA}} \times 100\%$$

where I_s is the fluorescence intensity of the sample. I_0 is the fluorescence intensity of untreated cells and I_{IPA} is the fluorescence intensity of cells treated with isopropanol.

3.2.8 Statistical analysis

For the results of the protein activity and protein stability tests, the student's t-test was performed to evaluate whether or not there was a statically significant difference between protein in solution and hydrogel samples. The null hypothesis of these tests was that there is no difference between the samples (i.e. between protein in hydrogels and protein in solution). The experiments with a p-value less than 0.05 indicate that the null hypothesis was rejected and are denoted by an asterisk in the relevant figures.

3.3. Results and discussion

3.3.1 Zwitterionic pSB hydrogel beads

SEM micrographs of the lyophilized (freeze dried) hydrogel beads (Figure 3.2) show that most of the hydrogel beads formed are within 30-100 microns in size. The micrographs also indicate significant differences in the morphology of the hydrogel formed by the inverse emulsion polymerization technique compared to the bulk polymerization technique (in which no oil phase exits). The hydrogel prepared by the bulk technique has larger pores after lyophilization (10-20 microns in size). These large pores would lead to the burst release of the loaded molecules.

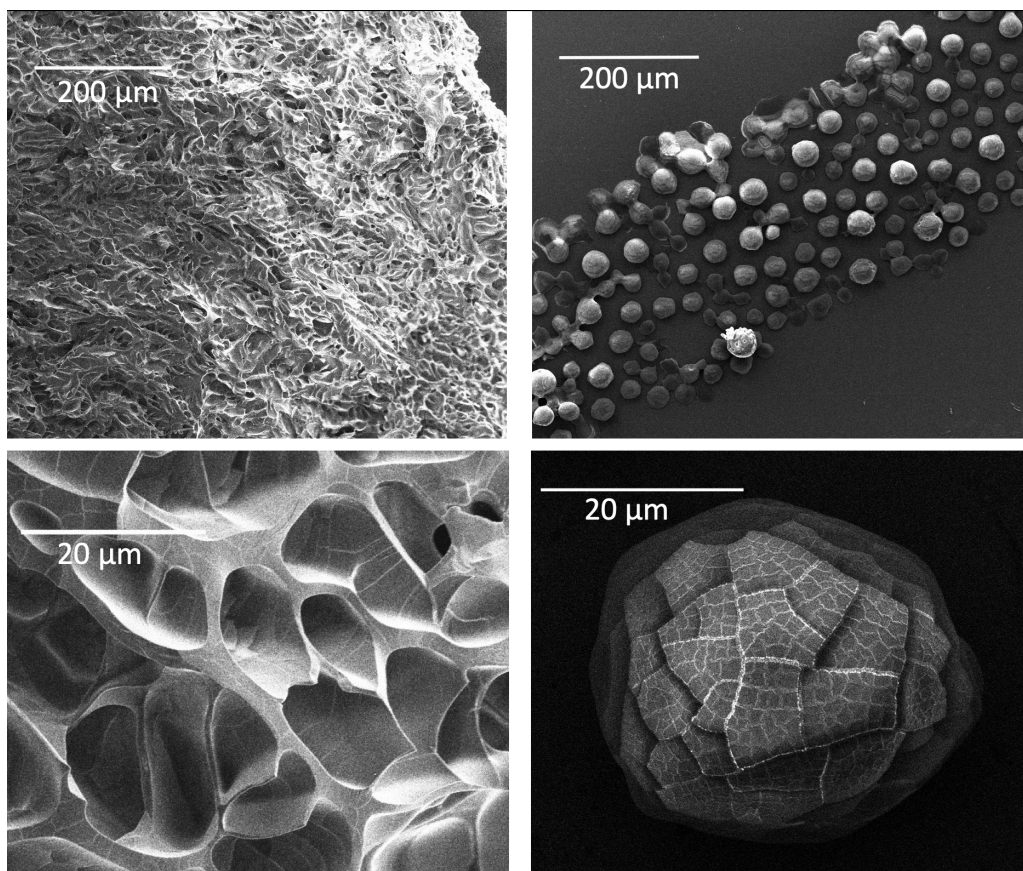


Figure 3.2. SEM of the freeze-dried hydrogels. *Left* (top and bottom): Hydrogel synthesized using bulk polymerization technique. *Right* (top bottom): Hydrogel beads formed using inverse emulsion polymerization. The (crosslinker: monomer) ratio for these samples was set to 1:15 molar.

3.3.2 Physicochemical properties

Water content

The water content of the different hydrogels was measured, and the results are presented in Figure 3.3. Our measurements indicate a decrease in water content associated with increasing crosslinking density (Figure 3.3). The water content of the pSB is similar to that reported for pCB hydrogels [29]. Only at low crosslinking densities does pSB have a higher water content than the pCB hydrogel (0.90 compared to 0.83).

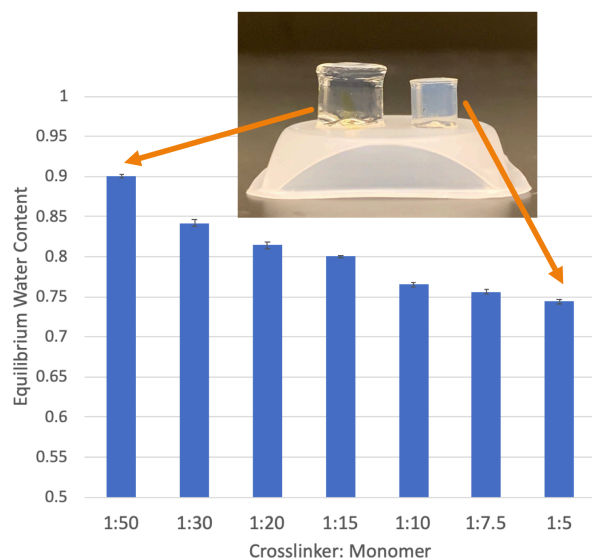


Figure 3.3. Equilibrium water content (PBS as the water phase) of the zwitterionic hydrogels with different crosslinking densities. The hydrogels illustrated in the figure were prepared using the bulk polymerization technique.

Thermoresponsivity

The measured water contents of pSB hydrogels over a range of temperatures (Figure 3.4) shows a positive temperature dependency behavior. The positive temperature dependency of water content for pSB is different from many previously studied hydrogels such as N,N-diethylacrylamide (PDEAM) or N-isopropylacrylamide (pNIPAAm) which have shown negative temperature dependency of swelling (lower critical solution temperature behavior) [209]. For PDEAM and pNIPAAm, at low temperatures, the gel is in its swollen state. For materials like

PNIPAAm, the negative thermosensitivity is explained by hydrogen bond thermosensitivity (higher temperature, weaker the water-polymer interactions). The positive temperature dependency of pSB indicates that the water-polymer association is limited by polymer self-association. As zwitterionic polymer chains are known to self-associate [100], due to the dipole moment of zwitterions, as the temperature increases the self-association weakness resulting in increasing water content.

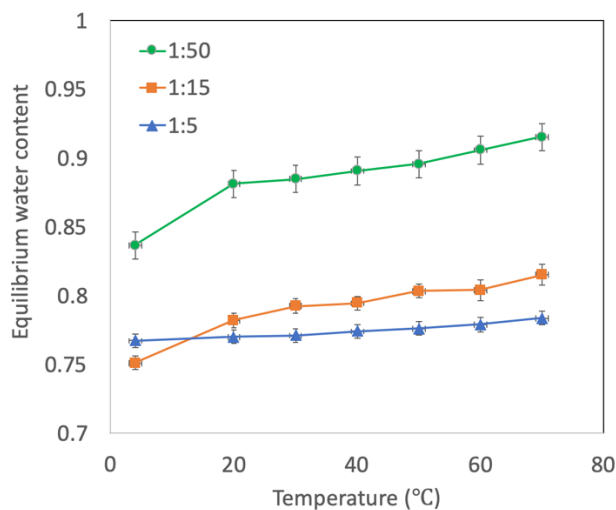


Figure 3.4. Effects of temperature on equilibrium water content of zwitterionic pSB hydrogels. Zwitterionic poly(sulfobetaine) (pSB) hydrogels show a positive temperature dependency behavior.

Ionresponsivity

As can be seen in the Figure 3.5, the hydrogel lost its water content by changing the solvent from PBS to DI water. In poly zwitterions solutions, short range interactions (i.e., attraction and repulsion) between polymer chains due to local charges can make the dynamics of such systems extremely complicated to understand [210]. Nevertheless, zwitterionic polymers have shown anti-polyelectrolyte effects. One of the implications of such behavior is that pSB is insoluble in DI water but is highly soluble when small quantities of salts are present. With this in mind, I would expect the anti-polyelectrolyte behavior of the polymer to affect the ability of the

hydrogel (hydrate crosslinked polymer) to maintain its water content. I postulate that in the absence of ions, the interchain association of the zwitterionic polymer chains results in packing of polymer chains and exclusion of the water that is otherwise stored within the hydrogel. Interestingly, the ionresponsivity is more significant for the low crosslinked hydrogel.

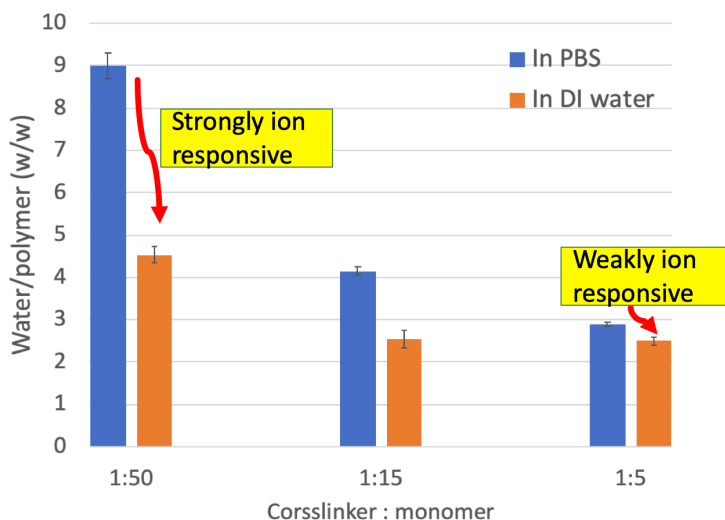


Figure 3.5. Schematic of the ionresponsivity of the zwitterionic poly(sulfobetaine) (pSB) hydrogels. pSB hydrogels swell in the presence of ions and shrink in DI water.

NMR analysis of the hydrogel reduced diffusivity

Diffusion NMR was performed to characterize directly the transport properties of the zwitterionic hydrogels. Utilization of hydrogels, whether for sustained release or for protein immobilization, requires a good understanding of the diffusivity inside the hydrogels. For this purpose, the measured, reduced diffusivity coefficients of different studied gels are presented in Table 3.1. As can be seen in the table, the effective self-diffusion of water (related to the mean square random displacement of water molecules) and the tortuosity of the zwitterionic hydrogel can be controlled by the crosslinking density. Water inside hydrogels can exist in different microscopic states [211]. Previous studies on hydrogels observed bound and unbound water in hydrogels using NMR [212]. The bound water is defined as the fraction of water that at any specific time is effectively immobilized by the hydrogel [212]. The bound and unbound water

within the hydrogel was also observed using ^1H NMR. Figure 3.6 illustrates the ^1H NMR spectra of two different crosslinking densities of pSB hydrogel. The unbound/bound water ratio is also summarized in Table 3.1. Our results indicate that at low crosslinking densities (1:50), all of the water molecules in the hydrogel are bound. In comparison, other hydrogels such as pHEMA (poly hydroxyethyl methacrylate) hydrogels can have up to half of associated water unbound [212]. The small amount of unbound water in pSB indicates the strong water-polymer association in the hydrogel. The high water content and high bound water ratio of pSB compared to other hydrogels can be attributed to the super-hydrophilicity of pSB. For pSB hydrogels, the unbound/bound ratio can increase to 0.20 by increasing the extent of crosslinking. The direct relationship between unbound/bound water ratio and the crosslinking density indicates how the bis-acrylamide crosslinker disrupts the structure of the hydrogel.

Table 3.1. Measured solvent diffusion coefficients of different studied hydrogels

Gel crosslinked density (molar ratio)	H ₂ O/D ₂ O mixture diffusivity Coef. (10 ⁹ m ² /sec)	Tortuosity	Unbound/bound water ratio	Reduced Diffusion Coef. (D _{eff} /D ₀) zwitterionic gel	Reduced Diffusion Coef. (D _{eff} /D ₀) poly vinyl alcohol gels[213]
Low (1:50)	1.424	1.30	0.000	0.77	0.79
Medium-low (1:30)	1.200	1.54	0.004	0.65	--
Medium (1:15)	1.010	1.81	0.103	0.55	0.65
Medium-high (1:10)	0.888	2.08	0.139	0.48	--
High (1:5)	0.796	2.33	0.170	0.43	0.61

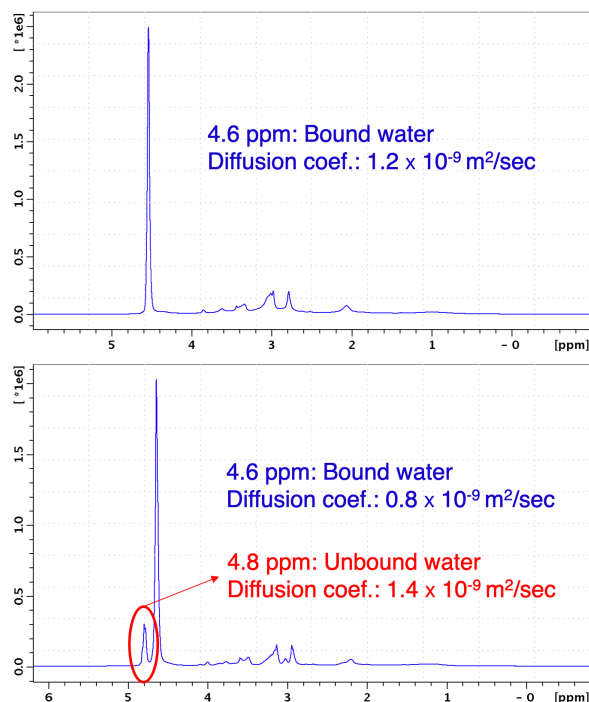


Figure 3.6. ^1H NMR spectra of zwitterionic hydrogel. *Top*: Low crosslink density (1:50 molar). *Bottom*: High crosslink density (1:5 molar)

3.3.3 Post-fabrication protein loading

Unwanted chemical reactions between the hydrogel and the protein amino acid residues can be prevented by loading the protein after the hydrogel formation [214]. Figure 3.7 illustrates the confocal fluorescence microscopy of the hydrogels loaded with fluorescently tagged BSA. As can be observed in the figure, all beads are loaded with protein. Several confocal microscopy studies were carried out to investigate the distribution of the protein inside the bead at multiple planes. Figure 3.8 shows the averaged projection of a series of optical sections at different depths of the bead. This figure demonstrates that the protein molecules have been homogeneously loaded inside the hydrogel and are not surface bound. The amount of protein loaded per weight of dried hydrogel is illustrated in Figure 3.9. The protein loading occurs as a result of capillary and osmotic pressure that forms when the lyophilized hydrogel beads are immersed in a protein solution. Such a loading strategy can only be applied if the hydrogels are small enough for the diffusional loading to take place in a reasonable time.

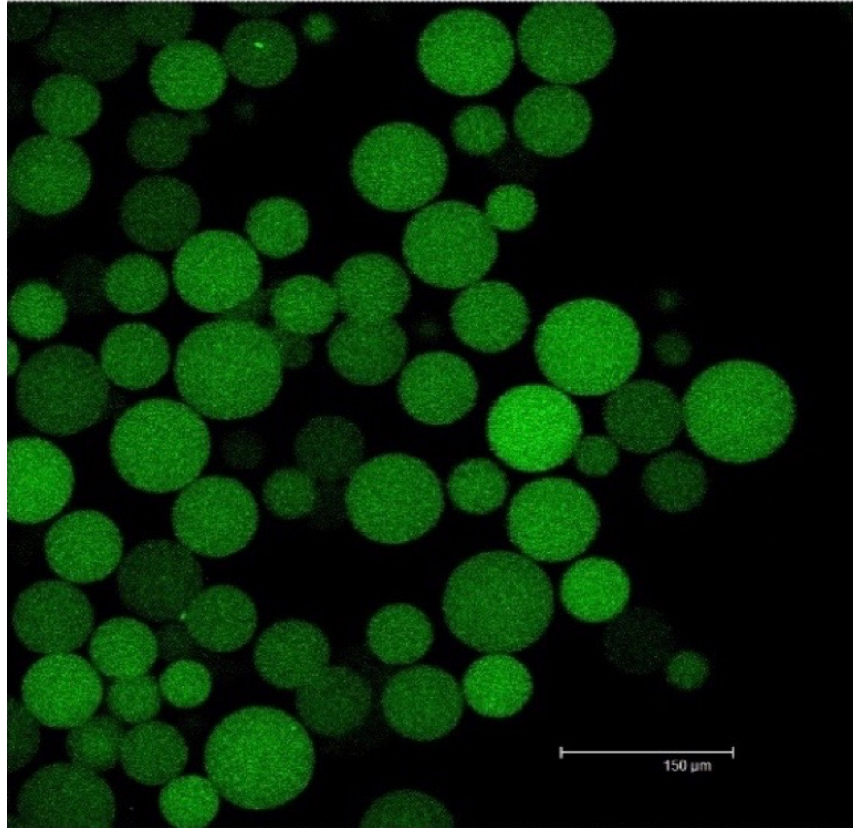


Figure. 3.7 Confocal microscopy of the hydrogels loaded with fluorescently tagged albumin using the post-fabrication loading technique. The crosslinker: monomer ratio was set to 1:15 molar. The hydrogel beads were dispersed in PBS buffer solution

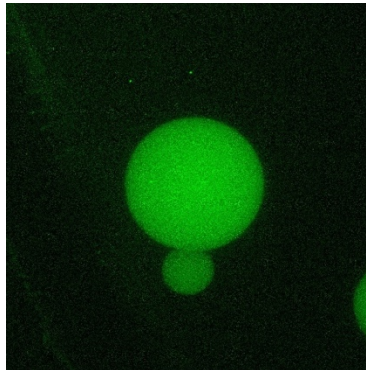


Figure 3.8. The averaged projection of series of optical sections at different depths of the beads. The crosslinker: monomer ratio was set to 1:15 molar. The hydrogel beads were dispersed in PBS buffer solution

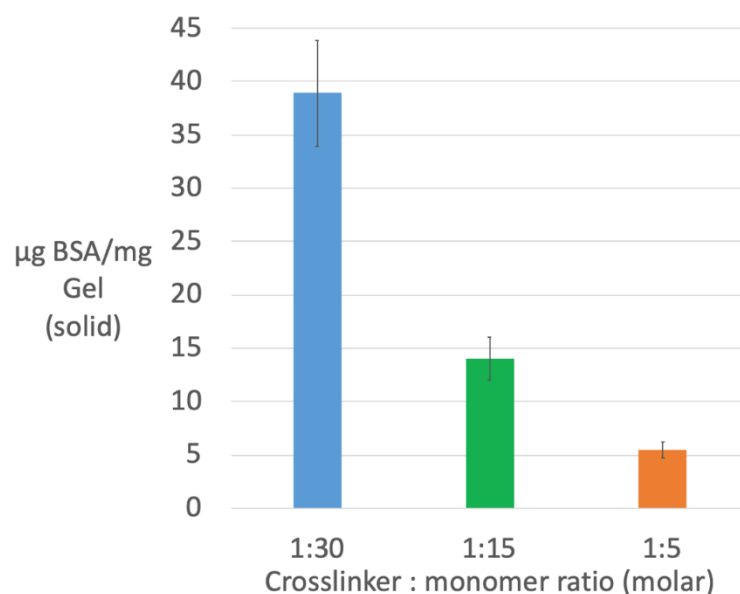


Figure 3.9. The amount of protein loaded inside hydrogels. The amount of protein loading was evaluated after release of FITC-albumin inside PBS.

3.3.4 Protein release and released protein bioactivity

To measure protein release, hydrogels were prepared at their equilibrium water content and loaded with fluorescently labeled BSA. The release was carried out at 37 °C in PBS (Figure 3.10). As seen in the figure, the lower crosslinked hydrogel released more protein than the higher crosslinked hydrogels at all times. The plots show that initially BSA was released following a zero-order relationship. The release of BSA from the pSB hydrogels was diffusion-controlled. As BSA diffused out of the hydrogel, the effective diffusivity of the BSA within the hydrogel increased, offsetting the decreasing driving force (i.e., concentration gradient) for diffusional mass transfer. Similar zero-order release of BSA from hydrogels has been reported previously [215]. Although sustained release was limited to ~48 hrs, there are strategies to slow the release rate and extend release over longer periods of time by tuning the polymer-protein interactions. For example, in our previous work I showed the effectiveness of electrostatic interactions on the encapsulation of different proteins [208, 216, 217]. Using such interactions in combination with

a zwitterionic hydrogel network could potentially slow release of protein from the hydrogel. Manipulating the hydrogel-protein interactions for different release rates, however, is beyond the scope of this article.

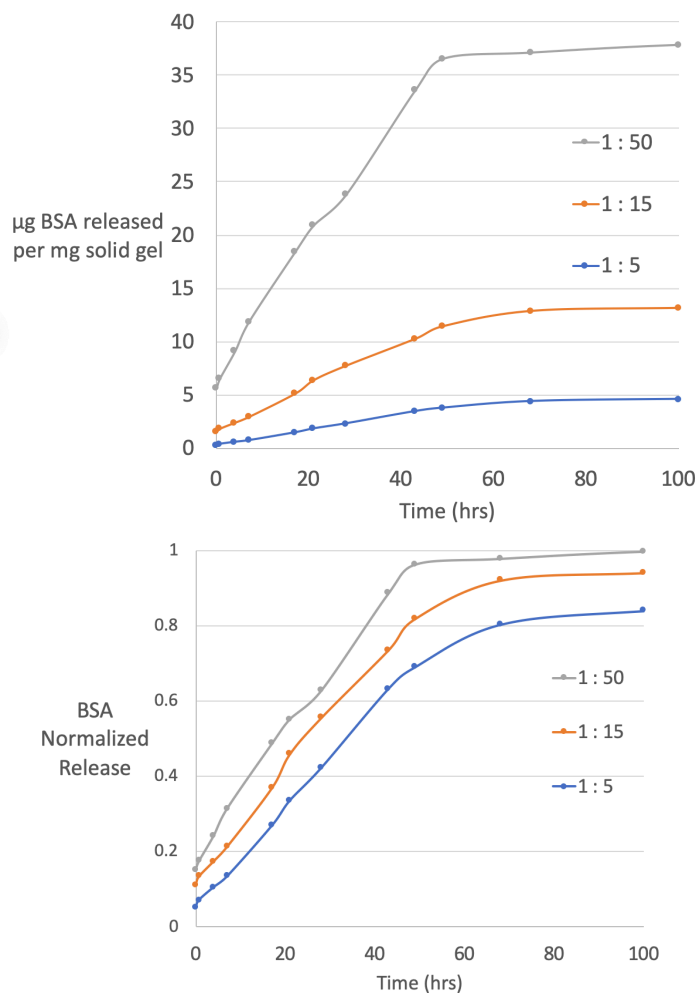


Figure 3.10. Release plots for three different zwitterionic pSB hydrogel crosslinking densities. *Top*: Total amount of BSA released per mass of the solid hydrogel (excluding water). The less crosslinked hydrogel released more amount of protein. *Bottom*: Normalized release of BSA for different crosslinking densities. The amount of BSA release was normalized by the total amount of BSA encapsulated in each hydrogel.

The enzymatic activities of the released proteins (Figure 3.11) shows that for crosslinker: monomer ratios of 1:30 to 1:5, no significant changes in activity were observed. The activity of the BSA suggest that protein molecules were not denatured. The ability of the zwitterionic

hydrogel beads to load and release BSA without loss of esterolytic activity is significant when compared to similar protein encapsulation technologies. For instance, studies on BSA encapsulation in PLGA microspheres indicated that up to 50% of the BSA aggregated or was bound to the polymer in such a way that led to a substantial loss of activity during fabrication [218].

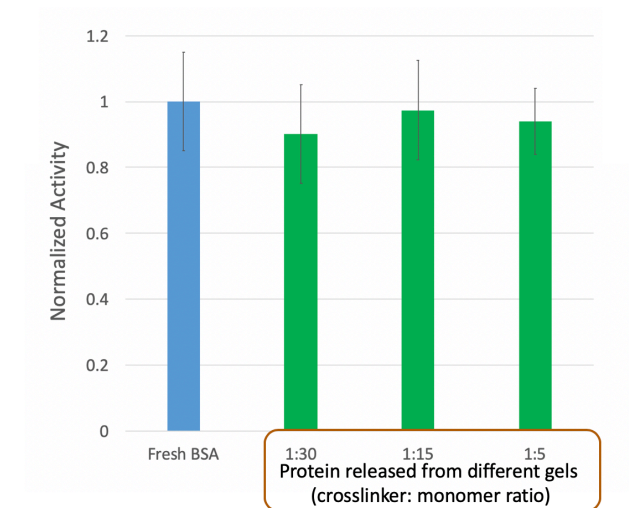


Figure 3.11. The enzymatic activities of the released proteins. The esterolytic activity of fresh BSA solution with known concentration was used to normalize the data.

3.3.5 Protein stability

The thermal stability of encapsulated BSA inside the zwitterionic hydrogel network was studied and compared to BSA in solution (buffered at 7.6 PBS). As shown in Figure 3.12 (left), while the BSA tended to aggregate both in solution and inside hydrogels (at 70 °C), the aggregation rate inside the hydrogel was significantly slower. For example, after 8 hours the quantity of monomers in solution was less than 40% while for the hydrogel it was around 70%. This lower aggregation rate can be attributed to the smaller diffusion coefficients inside the hydrogel (compared to free water, which slows down molecular motion) and is accordance with the ability of the zwitterions to affect the activation energy gaps in protein aggregation

previously reported [219]. The difference between the enzymatic activity of BSA molecules exposed to high temperature showed an even more interesting behavior. As illustrated in Figure 3.12 (right), while the BSA in the solution lost more than half of its enzymatic activity (due to significant tertiary structure changes), the proteins released from the zwitterionic hydrogel retained all of their enzymatic activity. The ability of the zwitterionic hydrogel to improve protein stability can have significant implications both for sustained protein delivery and protein immobilization inside the hydrogels.

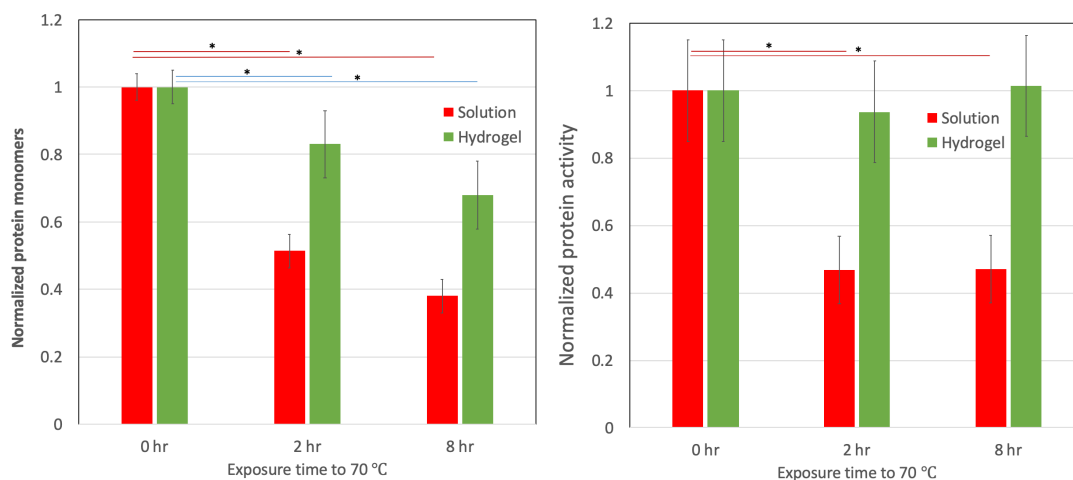


Figure 3.12. *Left*: BSA aggregation when exposed to 70 °C for 0-8 hours. *Right*: BSA enzymatic activity after being exposed to 70 °C. The BSA loaded inside zwitterionic hydrogel (crosslinker: monomer 1:15) can maintain the protein enzymatic activity. The “*” denotes statistically significant changes between the two data points.

3.3.6 Cytotoxicity

The pSB cytotoxicity was studied for concentrations up to 3 mg/ml. The polymer had an estimated average molecular weight of 40 kDa (measured by ¹H NMR and evaluating the number of the polymer end-groups). Cell viability of 100% was observed for concentrations up to 3 mg/ml. For the zwitterionic hydrogel beads, the cell viability assay was carried out by treating the cells with hydrogel beads, which settled onto the cell surface. Figure 3.13 illustrates

different concentrations of hydrogels in the cell medium. Increasing concentrations of the microgel were added and at 2% w/v microgel in the medium, all the cells were covered with hydrogels. Cell viability of 100% was observed for concentrations up to 2% (w/v) of pSB hydrogel beads.

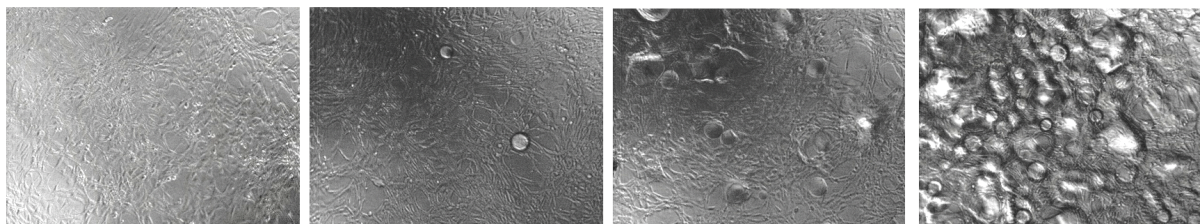


Figure 3.13. Fibroblast cells treated with different amounts of hydrogel beads. From left to right: 0%, 0.02 %, 0.2 %, and 2% (w/v) of hydrogel beads in the medium. Magnification: 10 X.

3.4 Conclusions

Zwitterionic poly(sulfobetaine) (pSB) hydrogel beads were fabricated and BSA was loaded inside the beads following synthesis. pSB hydrogels are ionresponsive as evidenced by the swelling behavior when exposed to ions. Furthermore, a positive temperature dependency of swelling was observed for the pSB hydrogel. The NMR analysis indicated two states of water (i.e. bound and unbound) for highly crosslinked pSB hydrogels. At low crosslink densities, all the water was gel-bound, while at high crosslinking densities, up to 20% of the water was unbound. In addition to the excellent dispersion characteristics of hydrogel beads, the small size of these beads facilitated post-fabrication protein loading due to enhanced surface area. The release of protein from the hydrogel beads was tunable by changing the crosslinking density. High permeability of the hydrogel limited the release of the protein to short timeframes (less than a week). Proteins loaded and released from the hydrogel maintained their native structure (probed by the enzymatic activity). Most importantly, our results indicated that proteins loaded inside the zwitterionic hydrogel beads were thermally more stable (aggregated slower and

retained tertiary structure) than protein in solution. The ability of the zwitterionic hydrogel to improve protein stability has significant implications both for sustained delivery of protein and immobilization of protein within a pSB hydrogel.

Acknowledgements

This chapter was previously published as: Erfani, Amir, Nicholas H. Flynn, Clint P. Aichele, and Joshua D. Ramsey. “Encapsulation and delivery of protein from within poly (sulfobetaine) hydrogel beads” *Journal of Applied Polymer Science* 137, no. 40 (2020): 49550.

CHAPTER IV

Biodegradable Zwitterionic Poly(Carboxybetaine) Microgel for Sustained Delivery of Antibodies with Extended Stability and Preserved Function

Chapter Overview

In this chapter, I will explore using zwitterionic microscale hydrogels for delivery of antibodies. Many recent innovative treatments are based on monoclonal antibodies (mAbs) and other protein therapies. Nevertheless, sustained subcutaneous, oral or pulmonary delivery of such therapeutics are limited by the poor stability, short half-life, and non-specific interactions between the antibody molecules or antibody (ab) and delivery vehicle. A biodegradable zwitterionic poly(carboxybetaine), pCB, based microgel covalently crosslinked with tetra(ethylene glycol) diacrylate (TTEGDA) was synthesized for Ab encapsulation. The microgels were found to contain up to 97.5% water content and showed excellent degradability that can be tuned with crosslinking density. Cell compatibility of the microgel was studied by assessing the toxicity and immunogenicity *in vitro*. Cells exposed to microgel showed complete viability and no pro-inflammatory secretion of interleukin 6 (IL6) or tumor necrosis factor-alpha (TNF α). Microgel was loaded with Immunoglobulin G (as a model Ab), using a post-fabrication loading technique, and Ab sustained release from microgels of varying crosslinking densities was studied. The released Abs (especially from the high crosslinked microgels) proved to be completely active and able to bind with Ab receptors.

4.1 Introduction

Monoclonal antibodies (mAbs) are effective in treating many health conditions including cancer [220], infectious diseases [221], and respiratory diseases [222, 223]. In fact, many recent innovative therapies are based on mAb treatments [224, 225]. Low stability, short half-life, and low bioavailability of mAbs limit their administration to only intravenous (IV) therapy [226], and there is a need for other methods of delivery including oral [227], pulmonary [228], and subcutaneous (SC) [229]. For respiratory diseases, it has been shown that pulmonary delivery of mAbs can be more effective potentially than IV administration [230]. Recently, SC administration of mAbs has gained attention in the area of oncology with medications such as rituximab and trastuzumab being studied for SC administration [229]. Similarly, biodegradable particulate delivery carriers such as microgels can enable direct delivery of therapeutic agents to tumors with reduced side effects as compared to IV administration [231]. Despite these advances, sustained delivery of therapeutic mAbs using protein-compatible materials is still a significant unmet need [232].

One important obstacle in delivery of mAbs using polymers is the conformational changes and aggregation during mAb encapsulation in polymeric networks [194]. This can be caused by mAb conformational instability, mAb-mAb interactions, or unwanted interactions between the mAb and delivery vector. Extended release of mAbs will require that antibodies display stability at body temperature for the duration of the release period. Although mAbs are known to be quite stable at 4 °C, they are unstable when subjected to body temperature for extended periods at high concentrations. An ideal hydrogen/polymer network for delivering mAbs must be able to improve the stability of the mAbs, if the approach is to be successful [233-236]. Previous efforts to deliver proteins through polymeric networks have utilized poly(lactic-

co-glycolic acid) (PLGA) microspheres; however, these polymer networks can result in protein aggregation and denaturation [194-196, 199, 237] which has hindered the development of this technology for encapsulation of proteins such as mAbs. Similarly, poly(ethylene glycol) (PEG) based hydrogels have been studied widely [238] but are likely not suitable for delivering proteins such as mAbs. Firstly, PEG-based hydrogels can promote a degree of nonspecific protein adsorption [239-241]. Secondly, PEG-based hydrogels have shown some level of macrophage activation and pro-inflammatory cytokine secretion [242]. Finally, PEG does not increase protein stability [243]. There is a need for materials that can address these shortcomings, and one approach is to incorporate biomimetic natural zwitterionic osmolytes to prevent nonspecific biomolecule interactions, eliminate/reduce/improve immunogenicity, and increase mAb stability. While emerging evidence indicates zwitterionic polymer conjugates can increase protein half-life, there is little empirical information of using such materials for sustained mAb delivery (encapsulation/release) especially in the form of microgels. This strategy has the potential to address the mentioned unmet needs in delivery of antibodies.

Utilization of hydrogels for biomedical applications has gained increasing attention [182, 187, 188, 244]. Injectable hydrogels such as microgel beads have been investigated for oral [187], subcutaneous [192], intramuscular [245], ocular [246], and pulmonary [247] administration of therapeutics. Degradable microgels can eliminate the need for surgical removal after drug delivery is accomplished. The degradation can be achieved by different strategies such as physical degradation for chain-entangled hydrogels, using degradable polymer backbones, or employing degradable crosslinkers such as tetra(ethylene glycol) diacrylate (TTEGDA) [238].

To our knowledge, there is no published report studying biodegradable zwitterionic microgels. More importantly, encapsulation and release of antibody (Ab) within zwitterionic

microgels have not been investigated. Our hypothesis was that the nature of a super-hydrophilic zwitterionic polymer network can enhance Ab stability resulting in release of bioactive antibodies from the hydrogel. The overall objective of this work was to synthesize and evaluate biodegradable zwitterionic microgels to enable cell-compatible and non-immunogenic Ab delivery. Carboxybetaine, a natural osmolyte, was used as the repeating unit of the polymer crosslinked with TTEGDA. I investigated how a post-fabrication Ab loading technique can result in loading and enhanced stability of a model Ab (IgG).

4.2 Experimental section

4.2.1 Chemicals

N-(3-(Dimethylamino)propyl) methacrylamide (DMPAA) and β -propiolactone were purchased from Sigma Aldrich. Human total IgG was purchased from VWR. TTEGDA, tetra methyl ethylene diamine (TEMED), span 80, cyclohexane, fluorescein isothiocyanate (FITC), anhydrous acetone, and ammonium persulfate (APS) were purchased from Fisher Scientific. All chemicals used were of analytical grade and used without any further purification.

4.2.2 Synthesis of the poly(carboxybetaine) microgels

Firstly, the carboxybetaine methyl methacrylate monomer (CBMA) was synthesized through reacting DMAPAA and β -propiolactone. DMAPMA (20.7 g) was mixed with 450 ml anhydrous acetone, and β -propiolactone (9 ml, in 90 ml anhydrous acetone (10 v/v%)) was added slowly to the DMAPAA solution. The reaction was carried out at 25 °C in a nitrogen-purged container for 6 hours under gentle mixing. The product was insoluble in acetone; as such, the precipitate was separated from the solution by centrifugation upon completion of the reaction.

The product was washed in acetone twice and dried under vacuum for 48 hours before storage at 4°C.

Next, an inverse emulsion, free radical polymerization technique was used for preparation of the microgel. Monomer, crosslinker (TTEGDA), and the initiator (APS) were dissolved in phosphate buffer saline (PBS) to constitute the aqueous phase. The molar crosslinker to monomer ratio was varied from 1:50 (low crosslinking density) to 1:3 (high crosslinked density), while the concentration of APS was held constant at 3 w/w%. The monomer concentration in the aqueous phase was set to 22 w/w%. The oil phase consisted of 1 w/w% span 80 in cyclohexane to assist the formation of a water-in-oil emulsion. Furthermore, TTEGDA was also dissolved in cyclohexane at concentrations between 5 mg/ml (for low crosslinking) to 10 mg/ml (for high crosslinking) to prevent partitioning. The aqueous phase was slowly added to the oil phase and mixed using a vortex mixer to generate a water-in-oil emulsion with a fixed oil to aqueous phase volume ratio of 9:1. After emulsion formation, the catalyst, TEMED, was added to the emulsion (1% v/v) in 6 aliquots while the sample was mixed. The reaction was allowed to proceed at room temperature for 6 hours on a shaker table to prevent settling of the microgel. After the reaction was completed, the samples were washed with cyclohexane to remove the span 80 and were later washed with DI water. The oil and unreacted chemicals were separated from the microgel particles using centrifugation. The microgel was equilibrated in DI water for 3 days and later freeze-dried under vacuum (lyophilized) and stored at 4 °C. Images of the microgel were taken using an FEI Quanta 600 field-emission scanning electron microscope (SEM) with a voltage of 2 kV and magnification of 1,000 and 10,000 X after carbon coating.

4.2.3 Post-fabrication Ab loading

A post-fabrication Ab loading technique was utilized. The dried microgel was suspended in a 40 mg/ml Ab solution for 5 days at 4 °C in Tris HCl buffer (pH 8). As the microgel is hydrophilic, the Ab solution soaked into the microgels to hydrate the polymer structure. The microgel beads were later washed with PBS to remove the excess Ab solution.

4.2.4 Ab labeling

IgG solution (10 mL at 15 mg/ml in 500 mM sodium carbonate buffer pH 9.5) was prepared and kept at 4 °C. Later, 400 µl of FITC solution (10 mg/ml in dimethyl sulfoxide) was added in 50 µl aliquots. The reaction was carried out at 4 °C for 10 hours (no mixing). The unreacted FITC was removed in three stages using a 3.5 kDa dialysis membrane in the exchange buffer (10 mM Tris buffer, 150 mM NaCl, pH 8.2) for 24 hours. The sample was later concentrated to 40 mg/ml (evaluated with UV-Vis) using a 10 kDa concentrator. The fluorescently labeled IgG (FITC-IgG) was used for confocal microscopy and the release studies.

4.2.5 Characterization of the microgel

Confocal microscopy

Confocal microscopy was used to investigate Ab loading within the microgel beads. The FITC-IgG was excited at 488 nm (argon/krypton laser) and visualized with a Leica DM E14 confocal laser microscope with a bandpass filter for the range 520 – 560 nm.

Fourier transform infrared spectroscopy (FTIR)

FTIR was carried out on the freeze-dried microgel samples of different crosslinking densities. A Thermo Scientific Nicolet iS50 ATR-FTIR instrument was used for this purpose.

Small-angle neutron scattering (SANS)

SANS was used to investigate the microstructure of the microgel. SANS provides structural information ranging from a few nanometers to a fraction of a micron. Measurements were carried out at the National Institute of Standards and Technology (NIST) Center for Neutron Research (NCNR) on the 10 m SANS beamline. Data was reduced to absolute intensity using the standard reduction protocols provided by the NCNR [248]. Microgel samples were immersed in D₂O for enhanced contrast and data was analyzed using Sasview software [249]. The scattering data was illustrated by defining the wavevector (q) as Equation 1, where λ is the neutron wavelength and θ is the scattering angle.

$$q = \left(\frac{4\pi}{\lambda}\right) \sin \frac{\theta}{2} \quad (1)$$

Results were analyzed using the correlation length model displayed in Equation 2, where A is the Porod scale, n is the Porod exponent, C is Lorentz scale, m is the Lorentz exponent, B is the background term, and ζ is the correlation length [250].

$$I(Q) = \left(\frac{A}{q^n}\right) + \left(\frac{C}{1 + (q\zeta)^m}\right) + B \quad (2)$$

The first term describes Porod scattering from clusters. In this work, the first term was removed by setting A to zero. Second term is the Lorentzian function describing scattering from polymer chains (exponent = m) and was fitted to experimental data to find the ζ .

Water content and swelling ratio

Water content and swelling ratio were measured after microgel samples were equilibrated in PBS for 4 days at 25 °C. Subsequently, the swollen microgels were weighed, washed/stored in with DI water (to removed salts), freeze-dried, and weighed again. For weighing the samples, microgel beads were moved to a plastic weighing boat and the excess PBS was removed using

wipes. Water content and swelling ratio were calculated from Equations 3 and 4, where W_s and W_d are the weight of the microgel samples in the swollen and dry state, respectively.

$$\text{Water content} = \frac{(W_s - W_d)}{W_s} \quad (3)$$

$$\text{Swelling ratio} = \frac{W_s}{W_d} \quad (4)$$

Diffusion NMR

Diffusion NMR was used to measure solvent mobility inside the microgel. This was achieved using a 400 MHz Bruker NMR spectroscope equipped with a gradient probe. Pulse field gradient NMR was used [203, 204] with stimulated echo sequence [205] and diffusion time of 0.100 seconds. Microgels with different crosslinker:monomer ratios were prepared at their equilibrium water contents. The solvent was prepared as a 1:9 H₂O/D₂O mixture and measurements were carried out at 25 °C. The reduced diffusivity of each microgel formulation was calculated with Equation 5 in which $D_{reduced}$ is the reduced diffusivity, D_{eff} is the measured, effective diffusivity in the microgel and D_0 is the diffusivity of the free H₂O/D₂O mixture.

$$D_{reduced} = \frac{D_{eff}}{D_0} \quad (5)$$

The $D_{reduced}$ compares the mobility of solvent within the material (D_{eff}) with the free solvent outside the material (D_0). Furthermore, the tortuosity (τ) and reduced diffusivity were related by Equation 6 [206].

$$\tau = \frac{1}{D_{reduced}} \quad (6)$$

4.2.6 Microgel hydrolytic degradation

To evaluate microgel hydrolysis-based degradation, microgels with different crosslinking densities were dispersed in PBS and stored at 40 °C. At different time intervals, samples were removed and washed using DI water to remove degraded water-soluble products. Samples were dried and weighed and the change of mass of the microgels was used to determine microgel degradation (samples were prepared in triplicate).

4.2.7 *In vitro* cell viability assay

Mouse fibroblast cells (NIH 3T3) were seeded in a 96-well plate at 2.5×10^4 cells/well in DMEM supplemented with 10% v/v calf serum 24 hours before the cell viability assay. Varying concentrations of the microgel (0.05%-5% v/v) were added to the wells for 24 hours. After treatment for 24 hours, the microgel beads were removed by rinsing the cells with PBS. The Cell Titer Blue cell viability assay (Promega) was performed (6 replications) to evaluate the cell viability *via* fluorescence intensity. In addition to the microgels, the degradation products of the microgels (soluble polymers) were separated and evaluated for cytotoxicity. The cell viability was calculated using Equation 7, where I_s is the fluorescence intensity of the sample. I_0 is the fluorescence intensity of untreated cells and I_{IPA} is the fluorescence intensity of cells treated with isopropanol.

$$\text{Cell Viability} = \frac{I_s - I_{IPA}}{I_0 - I_{IPA}} \times 100\% \quad (7)$$

4.2.8 *In vitro* immunogenicity assay

The immunogenic responses of mice macrophage cells to the microgels were evaluated by quantifying the cytokine expression *in vitro*. For this purpose, RAW 264.7 cells were seeded

at 3×10^5 cells/well in DMEM. The cells were treated with microgels at different concentrations (4 replicates) for 24 hours before cell media were sampled. Secretion of interleukin 6 (IL-6) and tumor necrosis factor-alpha (TNF α) were studied using two separate pre-coated enzyme-linked immunosorbent assay (ELISA) kits (Invitrogen) according to the manufacture's protocol.

4.2.9 Release of IgG and IgG activity

The FITC-IgG loaded microgels of different crosslinking densities were dispersed in PBS buffer and stored at 40°C (10 mg of microgel was loaded and immersed in 2 ml PBS). The PBS buffer was replaced with fresh PBS after each sample was taken, and the removed sample was stored at 4 °C. FITC-IgG concentrations were evaluated using a fluorescence plate reader and by comparing to a previously made calibration curve for the free FITC-IgG fluorescence intensity (samples in triplicates).

The ability of the released antibodies to bind with Ab receptors was studied with a separate ELISA. Released IgG (not labeled) solution from the microgels were diluted to known concentrations and evaluated using an anti-Ab pre-coated ELISA kit for total human IgG (Thermo Fisher). The test was repeated twice with each sample in duplicate (total of 4 replicates). The “student's t-test” was performed to evaluate whether there was a statically significant (p -value < 0.05) difference between activity of antibodies, and statistically significant differences are denoted by an asterisk in the relevant figures.

4.3 Results and discussion

4.3.1 Biodegradable pCB microgels

polymer strands. Furthermore, the microgels with the lowest crosslinking ratio (1:30) have more structural imperfections. Although distinct particles can be observed, most particles are agglomerated together. One can speculate that 1:30 crosslinker:monomer ratio was close to the critical crosslinking concentration that can result in gel formation and that lower concentrations may not form particles with sufficient rigidity to keep their particle-like form.

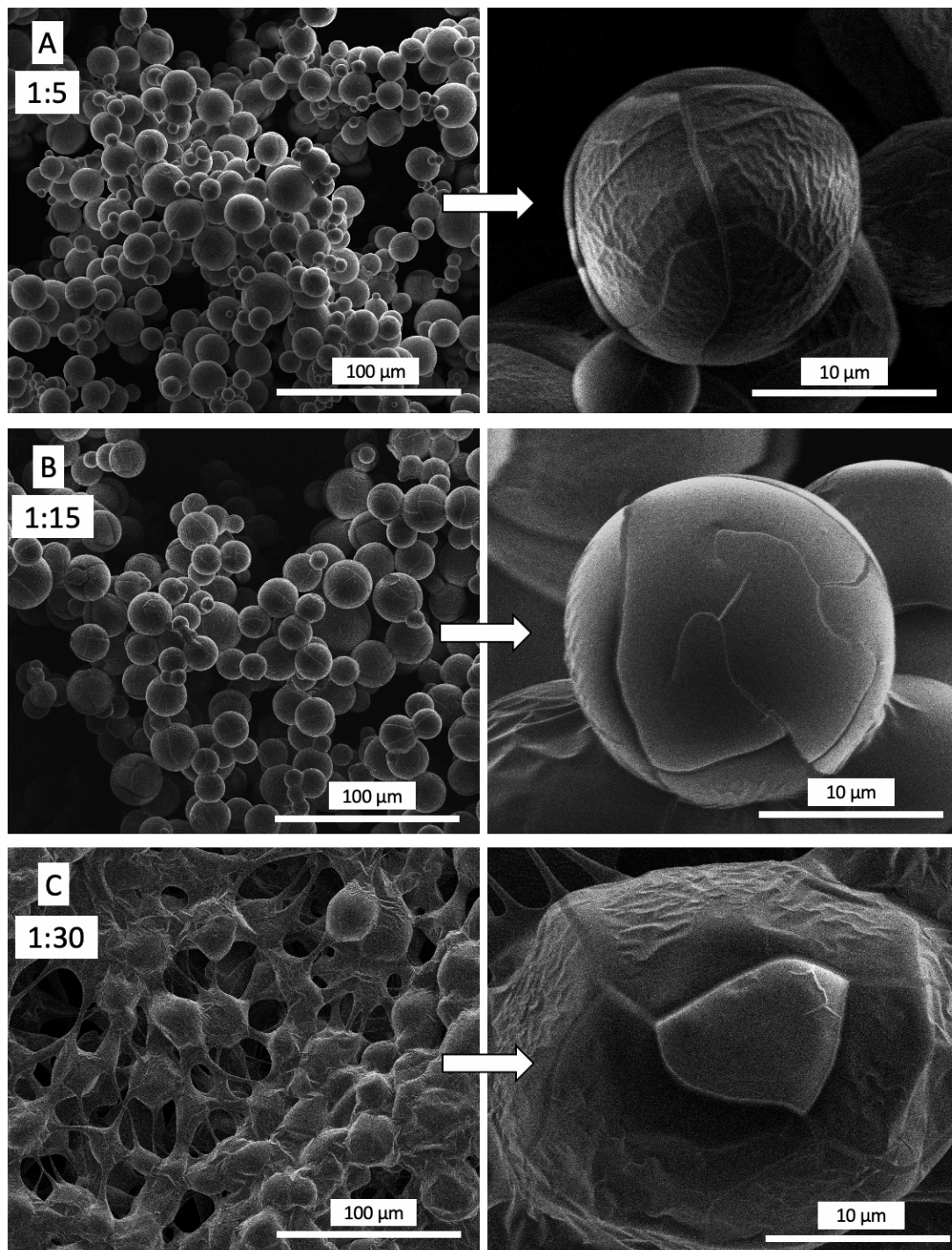


Figure 4.2. SEM of the freeze-dried zwitterionic pCB microgels formed with different crosslinking densities. The molar (crosslinker: monomer) ratio for these samples are **A**: 1:5, **B**: 1:15, and **C**: 1:30.

The synthesized microgels were extremely hydrophilic and swelled with high water contents at all crosslinking densities (Figure 4.3A). We observed water content up to 97.4% and a swelling ratio of approximately 38 for the low crosslinked microgels (1:30) which is higher than several previously studied pCB hydrogels [29, 251, 252]. For the high crosslinked microgel (1:3), the water content was 88.0%. In comparison, pCB hydrogels crosslinked with methacrylate were previously shown [29] to have a lower water content of 70%. The high water content of the TTEGDA-crosslinked microgel indicated that the flexibility of the crosslinker did not prevent hydration even at high crosslinking densities.

The FTIR spectra (Figure 4.3B) of the monomer was compared to microgels with different crosslinking densities. For the monomer, we observed a peak at 1670 cm^{-1} for the C=C bond which disappeared after polymerization. Also the 1080 cm^{-1} peak corresponding to the C-O-C bond [253] was associated with the TTEGDA crosslinker. This is important as TTEGDA can potentially partition in the oil phase, which can reduce control of the extent of crosslinking. The intensity of the peak increased at higher crosslinking densities, indicating that crosslinking densities of the samples were correctly controlled. The NR_4^+ bond was observed at 3250 cm^{-1} . Furthermore, peaks for the asymmetric and symmetric $-\text{COO}^-$ stretching were observed at 1590 cm^{-1} and 1370 cm^{-1} accordingly, indicating a negative charge due to unprotonated carboxylic acid for all crosslinking densities. Similarly, the positively charged ammonium was observed at $2800\text{--}3000\text{ cm}^{-1}$, confirming the zwitterionic nature of the microgels.

The mobility of solvent within the microgels was evaluated using diffusion NMR. I investigated if the nature of the microgel can effectively reduce the diffusivity of the confined solvent and whether the diffusivity can be tuned by the crosslinking density. The studied

microgels showed reduced diffusivity (defined as $\frac{\text{diffusivity within the microgel}}{\text{diffusivity outside the microgel}}$) of 0.67 for the 1:30 microgel which indicated that the microgel was very permeable. For the 1:5 microgel the reduced diffusivity was as low as 0.52 (equivalent to a tortuosity of 1.9).

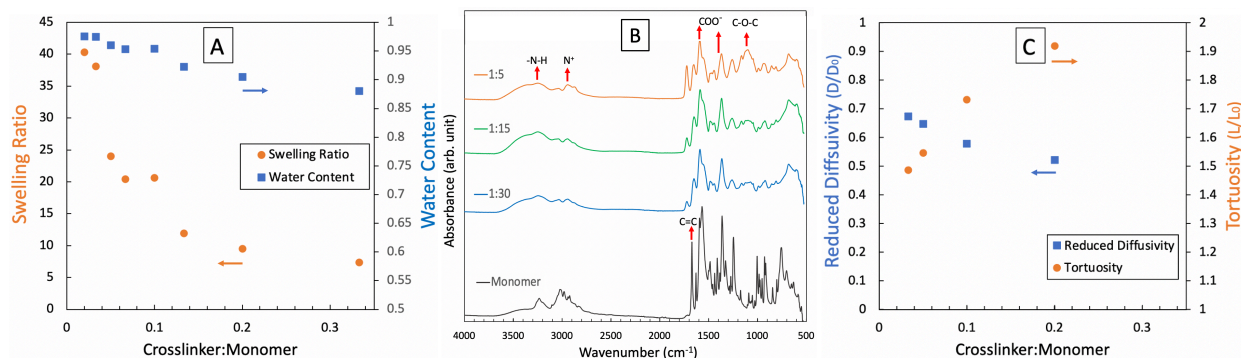


Figure 4.3. Characterization of the synthesized zwitterionic poly(carboxybetaine) microgel crosslinked with tetra (ethylene glycol) diacrylate at 25 °C. **A:** Water content and swelling ratio of microgels with different crosslinker:monomer ratios. **B:** FTIR spectra of the carboxybetaine methyl methacrylate monomer and the microgels. **C:** Reduced diffusivity and tortuosity of the microgels measured using diffusion NMR.

The microstructure of the microgels was further studied using SANS (Figure 4.4). The significance of evaluating microstructure of the microgels experimentally compared to using theoretical methods such as Canal-Peppas and Flory Huggins lies with that fact that these models significantly underestimate the pore size of microparticles. The correlation length of the polymer chains, which is an estimate of the average distance between entanglements that form within the microstructure of the hydrogel, was evaluated using the correlation length model [250, 254]. Overall, the correlation length varied from 24.2 nm for low crosslinking (1:30) to 3.0 nm for high crosslinking (1:5). Analysis of the 1:30 and 1:15 crosslinking densities used a single correlation length fitting parameter (see Figure 4.4B and 4.4C), which fit all the features of the scattering data and indicated that the distance between the fixed linkage point in the microgel was 24.2 and 7.6 nm for the 1:30 and 1:15 microgels, respectively. For the 1:5 microgel, two

correlation lengths were observed (noted with the red and green arrows) resulting in two fitting parameters (Figure 4.4D). To fit these correlation lengths, two Lorentzian functions were summed (each having one correlation length as the fitting parameter). The two correlation lengths describe static (representing the distance between fixed linkage points) and dynamic (representing fluctuating polymers in the gel matrix) components of scattering by the hydrogel polymeric network [255, 256]. The 1:5 microgel had a static correlation length (red arrow) of 3.0 nm, and a dynamic correlation length (green arrow) of 1.0 nm. For the low crosslinked microgels the higher water content means the polymer concentration is significantly smaller. This lower concentration can explain why we don't see a dynamic correlation length as the polymer chains can fully extend in the solvent.

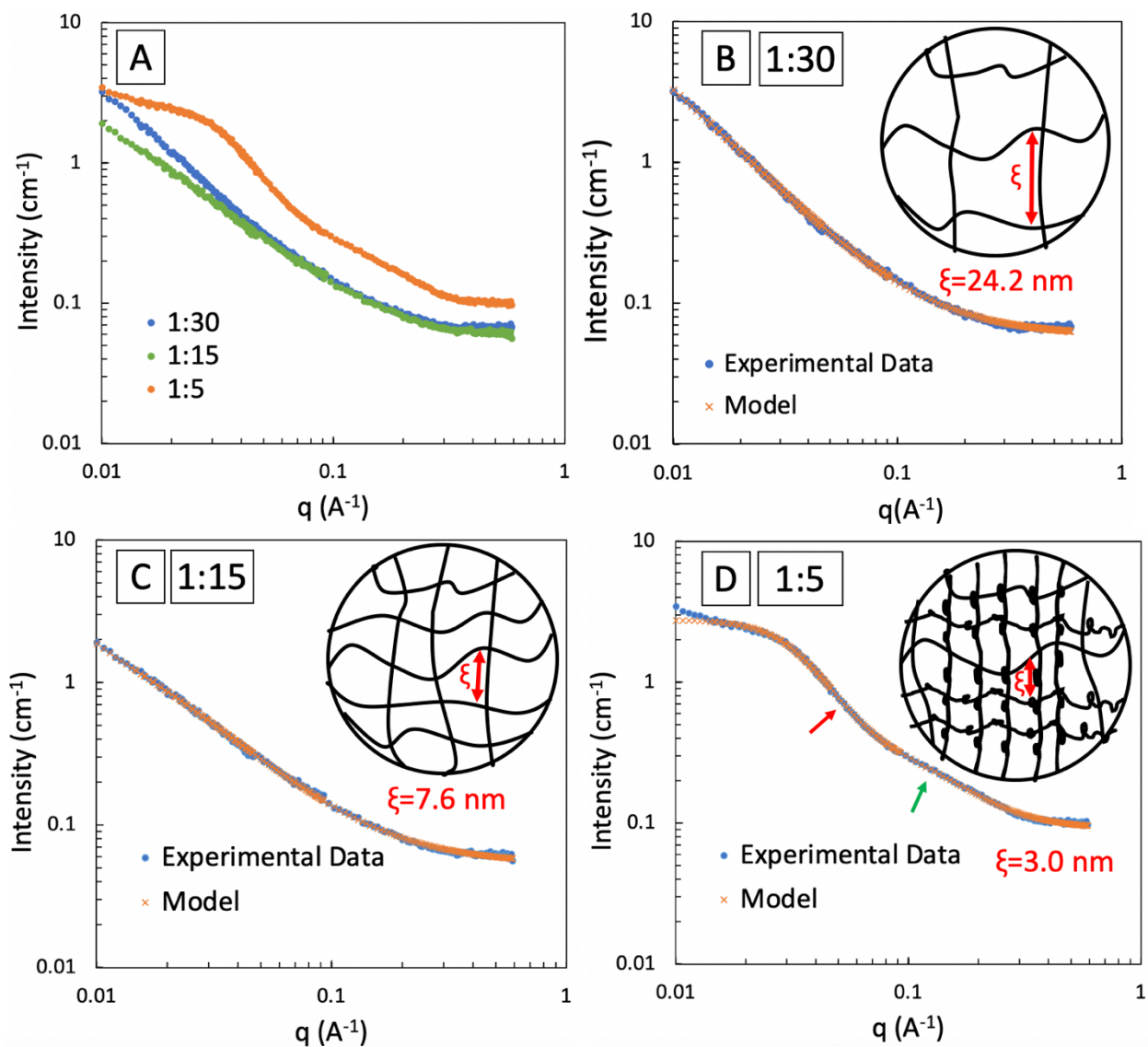


Figure 4.4. Small-angle neutron scattering (SANS) of the zwitterionic poly (carboxybetaine) microgels crosslinked with TTEGDA. **A**: Scattering intensity vs wavevector (q) for three different crosslinking densities. **B**: Experimental data and fitted model for the 1:30 crosslinker: monomer ratio. The calculated correlation length (average distance between entanglements) was 24.2 nm. **C**: Experimental data and fitted model for the 1:15 crosslinker: monomer ratio. The calculated correlation length was 7.6 nm. **D**: Experimental data and fitted model for the 1:5 crosslinker: monomer ratio. The highly crosslinked microgel had two correlation lengths. The static correlation length (red arrow) was 3.0 nm (representing distance between linkage points). The dynamic correlation length (green arrow) was 1 nm (representing polymer-solvent interaction).

4.3.2 Degradation of the microgel

Figure 4.5A illustrates the chemistry of the zwitterionic microgel and its degradation. In aqueous solution, the cleavable ester bond in TTEGDA can hydrolytically degrade and form water-soluble pCB polymers. The hydrolytic degradation of the different crosslinking densities was studied and is illustrated in Figure 4.5B. Microgel degradation was a function of crosslinking density. While the low crosslinked (1:30) microgels fully degraded in approximately 7 days, it took about 30 days for the high crosslinked (1:5) microgels to degrade. Interestingly, the degradation of all the studied microgels follow a linear behavior throughout the degradation process. The microgels will degrade into single chain zwitterionic polymers of a few nanometers for renal clearance.

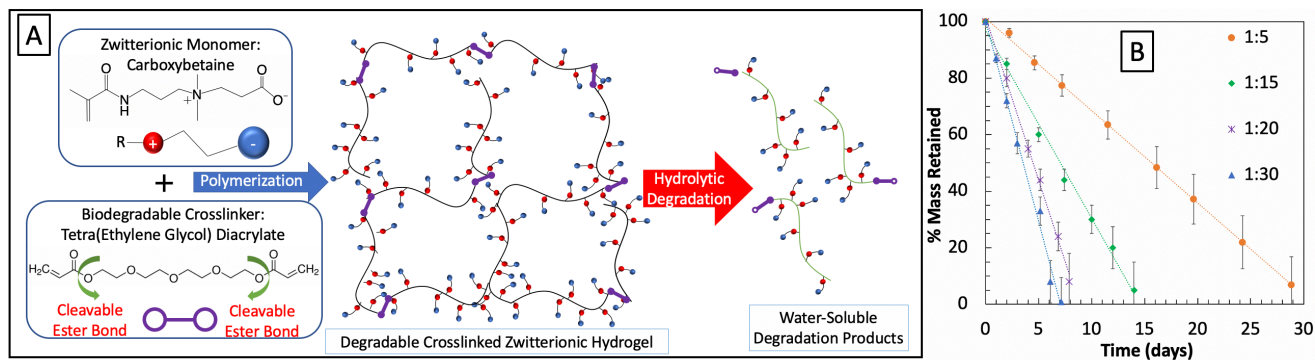


Figure 4.5. Microgel degradation. **A:** Schematics of the zwitterionic pCB-TTEGDA and its hydrolytic degradation. The cleavage of ester bond in the crosslinker results in water-soluble pCB polymer to separate from the microgel. **B:** Biodegradability of the microscale hydrogels in PBS. Degradation of the microgels over time in PBS at 40 °C. While low crosslinked microgel degraded in approximately 7 days, the more crosslinked microgel degraded in more than 30 days.

I also observed the microgel shape and structure during the degradation process (Figure 4.6). For the high crosslinking density, the particles kept their overall shape during the degradation process, but their surface became increasingly smoother over time. In contrary, the less crosslinked microgel particles tended to aggregate during the degradation process.

Furthermore, we observed microgel aggregation during the course of degradation. The microgel aggregation (as opposed to agglomeration) is dependent not only on the adhesion forces between the particle, but also on the mechanical strength of the microgel. For the low crosslinked microgels the weakened mechanical strength during degradation promotes the particle aggregation which. The adhesion forces between the microgels can be caused by the interactions between the zwitterionic polymer chains or by interaction between the TTEGDA moieties.

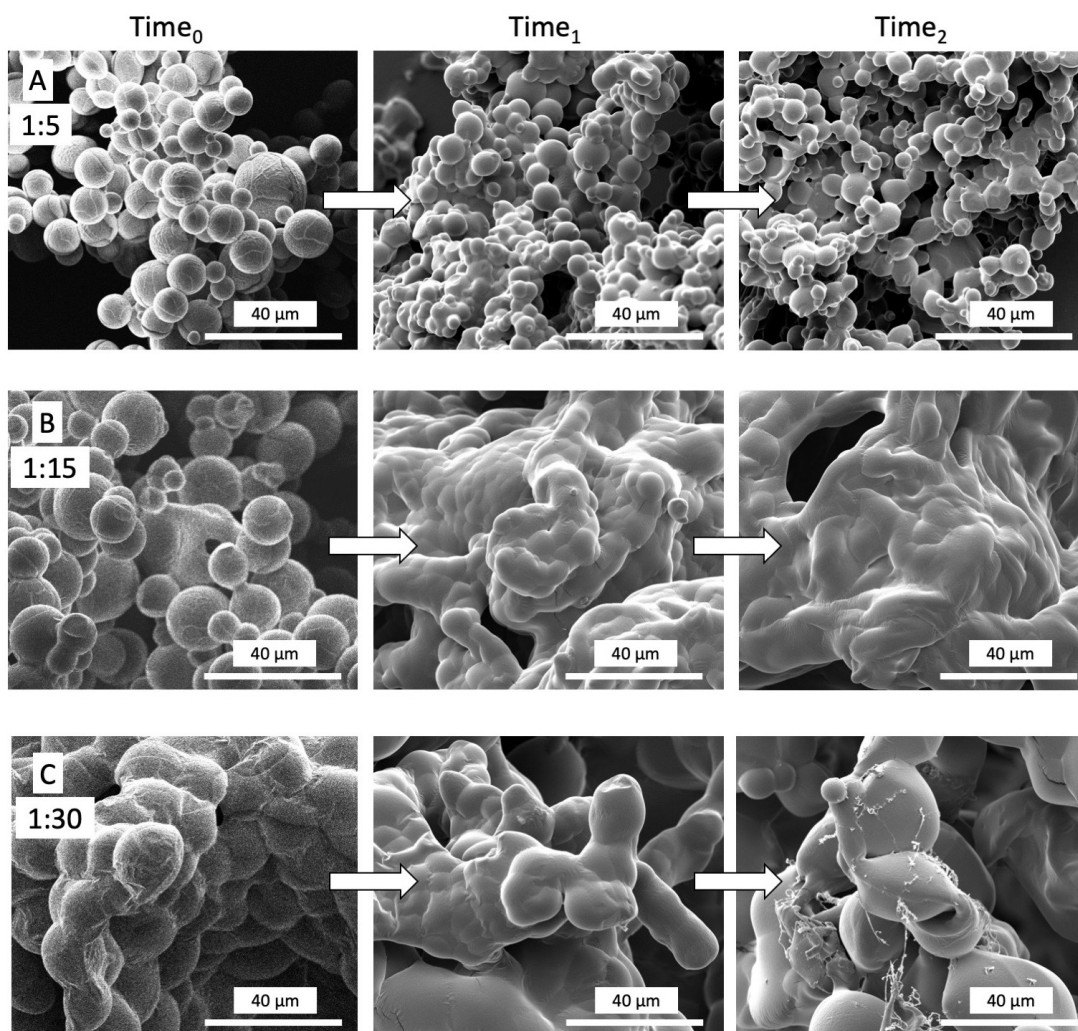


Figure 4.6. Biodegradability of the microgels in PBS observed in SEM micrographs. Time₀ is the fresh microgel. At Time₁, 30% of the microgel is degraded and at Time₂, 60% of the mass of microgel is degraded. The less crosslinked microgel tend to aggregate more during the degradation process.

4.3.3 *In vitro* cytotoxicity and immunogenicity of the microgel

Cell compatibility is essential for the soft delivery of biomolecules. Because of the abundance of the fibroblasts in SC tissue, I evaluated the viability of these cells when exposed to the microgels (Figure 4.7A). For this purpose, microgels were added to cell culture wells and cell viability was evaluated after 24 hours of exposure. The cells exposed to microgels showed complete cell viability (no statistically significant difference between exposed and control cells). Furthermore, I investigated the cell viability for cells exposed to the degradation products of the microgels at concentrations of up to 2 mg/ml and observed 100% cell viability.

The immunogenic reaction to the zwitterionic microgels was studied by quantifying cytokine secretion from macrophage cells (Figure 4.7B). The secretion of cytokines IL-6 and TNF α were evaluated as they play a major role in development of inflammation [257]. After 24 hours exposure to the microgel, the cells did not secrete any measurable amount of IL-6. For TNF α , the cells secreted approximately 500 pg/ml TNF α with or without exposure to the microgels. This amount of TNF α is significantly smaller than secretion caused by an immunogenic reaction to an endotoxin molecule such as lipopolysaccharides which can be approximately 8000 pg/ml or higher [258].

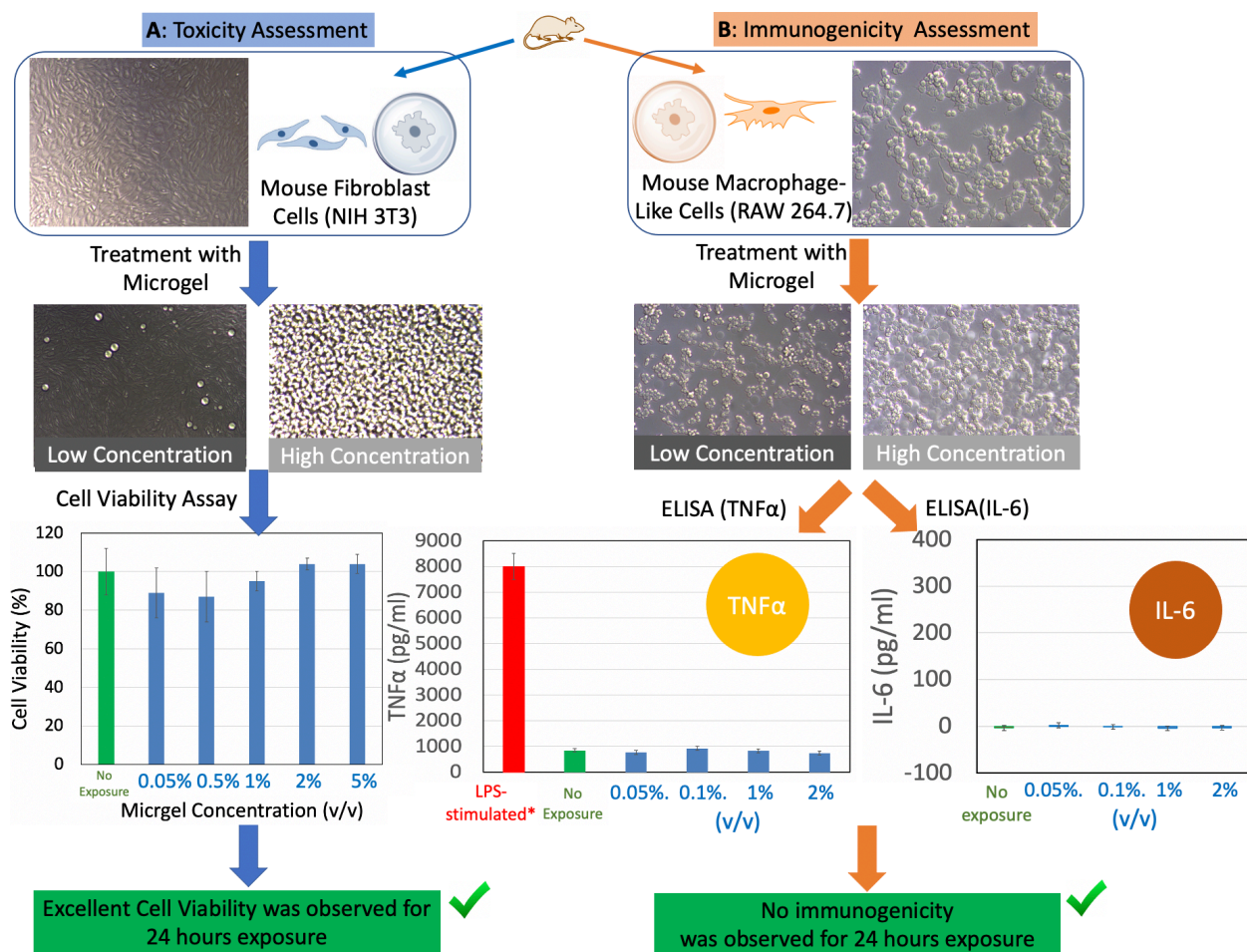


Figure 4.7. Cytotoxicity (A) and immunogenicity (B) of biodegradable zwitterionic pCB microgels. Microgel with a crosslinker:monomer ratio of 1:15 was used. Mouse fibroblast cells (NIH 3T3) showed complete cell viability when exposed to the different concentration of microgels. The section of interleukin 6 (IL6) and tumor necrosis factor-alpha (TNF α) were investigated after exposure of macrophage cell (RAW 264.7) with the microgel. LPS-stimulated*: For cells stimulated using the lipopolysaccharides (a well-known endotoxin) as a positive immunogenic control [258].

4.3.4 Ab loading and release

One of the key advantages of our methodology was that the Ab (IgG) was loaded after the microgel synthesis. This prevented unwanted chemical reactions and biomolecule aggregation/denaturing during the polymerization reaction and particle formation. Such a strategy was especially important for a biomolecule with limited stability such as an Ab. The Ab

loading occurs as a result of capillary pressure and a concentration gradient that forms when the freeze-dried microgel is immersed in the Ab solution. Such a loading strategy can only be applied if the microgel beads are small enough for the capillary pressure-based loading to take place in a reasonable time.

Confocal fluorescence microscopy of the microgels loaded with FITC-IgG (Figure 4.8A) showed that all beads are loaded with the Ab. Figure 4.8B illustrates the averaged projection of a series of optical sections at different depths of the bead to investigate the distribution of the FITC-IgG within the microgel. This study demonstrated that the FITC-IgG molecules were homogeneously loaded within the microgel and were not only surface bound.

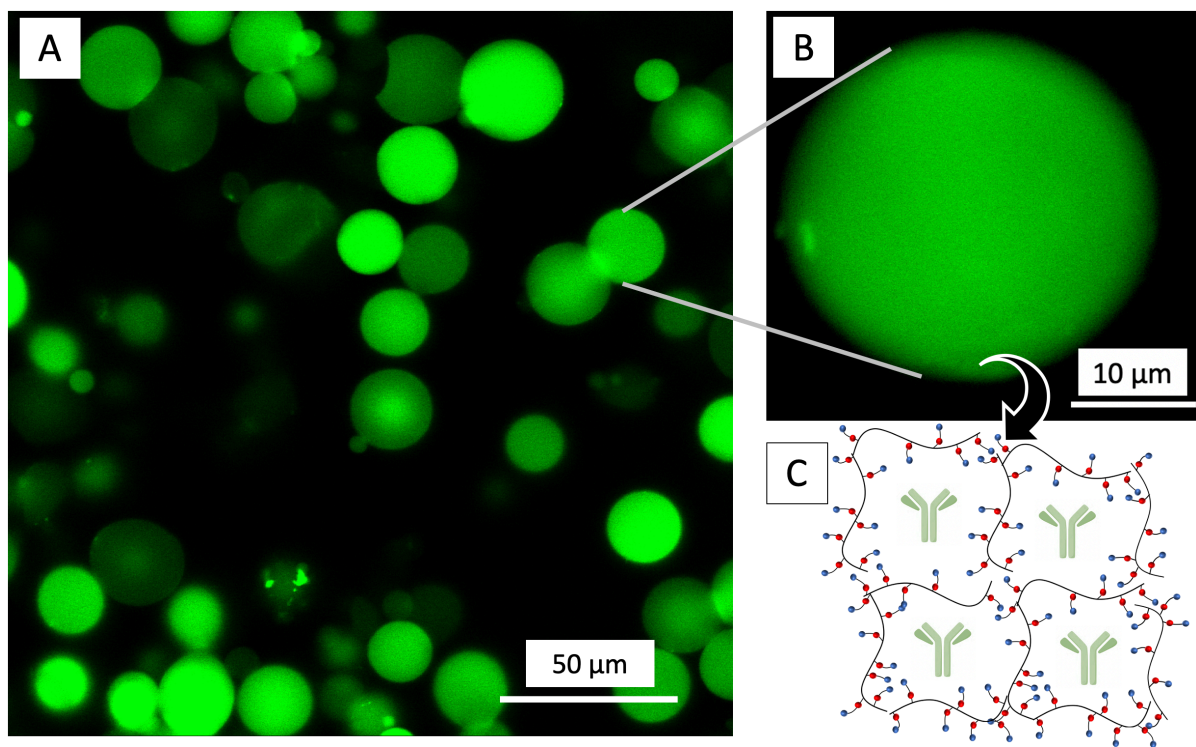


Figure 4.8. Immunoglobulin G (IgG) loaded zwitterionic microgels. **A:** The confocal microscopy of fluorescently labelled IgG (FITC-IgG). **B:** Averaged projection of different planes of the beads indicated that the antibody (Ab) is loaded within the microgel and is not surface bound. **C:** Schematics of the Ab loaded within the crosslinked polymeric structure of the microgel. The molar crosslinker:monomer ratio was set to 1:15. The microgel beads dispersed in PBS buffer.

The release of Ab from microgels in PBS at 40 °C was studied (Figure 4.9A). The results indicated that the total amount of Ab that can be released from the microgels decreased with increasing the crosslinking density. For the 1:30 crosslinking ratio, all the Ab was released within the 72 hours of dispersion in buffer. The release profile can be understood by comparing the release plots with the SANS microstructure data (Figure 4.4). For the 1:30 microgels, as the correlation length of the polymers is significantly larger than that of the Ab (24.2 nm comparing to ca. 14 nm), the Ab escapes primarily through a burst release mechanism. For the 1:15 and 1:5 crosslinking, as the correlation length of the polymer networks is smaller than of the Ab, we observe the entanglement and slower diffusion of Ab, which is more favorable for sustained delivery.

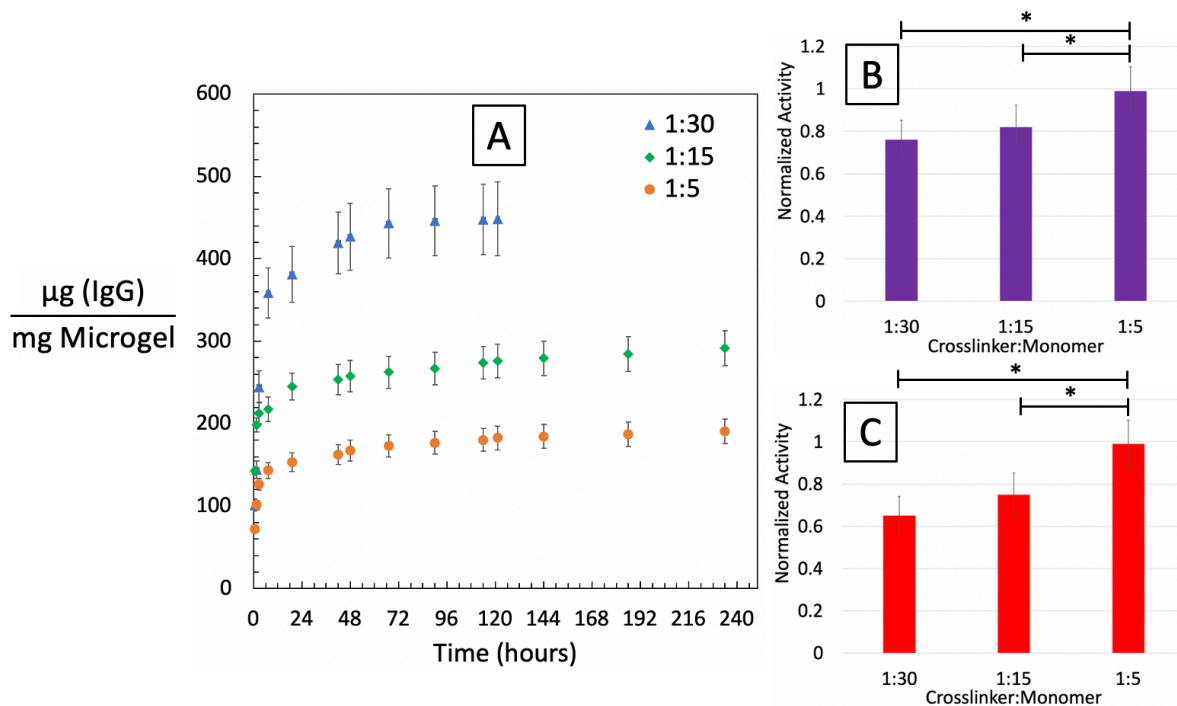


Figure 4.9. Antibody (Ab) release from zwitterionic microgels and activity of released Ab activity evaluated using human IgG ELISA kit. **A:** Ab release at 40°C, over time for three different crosslinking densities (fluorescently labelled IgG) **B:** Activity of the released Abs for

the Ab released during early release stage (the first 18 hours). C: Activity of the Abs released during the slow-release stage (18 to 120 hours). The Ab activity indicates the ability of the Ab to bind with the Ab receptors. Statistical significance indicated by (*).

The high permeability of the microgels can be observed by both fast release and the high diffusivity of the microgels. This is especially important when comparing the microgel with materials such as PLGA microspheres. While PLGA particles cause aggregation and instability of biomolecules, their permeability can be controlled to achieve lower release rates. Based on the release rate, the studied microgels are suitable for short-term release needs.

The activity of released Abs was evaluated using an anti-Ab ELISA (Figure 4.9B and 4.9C). While many studies report encapsulation and release of Abs, only few have investigated the ability of the released Ab to bind with Ab receptors to confirm that the Abs maintain the conformation and function. Even for highly stable and less sensitive bovine serum albumin (BSA), encapsulation in PLGA microspheres indicated up to 50% BSA aggregation or denaturation during fabrication [218]. This indicates why much of the published research lacks the activity of the released Abs. The post-release functionality of Ab from the sustained delivery matrix is critical, as concentrated Ab solution is susceptible to aggregation and denaturation at body temperature. Our results indicated that the Abs released from the 1:5 microgel completely retained their function. This was true for the early stage released Abs (first 18 hours of release) and later stage of release (18 to 120 hours). Such results clearly indicated the benefit of using zwitterionic microgels. For the lower crosslinking density of 1:30, we see that while the majority of the released Abs are active, the activity is significantly lower. For the early state released Abs 78% and for later stage released 67% of Ab molecule were active.

To our understanding, loading and release of Abs from zwitterionic microgels have not been carried out before. While this research advances the design of materials to enhance Ab stability for non-intravenous administration, it also raises further questions that needs to be separately investigated. For instance, while zwitterionic microgels can enhance Ab stability, long-term, sustained delivery of Ab will require the particles to be modified with other means to include another level of control over release. This can be achieved by methods such as coating the microgels particles [259]. Furthermore, the mechanism of Ab denaturation within the microgel needs to be investigated and is beyond the scope of this paper. Similarly, investigation of responses to Abs released from microgels can be considered a future step for this research.

4.5 Conclusions

Biodegradable zwitterionic poly(carboxy) (pCB) microgels were fabricated using tetra (ethyne glycol) diacrylate (TTEGDA) as the crosslinker with a water-in-oil emulsion technique. The synthesized microgels showed water content as high as 97.5% and were in the range of 5-30 micrometers in diameter (freeze-dried). The microgels showed excellent hydrolytic degradability, which could be tailored by changing the crosslinking density for different drug delivery administration applications. Microgels characteristic lengths were evaluated using small-angle neutron scattering and were found to range from 3.0 to 24.2 nm. The studied microgel showed excellent cell compatibility, complete fibroblast cell viability and lack of immunogenic responses observed by monitoring secretion of interleukin 6 (IL6) and tumor necrosis factor-alpha (TNF α). The small size and dispersibility of these microgels facilitated post-fabrication loading with delicate biomolecules due to enhanced surface area. The biodegradable microgel was loaded with Immunoglobulin G (IgG) as a model antibody (Ab). Ab molecules were able to diffuse inside the microgels during encapsulation and were later released.

The release of Ab from the microgel was tunable by changing the crosslinking density. High permeability of the microgel limited the release of the Ab to short-term release needs. Abs loaded and released from the microgel at 40°C maintained their native structure, which was probed by the binding ability of the IgG molecules. The ability of the zwitterionic microgel to prevent non-specific interactions of Ab has significant implications for sustained local delivery of Ab. Controlling and reducing the release rate of Ab to enable long-term release needs is a future step of this research.

Acknowledgements:

This chapter is pending publication as an article: Erfani, Amir, Abanoub Hanna, Payam Zarrintaj, Saeed Manouchehri, Katie Weigandt, Clint P. Aichele, and Joshua D. Ramsey. “Biodegradable Zwitterionic Poly(Carboxybetaine) Microgel for Sustained Delivery of Antibodies with Extended Stability and Preserved Function”

CHAPTER V

Zwitterionic Poly(carboxybetaine) Microgels for Enzyme (Chymotrypsin) Covalent Immobilization with Extended Stability and Activity

Chapter Overview

In this chapter, I explore a zwitterionic poly (carboxybetaine) (pCB) based microgel for enzyme immobilization. The microgel was loaded with a model enzyme, α -chymotrypsin (ChT), using a post-fabrication loading technique. A reaction scheme was developed and studied for covalent immobilization of ChT within the microgel. Confocal laser microscopy studies showed that immobilized ChT (i-ChT) was distributed within the hydrogel. The enzyme-immobilized microgels showed excellent reusability (72% of its initial activity after 10 uses) and could undergo several freezing/drying/rehydration cycles while retaining enzymatic activity. The i-ChT activity, half-life, and conformational stability were studied at varying pH and temperatures with results compared to free ChT in buffer. ChT immobilized within pCB hydrogel showed increased enzymatic stability as observed by a 13 °C increase in the temperature at which i-ChT loses activity compared to free ChT. Furthermore, enzyme half-life increased up to seven-fold for the pCB immobilized ChT, and the increased stability resulted in higher activity at elevated pH. The i-ChT was most active at pH of 8.5 and was partially active up to the pH of 10.2.

5.1 Introduction

Enzymes are useful in industrial chemistry [260], biosensors [261], and medicine [262]. Moreover, they are expected to be increasingly used in sustainable chemical processes as a result of advancements in enzyme engineering [263, 264]. The global enzyme market is expected to grow to over \$17 billion by 2027 [265]. Nevertheless, enzymes are comparably expensive and not compatible with many environments, and there is a growing need to design technologies that help with enzyme reusability and enzyme compatibility [266, 267]. The key to successfully utilizing enzymes as therapeutics, biocatalysts, or biosensors is to maintain their conformation and function. This can be achieved by using protein compatible materials that prevent undesired non-specific protein binding, aggregation, and structural changes.

Protein stability can be hindered at elevated temperatures sometimes required in chemical processes [268] or within complex biological environments [197, 198]. Elevated reaction temperatures provide better solubility, lower diffusion limitations, and favorable reaction thermodynamics/kinetics, thus necessitating the need for enzymes that are functional at high temperatures [269]. Likewise, the therapeutic potential of proteins is promising, with proteins having been explored for treatment of cancer [270, 271], enzyme deficiency [262], cystic fibrosis [272], organophosphate intoxication [273], and gastrointestinal diseases [274]. Within the complex environment found in the body, however, undesirable interactions between the therapeutic protein and endogenous proteins can result in unfolding and deactivation of the protein [194]. Encapsulation of proteins within polymer networks has been studied to address both temperature stability and undesirable protein-protein interactions that lead to loss of enzyme activity [194-196]. For immobilization of proteins within such polymer networks, a major challenge arises from the fact that many materials, such as silicon and other hydrophobic

coatings, are inherently incompatible with proteins and lead to protein binding and aggregation [275, 276]. For instance, protein aggregation, structural changes, and denaturation have hindered the development of poly(lactic-co-glycolic acid) (PLGA) microsphere technology for protein encapsulation [199]. Additionally, protein structure and function have a significant impact on the immunogenicity of a protein and can result in unwanted immunogenic reactions [200]. Similarly, biofouling can hinder the specific bio-affinity of biosensors [277]. Clearly, there is a need for more compatible materials that increase protein stability while providing a permeable environment with high water content essential for enzyme activity and protein/substrate interactions.

Protein stabilization by zwitterionic moieties within living organisms provides an example of how we might approach the problem [16, 17, 28, 50, 51, 278]. A biomimetic approach would use the natural osmolyte properties of zwitterionic moieties by generating a super-hydrophilic network and to immobilize an enzyme within that network. Zwitterionic hydrogels also have super-hydrophilic characteristics and increase protein stability [179, 244] while maintaining high water content that is important for protein stability and enzymatic activity. Previously zwitterionic nanogels were formed by conjugating the enzyme with zwitterionic polymers of a few nanometers [10]. These nanogels improved stability of the studied enzyme. Yet these particles were synthesized with method and chemistry that are not suitable for enzyme immobilization (small size, soluble particles). Here I studied if microgel particle of a few microns composed of zwitterionic polymers can also enhance enzyme stability. Compared to bulk hydrogels, microgels have several advantages including low diffusional limitations and better dispersibility, which can be helpful in enzyme immobilization. Additionally, the soft nature of microgels can help with their use in bioreactors.

For the purpose of this study, I was interested in using a zwitterionic hydrogel to stabilize the enzyme chymotrypsin (ChT). ChT is a serine protease and is one of the most industrially utilized enzymes [260]. ChT has limited stability and a short half-life at conditions in which it is active. Furthermore, ChT activity is very well studied [279-283]. Notable residues in the ChT active site that directly interact with the substrate include histidine 57, aspartate 102, and serine 195 [284] (see Figure 5.1 for the protein structure). The combination of industrial relevance, poor stability, and knowledge about its activity mechanisms make ChT an ideal model for our study. Furthermore, enzymes such as ChT have applications in organic chemistry [285]. As many reactions are carried out in organic solutions, it is important to develop technologies that enable use of enzymes in organic media [286]. More specifically, ChT has been used to synthesize peptides in organic media [287]; yet like many other enzymes, ChT is not stable in organic media and has limited activity in hydrophobic environments. Additionally, protease enzymes such as ChT are gaining significant attention in the food industry, where the enzymes must function under harsh conditions such as elevated temperature [288]. Protease enzymes, for example have been used to reduce the chance that a consumer will have an allergic response to a food product, to tenderize meat, and to improve digestibility [288].

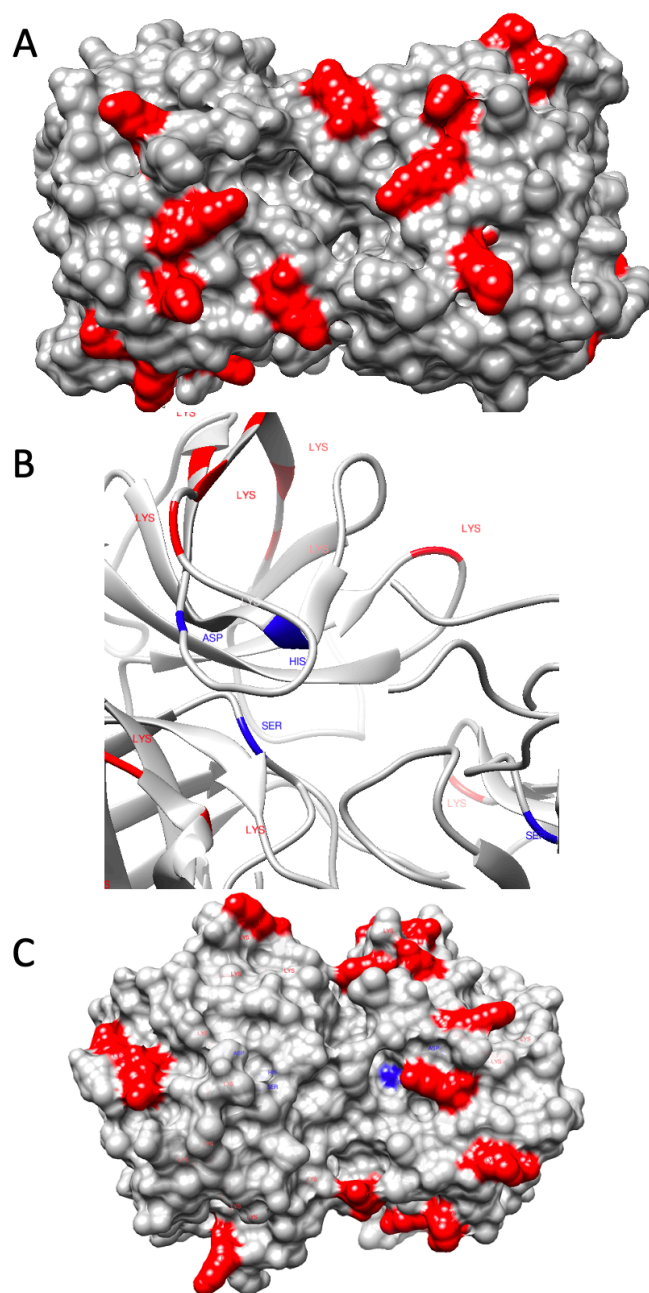


Figure 5.1. Molecular structure of α -chymotrypsin. **A**-Chymotrypsin is consisted of three poly peptide chains each repeated twice (total number of residues 482 total with molecular weight of 25 kDa). **A**: Chymotrypsin has 28 lysine residues (depicted in red) that are all on the solvent accessible surface of the protein. **B**: Enzymatic active site (residues depicted in blue) of chymotrypsin is consist of histidine 57, aspartate 102 and serine 195. [284] **C**: Surface accessible surface of chymotrypsin with lysine residues depicted in red and the active site residues depicted in blue. α -chymotrypsin structures from the protein data bank (PDB) entry 1YPH and was generated by UCSF Chimera [289].

To stabilize ChT using a zwitterionic hydrogel I expect that the protein needs to be immobilized within the hydrogel matrix. The main strategies for protein immobilization are physical, covalent, and bio-affinity binding [290]. The way in which proteins are immobilized can play a major role in loss of protein activity due to random orientation and structural deformations. Covalent immobilization is the most commonly used form as it can best prevent unwanted release of the enzyme [291]. Covalent immobilization can add a spacer arm length between the protein and the immobilization matrix or can be in the form of a zero-length crosslinking. To our knowledge, there is no published report studying the immobilization of enzymes within zwitterionic microgels. Furthermore, post-fabrication loading/immobilization of proteins inside these hydrogels has also not been previously investigated. Our hypothesis was that a network of super-hydrophilic polyzwitterions can result in immobilized enzymes with increased stability.

In this work, carboxybetaine, a natural osmolyte (protein stabilizer), was used as the repeating unit of the zwitterionic polymer. Zwitterionic pCB microgels were synthesized using inverse emulsion polymerization. A multi-point covalent immobilization scheme was studied to chemically immobilize ChT within the microgel. I investigated how a post-fabrication loading/immobilization procedure can result in loading of bioactive proteins within the microgel and compared the enzymatic activity of free and immobilized enzyme at different pHs and temperatures. I also investigated how immobilization within a super-hydrophilic network of polyzwitterions can affect the stability and half-life of a protein.

5.2 Experimental section

5.2.1 Chemicals

N-(3-(Dimethylamino)propyl)methacrylamide (DMPAA), β -propiolactone, (1-ethyl-3-(3-dimethylaminopropyl) carbodiimide hydrochloride (EDC), fluorescein isothiocyanate (FITC), and *p*-nitrophenyl acetate (NPA) were purchased from Sigma Aldrich. A-Chymotrypsin (ChT) from bovine pancreas, N, N'-methylenebisacrylamide, tetra methyl ethylene diamine (TEMED), span 80, cyclohexane, and ammonium persulfate (APS) were purchased from Fisher Scientific. All chemicals were of analytical grade and were used without any further purification.

5.2.2 Synthesis of the carboxybetaine methyl methacrylate monomers

Firstly, the carboxybetaine methyl methacrylate monomer (CBMA) was synthesized through reacting DMAPAA and β -propiolactone. DMAPAA (20.7 g) was mixed with 450 ml anhydrous acetone, and β -propiolactone (9 ml, in 90 ml anhydrous acetone (10%v v⁻¹)) was added slowly to the DMAPAA solution. The reaction was carried out at 25 °C in a nitrogen-purged container for 6 hours under gentle mixing. The product was insoluble in acetone; as such, the precipitate was separated from the solution by centrifugation upon completion of the reaction. The product was washed in acetone twice and dried under vacuum for 48 hours before storage at 4°C. The extent of the reaction was evaluated gravimetrically to be 80% and the molecular structure of the product was confirmed using ¹H NMR (Figure 5.2 and 5.3).

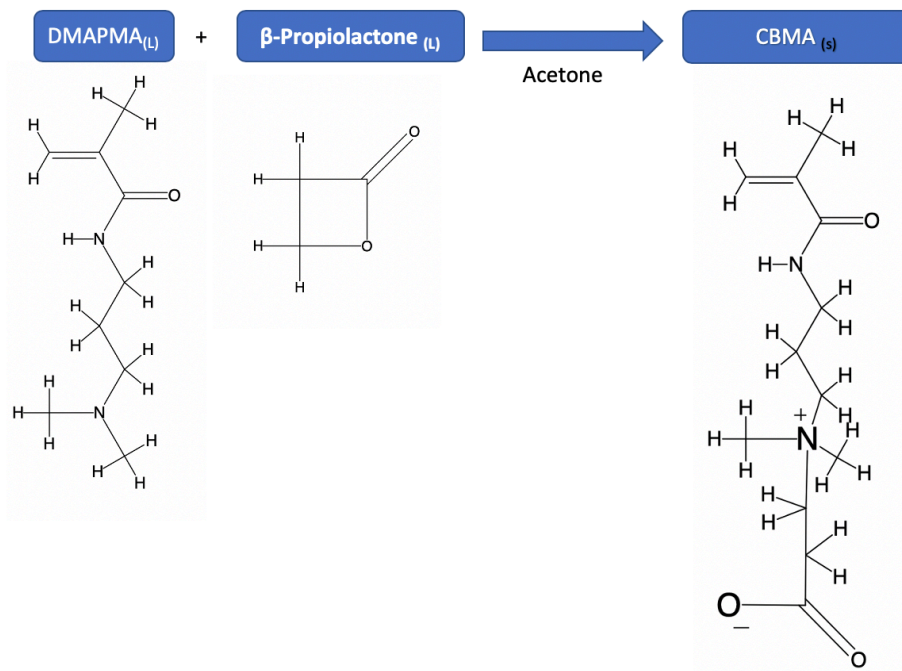


Figure 5.2. Monomer synthesis reaction scheme and the molecular structures of N-(3-(Dimethylamino)propyl) methacrylamide (reactant) and the synthesized monomer carboxybetaine methyl methacrylate (CBMA). While the reactants are soluble in acetone the product (zwitterionic monomer) is more polar hence precipitate in the acetone solution.

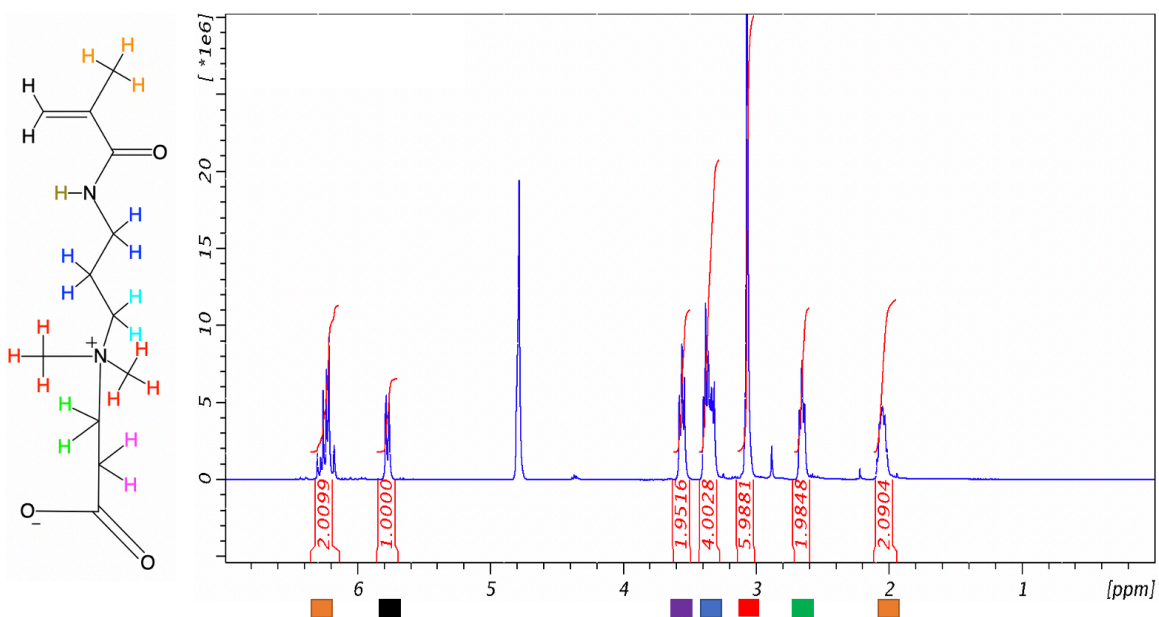


Figure 5.3. ^1H NMR spectra of the and the zwitterionic polymerizable carboxybetaine monomer. The alkylation reaction was carried out at 25 C.

5.2.3 Synthesis of the poly(carboxy betaine) microgel

An inverse emulsion (aqueous phase dispersed in a continuous oil phase) free radical polymerization reaction technique was used for preparation of the microgel beads. CBMA (300 mg/mL), crosslinker N, N'-Methylenebisacrylamide (bis-acrylamide) (13.6 mg ml⁻¹) and initiator APS (3 wt%) were dissolved in PBS to constitute the dispersed aqueous phase. A solution of 5 wt% emulsion stabilizer span 80 in cyclohexane was used as the continuous oil phase. The aqueous phase was added to the oil phase at a 1:9 v v⁻¹ ratio to prevent phase inversion and a vortex mixer agitated the sample for 30 seconds to generate the emulsion. Later, the catalyst TEMED was added to the emulsion (0.4 vol %) and vortexed for 30 seconds. The emulsion was placed on a shaker table to prevent microgel beads settling and the reaction was allowed to proceed at 25 °C (uncontrolled) for 4 hours. The microgel was washed once in cyclohexane to remove span 80, once with PBS followed by PBS equilibration for three days, and finally with DI water. This was followed by freezing at -80 °C and lyophilization at -35 °C.

5.2.4 Enzyme immobilization within the microgel

Here a post-fabrication protein loading/immobilization strategy was employed. ChT (10 mg/mL) and EDC (10 mg/mL) were dissolved in 100 mM sodium phosphate buffer (pH 5) that had been further modified with CaCl₂ (0.2 mg/mL) and NaCl (2 mg/mL) to form the reaction solution. The lyophilized microgel beads were resuspended in the reaction solution (40 mg microgel per ml) and the reaction was carried out at 25 °C for 3 hours. The beads were subsequently washed with phosphate buffer (pH 5) several times to remove the unreacted ChT before equilibration in DI water. The enzyme-immobilized microgel beads were lyophilized and later stored at 4 °C.

5.2.5 Characterization of the enzyme-immobilized microgel

Confocal microscopy and preparation of fluorescently labeled ChT

Confocal microscopy was used to investigate protein loading within the microgel beads. ChT was labeled using fluorescein isothiocyanate (FITC). For this purpose, 1 mL of ChT solution (2 mg/ml in pH 9 sodium phosphate buffer) was prepared at 4°C, and 50 µl of a FITC solution (5 mg/ml in dimethyl sulfoxide) were slowly added in 5 µl aliquots. The reaction was carried out at 4 °C for 10 hours before the solution was diluted 10-fold and unreacted FITC was removed using a 3.5 kDa dialysis membrane in exchange buffer (phosphate buffer with pH 5) for 12 hours. The fluorescently labeled ChT (FITC-ChT) was excited at 488 nm (argon/krypton laser) and visualized with a Leica DM E14 confocal laser microscope with a bandpass filter for the range 520 – 560 nm. The microgel beads were observed at multiple optical sections (~15 planes) and the intensity of the fluorescent light emitted from each section was compared for evaluating the protein loading.

UV spectra

The UV absorbance of the samples was acquired using a Beckman Coulter (DU 730) spectrophotometer. Blank and enzyme-immobilized microgel beads were suspended in pH 7 phosphate buffer at 15 mg microgel per ml, and free enzyme was dissolved in pH 7 phosphate buffer at 0.5 mg/ml.

Thermo gravimetric analysis

Microgel thermal properties were evaluated using a TA Instrument Q50. The sample chamber was continuously purged with nitrogen at a flow rate of 10 ml/min. The sample heating rate was 20 °C /min.

5.2.6 Activity assay for the free and immobilized enzymes

Activity assay for the free enzyme

ChT esterolytic enzymatic activity was measured using a nitrophenyl acetate (NPA) activity assay with a protocol similar to previous works [207, 292]. Enzyme solutions (0.25 mg/mL) were prepared in 100 mM phosphate buffer at the desired pH condition. Initially, 5 μ l of 8 mM NPA solution were added to 100 μ l of the ChT sample, and the mixture was subsequently stored at the desired temperature for 30 minutes. The absorbance of the samples was measured at 410 nm using a plate reader (Packard SpectraCount). The activity measurements were normalized between the highest measured absorbance and the absorbance of buffer and NPA mixture. The experiments were carried out in triplicate.

Activity assay for immobilized enzymes

First, 40 mg of enzyme-immobilized microgel beads were suspended in 1500 μ l phosphate buffer at the desired pH. Aliquots of the suspension (100 μ l) were incubated with 5 μ l of 8 mM NPA at desired temperatures for 30 minutes. Preliminary kinetic studies were carried out to make sure the amount of substrate per enzyme is enough to evaluate the enzyme activity and achieve an enzyme-controlled reaction rate. The absorbance of the samples was measured at 410 nm and normalized between the highest measured absorbance and the absorbance of the blank microgel. The experiments were carried out in triplicate.

5.2.7 Half-life measurements

The static (no substrate during the incubation) half-life of free and immobilized enzymes was measured at different pH (4 – 9) and different temperatures (30 – 60 °C). For each study, seven samples were stored at desired temperature and pH and subsequently removed at different time intervals and stored at 4 °C. Once all 7 sample were collected, the activity of all the samples were measured at 40 °C and pH 7.5. All the measured activities were normalized based on activity at time zero. The decay of the activity (U) was calculated to fit the half-life of the enzyme

$U = U_0 * \left(\frac{1}{2}\right)^{\frac{t}{t_{1/2}}}$, in which U_0 is the activity at time zero, t is time, and $t_{1/2}$ is the half-life.

5.3 Results and discussion

5.3.1 Poly(carboxy betaine) microgel

An inverse emulsion (aqueous phase dispersed in a continuous oil phase) free radical polymerization reaction technique was used for preparation of the microgel beads. Carboxybetaine methyl methacrylate (CBMA) was used as the monomer and was crosslinked with N, N'-methylenebisacrylamide (bis-acrylamide). The process for fabrication of the microgel is summarized in Figure 5.4.

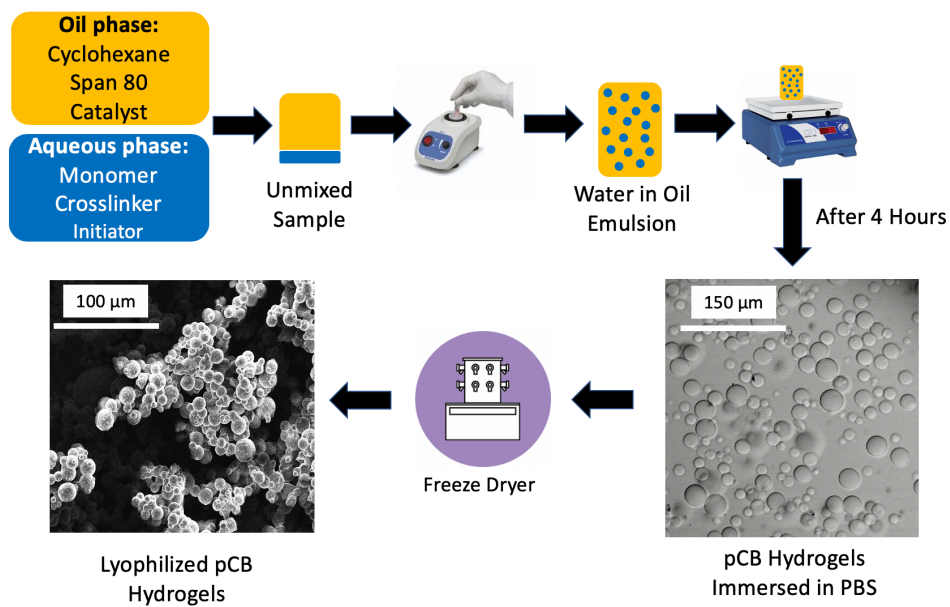


Figure 5.4. Schematics for the fabrication of poly(carboxybetaine) microgel, pCB, using inverse emulsion polymerization.

The SEM micrograph of the lyophilized pCB microgel (Figure 5.5) show that the microgel beads are individual spherical particles between 5-20 microns in diameter. This size is ideal for facile separation from the reaction medium by filtration. We observed that the crosslinking between the beads was very rare and almost all the particles were individual spheres. We attribute this to the relatively high concentration of the oil soluble surfactant. We speculate that Span 80 effectively partitioned at the surface of the particles during the reaction time and prevented the inter-particle crosslinking.

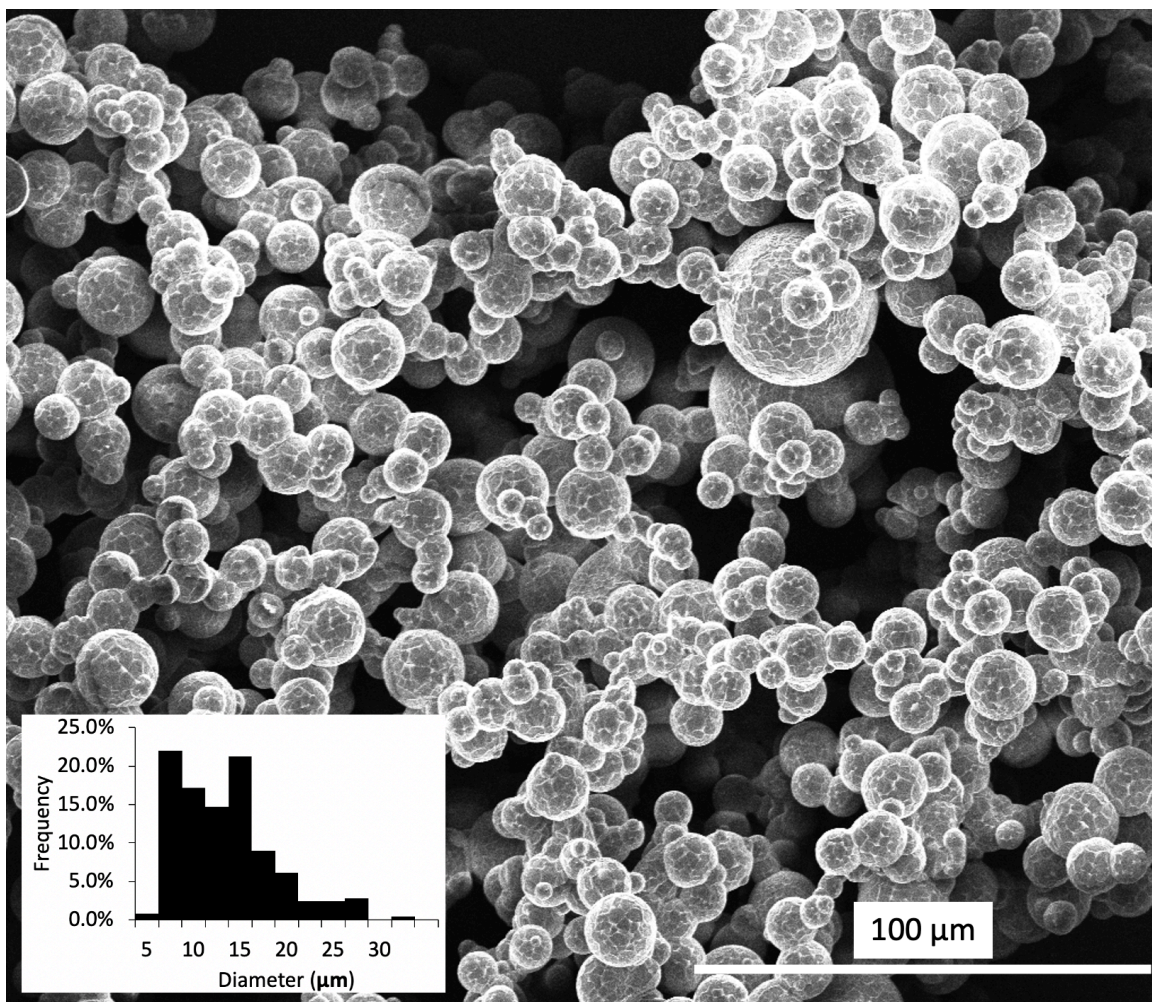


Figure 5.5. SEM micrograph of the lyophilized (freeze-dried) blank microgel (no enzyme) at 1000X magnification. Microgel particles were formed using inverse emulsion polymerization. The crosslinker:monomer molar ratio for the depicted sample was 1:16. The dried microgel beads are mostly within 5 – 20 μm in diameter.

5.3.2 Enzyme-immobilized zwitterionic pCB microgel

Here a post-fabrication protein loading/immobilization strategy was employed. The lyophilized microgel beads were resuspended in the reaction solution contacting ChT and (1-ethyl-3-(3-dimethylaminopropyl) carbodiimide hydrochloride (EDC). The EDC reaction scheme for enzyme immobilization within pCB is summarized in Figure 5.6.

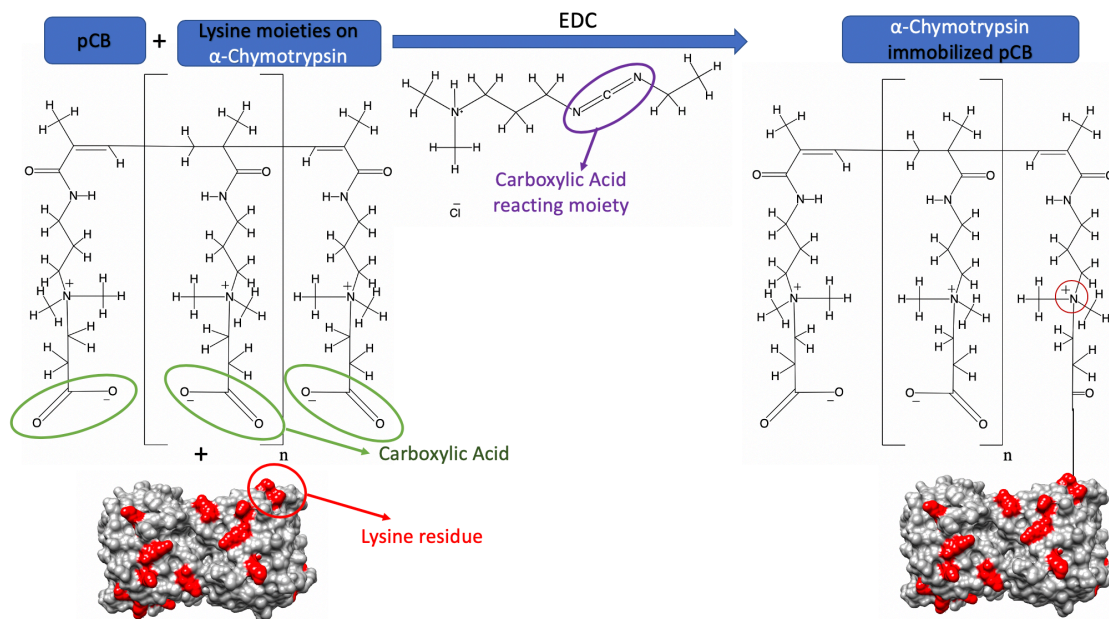


Figure 5.6. Reaction scheme for protein immobilization. The carboxylic acid groups of poly(carboxybetaine) (pCB) reacted with available lysine residues (depicted in red) on the α -chymotrypsin surface using EDC (1-ethyl-3-(3-dimethylaminopropyl) carbodiimide hydrochloride) as zero length crosslinker at pH 5. α -Chymotrypsin structure is for the Protein Data Bank (PDB) entry 1YPH and was generated by UCSF Chimera [289].

Figure 5.7 compares the surface structure of the blank pCB microgel and the enzyme-immobilized pCB microgel. The surface of the blank microgel beads displayed polygonal plates while the enzyme-immobilized microgel beads had a smoother surface.

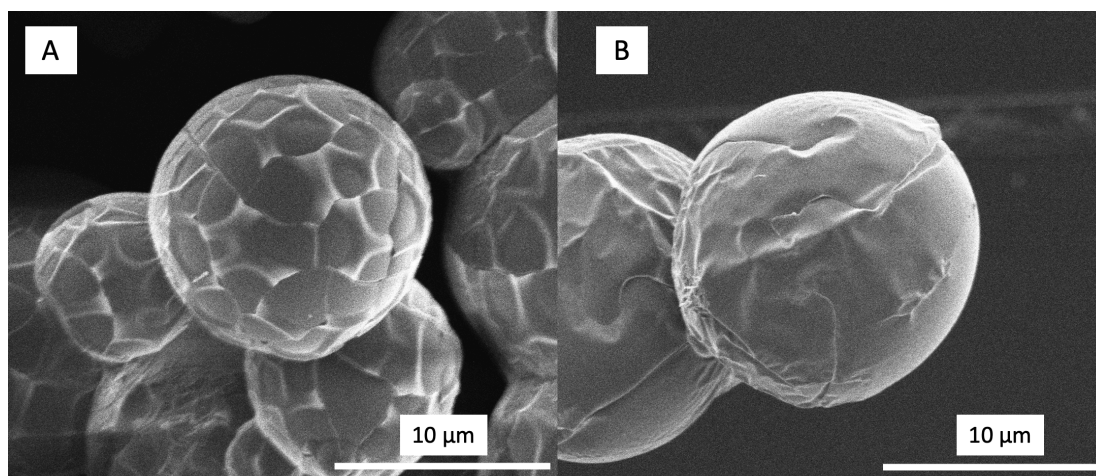


Figure 5.7. SEM of the lyophilized (freeze-dried) microscale hydrogel beads at 10,000 X magnification. **A:** Microgel beads with no enzyme (blank). **B:** Enzyme (chymotrypsin) immobilized microgel beads. While the surface of the blank microgel beads appeared to have been formed by plates the enzyme-immobilized microgel beads had a smoother surface.

Furthermore, confocal microscopy was used to visualize the fluorescently tagged ChT within the microgel beads (Figure 5.8). The enzyme-immobilized microgel beads were suspended in buffer for 5 days to remove free enzyme (that was not covalently bound to the microgel). The distribution of the enzyme inside the microgel was observed on multiple planes. Figure 5.8B shows the Z-stack image (averaged projection of a series of optical sections at different depths of the bead) and demonstrates that the protein molecules have been homogeneously immobilized inside the microgel and are not only surface bound.

The transport of protein and EDC crosslinker into the dried microgel occurred due to capillary action and osmotic pressure gradients that form when the lyophilized microgel beads are immersed in a protein and EDC crosslinker solution. Such a loading strategy can only be applied if the microgel beads are sufficiently small for capillary/osmotic loading to take place in a reasonable time. By comparing microgel beads in Figure 5.5 and Figure 5.8, the average diameter of dried microgel beads was 13 µm while the same swollen microgel beads had an

average diameter of 35 μm . Figure 5.9 shows a schematic representation of the chymotrypsin immobilized poly(carboxybetaine) zwitterionic microgel.

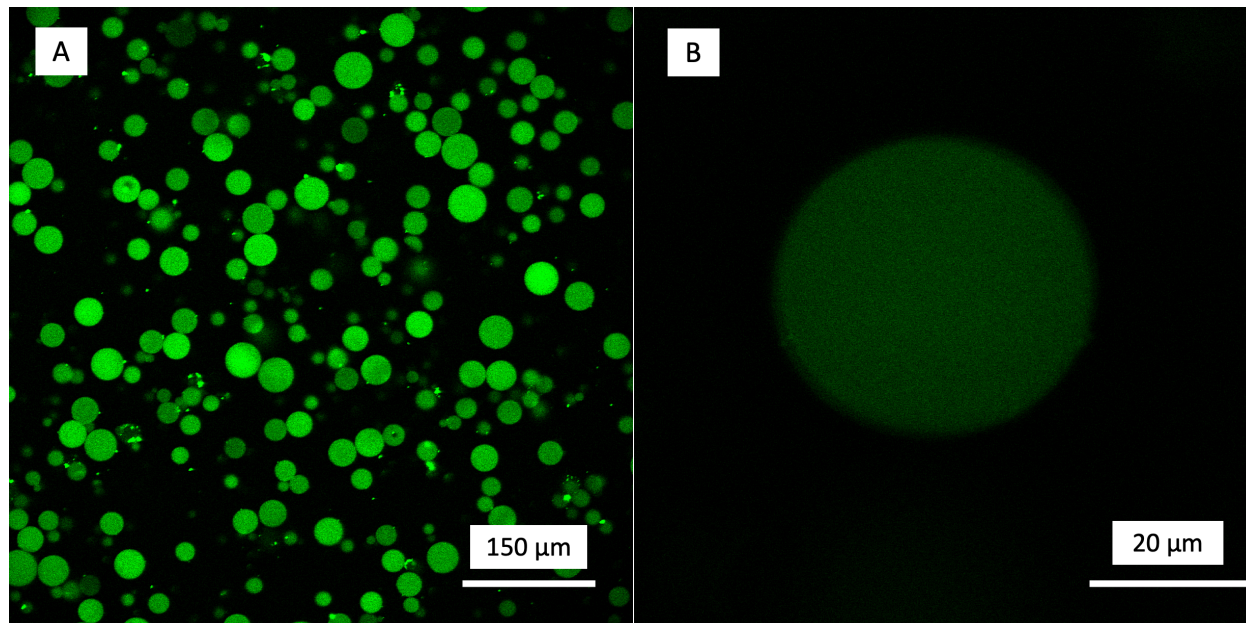


Figure 5.8 Confocal microscopy of the fluorescently labeled enzyme (chymotrypsin) immobilized microgel. Chymotrypsin was fluorescently tagged using FITC. **A:** magnification of 20X. **B:** Z-stack image, magnification of 60X, projection of several optical sections of a single microgel particle dispersed in phosphate buffer solution.

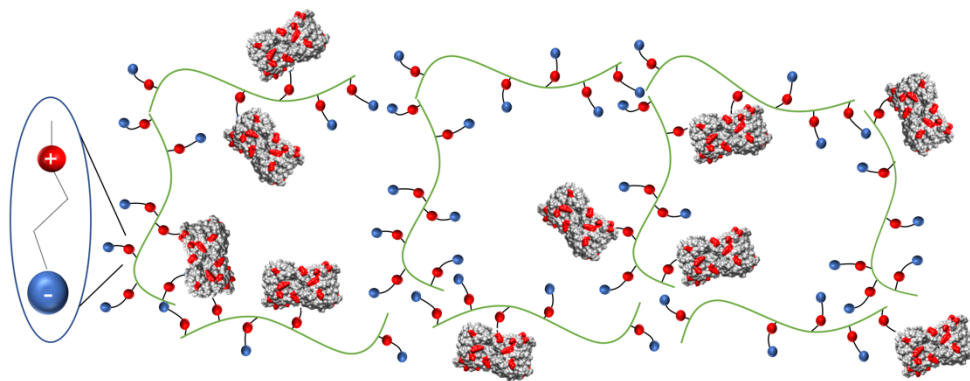


Figure 5.9. A schematic representation of the chymotrypsin immobilized poly(carboxybetaine) zwitterionic hydrogel.

To further characterize the microgel, the UV spectra of the enzyme-immobilized microgel was compared to that of the blank microgel and free enzyme (Figure 5.10A). The spectrum of the ChT immobilized microgel resembles the superposition of the blank microgel and the free ChT, indicating that the ChT was immobilized inside the microgel. Furthermore, the concentration of ChT in the microgel was estimated to be 1.3% w/w (Figure 5.10A) by comparing the absorbance of the blank and enzyme-immobilized microgel at 285 nm.

The TGA analysis of blank and enzyme-immobilized lyophilized microgel (Figure 5.10B) shows that the enzyme immobilization did not significantly affect the thermal properties of the microgel. Two notable transitions occurred within the ranges 10 – 100°C and 100 – 180°C. These transitions are likely because of two different water binding mechanisms. Interestingly, the lyophilized pCB microgel had an estimated water content of 35% (Figure 5.10B) that could not be removed by lyophilization. This amount of water corresponded to 7 H₂O molecule per monomer (CB.7 H₂O). Water molecules can orient around the zwitterionic dipole of carboxybetaine [293], which can account for 15 % of the retained water. Alternatively, water molecules can bind more strongly to the charged ionic groups of NR₄⁺ and COO⁻ present in the microgel [294], accounting for the remaining 20 % of water retained within the microgel structure.

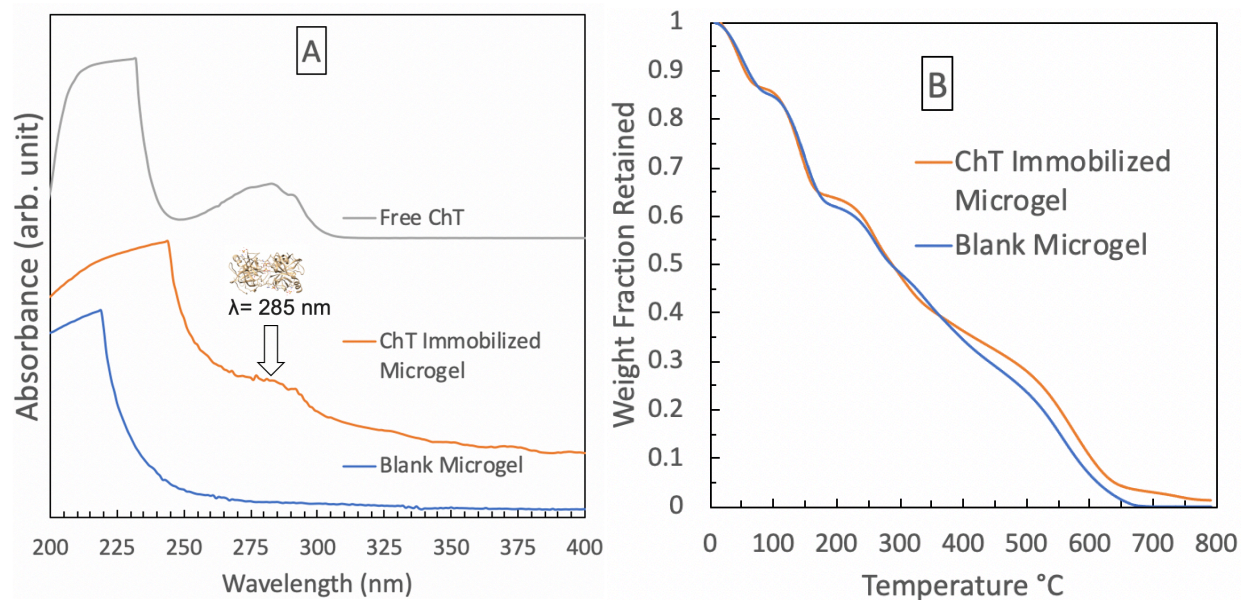


Figure 5.10. Characterization of the synthesized zwitterionic microgel. **A:** the UV spectrum of the free chymotrypsin (ChT), ChT (enzyme) immobilized microgel, and blank pCB microgel. The UV spectra confirmed that ChT was immobilized inside the microgel observed by the peak at 285 nm. **B:** Thermal gravimetric analysis of the blank and enzyme-immobilized microgel.

Enzyme reusability is one of the most important functionalities of an immobilized enzyme and is illustrated in Figure 5.11A. The immobilized enzyme retained 72% of its initial activity after 10 cycles of using the enzyme. Each cycle encompassed a 30 minute reaction followed by removing the reaction products by washing the microgel beads. One of the key advantages of our proposed methodology was the post-synthesis loading of ChT that prevented unwanted reactions, aggregation, and denaturation. This is important when the immobilized enzyme is costly or when denatured enzymes might show immunogenic reactions or lose their bio-affinity. Additionally, the hydrogel beads were lyophilized after enzyme immobilization, and the enzyme-immobilized, lyophilized microgel retained their enzymatic activity for four cycles of freeze drying/rehydration (Figure 5.11B). As a result, the microgel can be dried for storage and rehydrated prior to use without the need for a cryoprotectant.

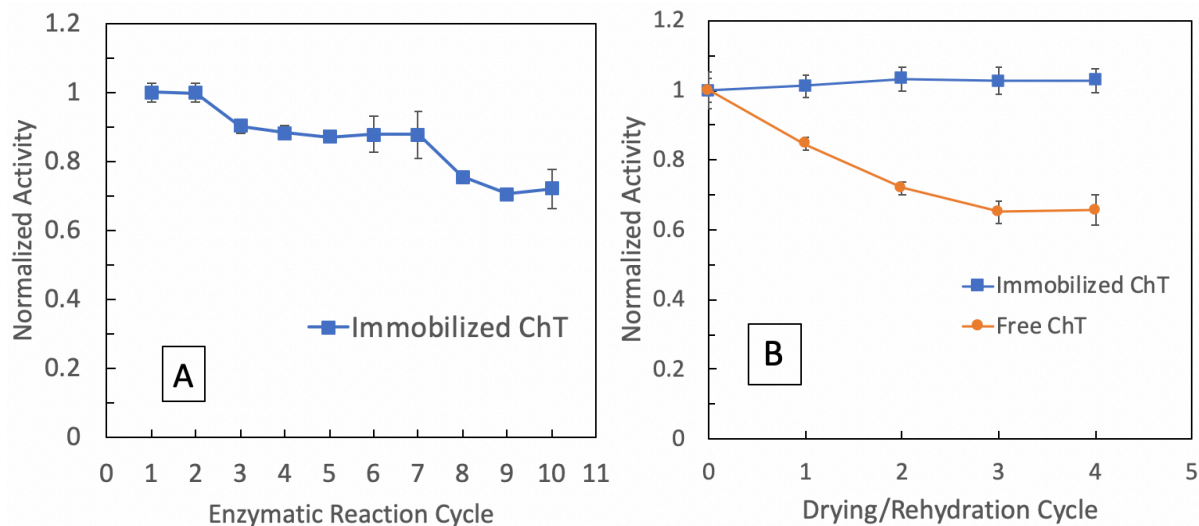


Figure 5.11. Reusability of chymotrypsin (ChT) immobilized within poly(carboxybetaine). **A:** Enzymatic activity for cycles of reusing the enzyme. The immobilized enzyme retained 72 % of its initial activity after 10 cycles. *Substrate hydrolysis in blank hydrogel (no enzyme) and water was used as the negative control.* **B:** Enzymatic activity for cycles of drying and rehydration of the enzyme-immobilized microgel and the free enzyme. Free chymotrypsin with no cryoprotectant lost some of its activity when dried/rehydrated at 1 mg/ml and pH 5. While the immobilized enzyme activity was retained after drying/rehydration. Activity was measured at 40 °C, pH 7.5, and 30 minutes of reaction duration.

5.3.3 Enzymatic activity of immobilized ChT at different temperatures and pHs

Enzymatic activity of ChT follows a temperature and pH dependent bell curve [279]. I compared the activity of immobilized and free enzyme (Figure 5.12). As indicated in Figure 5.12A, free ChT activity sharply decreased above pH 8. This can be explained by the isoelectric point of ChT as well as the autolysis. In contrast, the immobilized ChT (i-ChT) is significantly more active at pHs above physiological pH, being most active at pH 8.5 and partially active up to pH 10.2. To explain the enhanced activity of i-ChT at basic pHs, we need to consider that the free enzyme reaches its isoelectric point at pH 8.5. At this point, the neutralization of electrostatic charge would allow direct interactions between ChT, leading to structural changes

and protein aggregation [279]. In contrast, the i-ChT retains activity as the immobilization limits direct interactions of protein molecules. The loss of activity by free ChT at basic pH ranging from 8 – 10 has a different mechanism compared to loss of activity at pH ranging from 10 – 11. As mentioned previously, the loss of activity at pH 8 – 10 is caused by autolysis, physical aggregation and denaturing (thermophysical deactivation) [281]. In contrast, the α -amino group of isoleucine 16 becomes deprotonated at pH 10 – 11, breaking the activity-critical salt bridge between isoleucine 16 and asparagine 194 (chemical deactivation) [295]. As a result, the ChT changes to a chymotrypsinogen-like structure (proenzyme) [296]. Our results for the i-ChT indicate that i-ChT is active up to pH 10.2, which suggests that immobilization prevented thermophysical deactivation of the enzyme, but not its chemical deactivation.

In acidic environments free ChT was more active than i-ChT. This can be explained by the ability of the free enzyme to form dimeric chymotrypsin at low pH [297]. Although the activity of the dimer is small, it can cleave the substrate down to pH 3.7. I postulate that the immobilized enzymes were not as flexible and free to form active dimers, which explains the reduced activity of i-ChT in acidic environments in comparison to the free enzyme.

As indicated in Figure 5.12B, free ChT has its highest activity at 40 °C. At higher temperatures, the activity sharply decreased, and at temperatures above 54 °C free ChT completely lost its activity. This agrees well with the previously reported melting point of ChT of 53.4 °C [298]. In contrast, activity of i-ChT increased with increasing temperature up to 52 °C, and only after that did the activity decrease. Furthermore, i-ChT retained its activity up to 65 °C, indicating a significant increase in the thermal stability and thermal activity. At low temperatures, i-ChT showed normalized enzymatic activity below that of the free ChT, which

can be explained by the increased diffusion limitations caused by the low permeability of the microgel at low temperatures, resulting in a diffusion-controlled rate of reaction.

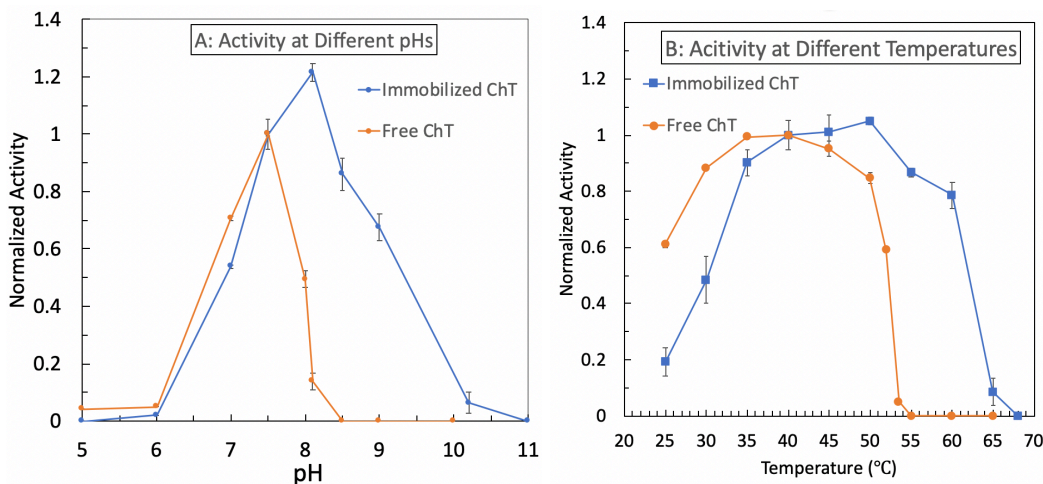


Figure 5.12. The esterase enzymatic activity of chymotrypsin immobilized within pCB microgel at different conditions compared with free chymotrypsin in solution. *Substrate hydrolysis in water (no enzyme) was used as the negative control.* **A:** effect of pH was measured at constant temperature of 40 °C and normalized for pH 7.5. **B:** effect of temperature was measured at constant pH 7.5. The enzymes immobilized within the zwitterionic microgel retained its activity at elevated pHs and temperatures.

For interpreting the effects of pH and temperature it is important to consider that pH and temperature can also affect the pCB structure and properties. Changes in the pH can induce protonation-deprotonation of the zwitterionic polymer. The pKa of the COO⁻ and NR₄⁺ are 3.3 and 9.7 respectively [12, 299]. As such, the pCB is in its zwitterionic state in the pH range of 3.3 to 9.7. pCB At pHs below 3.3 have a cationic and at pHs above 9.7 have an anionic nature, which could consequently affect the enzyme activity. Similarly, the intra- and inter-polymer interactions can be affected by increasing the temperature. The polymer chains correlations lengths within the microgel can also affect the enzymatic activity.

5.3.4 ChT deactivation and half-life

The increased conformational stability and enhanced activity of i-ChT at elevated pH/temperatures suggested that the half-life of ChT should also be affected by immobilization within the pCB microgel. As such, the permanent deactivation of the enzyme due to denaturation/aggregation was studied at different temperatures and pHs and is presented in Table 5.1 and 5.2 accordingly. While both free and immobilized ChT half-life decreased with increasing temperature, the i-ChT half-life was significantly improved at elevated temperatures. This lower denaturation/aggregation rate can be attributed to two important factors. Firstly, the reduced diffusivity inside the microgel as compared to free water can slow molecular motion and direct protein-protein interactions. Secondly, with the ability of the zwitterions to increase the activation energy gaps in protein denaturing [219], the zwitterionic environment can increase protein conformational stability. The increased stability of i-ChT within the zwitterionic microgel has important implications for the use of enzymes at elevated temperatures.

Table 5.1, Half-life of chymotrypsin at pH of 8 and different temperatures. The half-life measurements were carried out at conditions with equal volumetric activity (0.15 mg/ml chymotrypsin in solution and 30 mg/ml enzyme-immobilized microgel suspension)

Temperature (°C)	Half-life (min)		% Change in half-life after immobilization
	Free Enzyme	Immobilized Enzyme	
30	4680	4692	0.3%
40	512	2031	297%
50	44	196	346%
60	5	36	620%

As seen in Table 5.2, the half-life of free and i-ChT decreased with increasing pH for the studied pH conditions. Compared to the free enzyme, the immobilized enzyme half-life was improved significantly at neutral and basic pHs. Interestingly, this is not true for acidic pHs. At pH 3, the half-life of immobilized enzyme decreased by 24% in comparison to the free enzyme.

This observation can be explained by the effect lysine residues have on ChT stability in acidic environments. A previous report indicated that at a pH of 3 – 4, repulsive electrostatic charges of lysine residues can prevent ChT aggregation (ChT has a net charge of +14 mV at pH 4) [296]. In this study, immobilization was achieved by a carboxylic acid-lysine residue reaction; therefore, we have neutralized some of the lysine residues. Furthermore, at pH of 3 and 4 some of carboxylic groups are protonated which causes the polymer to lose its zwitterionic charge neutral nature. A combination of these effects can explain the smaller half-life for the immobilized enzyme at pH 3 and 4.

Table 5.2, Half-life of chymotrypsin in different pHs at T=40 °C. The half-life measurements were carried out at conditions with equal volumetric activity (0.15 mg/ml chymotrypsin in solution and 30 mg/ml enzyme-immobilized microgel suspension)

pH	Half-life (min)		% Change in half-life after immobilization
	Free Enzyme	Immobilized Enzyme	
3	14850	11321	-24%
4	12956	10714	-17%
5	4667	8980	92%
7	1500	3870	158 %
8	512	2031	297 %
9	115	822	615 %

To our understanding, immobilization of enzyme within zwitterionic microgel beads have not been carried out before. While this research advances the design of materials to enhance enzyme stability, it also raises further questions that needs to be separately investigated. For instance, efficacy of the EDC-mediated coupling of chymotrypsin was not measured in this work and needs to be investigated. Furthermore, the mechanism for loss of activity by the immobilized chymotrypsin at different pHs values should be further studied and is beyond the scope of this paper. Similarly, the effect of temperature on properties of the zwitterionic polymeric hydrogel (e.g. correlation length) should be studied to deconvolute effect of pCB changes on the enzyme activity as a future step for this research.

5.4 Conclusions

Zwitterionic poly(carboxybetaine) (pCB) microgel was synthesized. In addition to excellent dispersion characteristics, the size (5 – 20 μm) of these beads facilitated post-fabrication protein immobilization due to enhanced surface area. A protease enzyme, α -chymotrypsin (ChT), was immobilized within the beads following pCB hydrogel synthesis. The pCB-immobilized ChT retained 72% of its original activity after 10 reaction cycles. Most importantly, our results indicated that enzymes immobilized within the zwitterionic hydrogel beads displayed enhanced thermal stability over the free enzyme. This study paves the way for future work focused on developing enzyme immobilization inside biomacromolecule-compatible materials for reusability and enhanced functionality.

Acknowledgements:

This chapter was previously published as: Erfani, Amir, Joshua Seaberg, Payam Zarrintaj, Joshua D. Ramsey, and Clint P. Aichele. “Zwitterionic poly(carboxybetaine) microgels for enzyme (chymotrypsin) covalent immobilization with extended stability and activity” *Journal of Applied Polymer Science*, (2021).

CHAPTER VI

Conclusions and Future Directions

6.1 Conclusions

In this dissertation, I have described approaches to use zwitterionic polymers in the form of microscale hydrogels to enable protein encapsulation, release, stabilization and immobilization. We used inherent properties of zwitterionic polymers to increase the protein stability while encapsulated within the zwitterionic microscale hydrogels.

In Chapter 2, we reviewed literature on our expanding understanding of the interactions between zwitterionic moieties and water, salts, and biomolecules. Researchers have utilized the unique properties of zwitterionic monomers, polymers, and amphiphilic molecules to great effect with applications ranging from protein stabilization to stimulus-responsive drug delivery systems. I expect these materials to find applications in biosensors, protein separation, protein immobilization techniques, cryoprotectants, and biopharmaceuticals. I further expect to see growing interest from biopharmaceutical and biotech companies in the commercialization of such technologies.

In Chapter 3, zwitterionic poly(sulfobetaine) (pSB) hydrogel beads were fabricated and BSA was loaded inside the beads post synthesis. pSB hydrogels were ionresponsive as evidenced by the swelling behavior when exposed to ions. Furthermore, a positive temperature dependency of swelling was observed for the pSB hydrogel. In addition to the excellent dispersion characteristics of hydrogel beads, the small size of these beads facilitated post-fabrication protein loading due to enhanced surface area. The release of protein from the hydrogel beads was tunable by changing the crosslinking density. High permeability of the hydrogel limited the release of the protein to short timeframes (less than a week). Proteins loaded and released from the hydrogel maintained their native structure (probed by the enzymatic activity). Most importantly, our results indicated that proteins loaded inside the zwitterionic hydrogel beads

were thermally more stable (aggregated slower and retained tertiary structure) than protein in solution.

In Chapter 4, biodegradable zwitterionic poly(carboxy) (pCB) microgels were fabricated using tetra (ethyne glycol) diacrylate (TTEGDA) as the crosslinker with a water-in-oil emulsion technique. The synthesized microgels showed water content as high as 97.5% and were in the range of 5-30 micrometers in diameter (freeze-dried). The microgels showed excellent hydrolytic degradability, which could be tailored by changing the crosslinking density for different drug delivery administration applications. Microgels characteristic lengths were evaluated using small-angle neutron scattering and were found to range from 3.0 to 24.2 nm. The studied microgel showed excellent cell compatibility, complete fibroblast cell viability and lack of immunogenic responses observed by monitoring secretion of interleukin 6 (IL6) and tumor necrosis factor-alpha (TNF α). The biodegradable microgel was loaded with Immunoglobulin G (IgG) as a model antibody. High permeability of the microgel limited the release of the antibody to short-term release needs. Antibodies loaded and released from the microgel at 40°C maintained their native structure, which was probed by the binding ability of the IgG molecules. The ability of the zwitterionic microgel to prevent non-specific interactions of antibody has significant implications for sustained local delivery of antibody.

Finally, in Chapter 5, Zwitterionic poly(carboxybetaine) (pCB) microgel was synthesized. In addition to excellent dispersion characteristics, the size (5 – 20 μm) of these beads facilitated post-fabrication protein immobilization due to enhanced surface area. A protease enzyme, α -chymotrypsin (ChT), was immobilized within the beads following pCB hydrogel synthesis. The pCB-immobilized ChT retained 72% of its original activity after 10 reaction cycles. Most importantly, our results indicated that enzymes immobilized within the

zwitterionic hydrogel beads displayed enhanced thermal stability over the free enzyme. This study paves the way for future work focused on developing enzyme immobilization inside biomacromolecule-compatible materials for reusability and enhanced functionality. Furthermore, enzyme half-life increased up to seven-fold for the pCB immobilized ChT, and the increased stability resulted in higher activity at elevated pH. The i-ChT was most active at pH of 8.5 and was partially active up to the pH of 10.2. This research paves the way for the fabrication of enzyme-immobilized materials with extended enzyme lifetime and molecular turnover.

6.2 Future Directions

The work described in this dissertation can be extended in many areas, four of which are discussed below:

Surface modification to enable long-term release of biomolecules:

While this work demonstrates that encapsulation and release of active antibody from the zwitterionic microgel can be achieved, sustained long-term delivery of the biomolecules is still an unmet need. Surface modifications of the studied microgels with FDA approved slow degradable materials such as poly caprolactone can potentially result in core-shell particles that enable long-term sustained release

Enabling pulmonary delivery of antibodies by using microgels:

The global pandemic caused by SARS-CoV-2 shows the need for readily accessible treatments of infectious respiratory diseases, especially therapies that enable direct efficient

delivery of therapeutic biomolecules into the small airways of the lungs. Zwitterionic architectures, such as those that we explored in this project, are promising candidates due largely to the lack of pro-inflammatory response and minimal interaction with the loaded therapy. Such microgels if synthesized in ideal size ($\sim 1 \mu\text{m}$) can potentially penetrate and deposit into the small airways of the lung, thereby resulting in efficient delivery.

In-vitro assessment of zwitterionic microgels for delivery of cancer threatening mAbs:

In this research, we concluded that zwitterionic microgels can enable non-immunogenic delivery of a model antibody. Using the developed strategy, monoclonal antibodies such as Trastuzumab or Bevacizumab can be used to treat breast cancer and other appropriate cancer cells. Investigation of cancer cell responses to the microgel sustained released mAbs is a future step for this research.

Enzyme immobilized zwitterionic microscale to enable high temperature enzymatic CO₂ capture:

Our investigation on enzyme immobilization within zwitterionic microgels indicated significant increase in the thermal activity and thermal stability of the enzyme. This suggests that our strategy would be mostly useful if the enzyme would be used in a process with elevated temperatures. Enzymatic CO₂ capture using carbonate anhydrase is an example of such process.

REFERENCES

1. Paleg, L.G., G.R. Stewart, J.W. Bradbeer, *Proline and glycine betaine influence protein solvation*. Plant Physiol., 1984. **75**(4): p. 974-978.
2. Arakawa, T.S.N. Timasheff, *Preferential interactions of proteins with solvent components in aqueous amino acid solutions*. Arch. Biochem. Biophys., 1983. **224**(1): p. 169-177.
3. Zhang, W., M.W. Capp, J.P. Bond, C.F. Anderson, M.T. Record, *Thermodynamic Characterization of Interactions of Native Bovine Serum Albumin with Highly Excluded (Glycine Betaine) and Moderately Accumulated (Urea) Solutes by a Novel Application of Vapor Pressure Osmometry*. Biochemistry, 1996. **35**(32): p. 10506-10516.
4. Bonte, N.A. Laschewsky, *Zwitterionic polymers with carbobetaine moieties*. Polymer, 1996. **37**(10): p. 2011-2019.
5. Lowe, A.B.C.L. McCormick, *Synthesis and solution properties of zwitterionic polymers*. Chemical Reviews, 2002. **102**(11): p. 4177-4189.
6. Viklund, C.K. Irgum, *Synthesis of porous zwitterionic sulfobetaine monoliths and characterization of their interaction with proteins*. Macromolecules, 2000. **33**(7): p. 2539-2544.
7. Holmlin, R.E., X. Chen, R.G. Chapman, S. Takayama, G.M. Whitesides, *Zwitterionic SAMs that Resist Nonspecific Adsorption of Protein from Aqueous Buffer*. Langmuir, 2001. **17**(9): p. 2841-2850.
8. Ladd, J., Z. Zhang, S. Chen, J.C. Hower, S. Jiang, *Zwitterionic Polymers Exhibiting High Resistance to Nonspecific Protein Adsorption from Human Serum and Plasma*. Biomacromolecules, 2008. **9**(5): p. 1357-1361.
9. Cao, Z.S. Jiang, *Super-hydrophilic zwitterionic poly(carboxybetaine) and amphiphilic non-ionic poly(ethylene glycol) for stealth nanoparticles*. Nano Today, 2012. **7**(5): p. 404-413.
10. Keefe, A.J.S. Jiang, *Poly (zwitterionic) protein conjugates offer increased stability without sacrificing binding affinity or bioactivity*. Nat. Chem., 2012. **4**(1): p. 59.
11. Liu, S.S. Jiang, *Chemical conjugation of zwitterionic polymers protects immunogenic enzyme and preserves bioactivity without polymer-specific antibody response*. Nano Today, 2016. **11**(3): p. 285-291.
12. Laschewsky, A., *Structures and synthesis of zwitterionic polymers*. Polymers, 2014. **6**(5): p. 1544-1601.
13. Izquierdo-Barba, I., M. Colilla, M. Vallet-Regí, *Zwitterionic ceramics for biomedical applications*. Acta Biomater., 2016. **40**: p. 201-211.
14. He, M., K. Gao, L. Zhou, Z. Jiao, M. Wu, J. Cao, X. You, Z. Cai, Y. Su, Z. Jiang, *Zwitterionic materials for antifouling membrane surface construction*. Acta Biomater., 2016. **40**: p. 142-152.
15. Zurick, K.M.M. Bernards, *Recent biomedical advances with polyampholyte polymers*. J. Appl. Polym. Sci., 2014. **131**(6): p. 40069, 1-9.
16. Al Hassan, M., E. Estrelles, P. Soriano, M.P. López-Gresa, J.M. Bellés, M. Boscaiu, O. Vicente, *Unraveling salt tolerance mechanisms in halophytes: a comparative study on four Mediterranean Limonium species with different geographic distribution patterns*. Front Plant Sci., 2017. **8**: p. 1438, 1-21.
17. Bretscher, M.S.M.C. Raff, *Mammalian plasma membranes*. Nature, 1975. **258**(5530): p. 43.

18. Yuan, Y.Y., C.Q. Mao, X.J. Du, J.Z. Du, F. WangJ. Wang, *Surface charge switchable nanoparticles based on zwitterionic polymer for enhanced drug delivery to tumor*. *Adv. Mater.*, 2012. **24**(40): p. 5476-5480.
19. Li, Y., R. Liu, Y. Shi, Z. ZhangX. Zhang, *Zwitterionic poly (carboxybetaine)-based cationic liposomes for effective delivery of small interfering RNA therapeutics without accelerated blood clearance phenomenon*. *Theranostics*, 2015. **5**(6): p. 583.
20. Kato, T., M. Kawaguchi, A. Takahashi, T. OnabeH. Tanaka, *Adsorption of sulfobetaine polyampholyte on silica surfaces from aqueous salt solutions*. *Langmuir*, 1999. **15**(12): p. 4302-4305.
21. Kawata, Y., S. KozukaS.-i. Yusa, *Thermo-Responsive Behavior of Amphoteric Diblock Copolymers Bearing Sulfonate and Quaternary Amino Pendant Groups*. *Langmuir*, 2019. **35**(5): p. 1458-1464.
22. Kim, D., H. MatsuokaY. Saruwatari, *Synthesis and Stimuli Responsivity of Diblock Copolymers Composed of Sulfobetaine and Ionic Blocks: Influence of the Block Ratio*. *Langmuir*, 2019. **35**(5): p. 1590-1597.
23. Tu, Q., J.-C. Wang, R. Liu, Y. Zhang, J. Xu, J. Liu, M.-S. Yuan, W. LiuJ. Wang, *Synthesis of polyethylene glycol- and sulfobetaine-conjugated zwitterionic poly(l-lactide) and assay of its antifouling properties*. *Colloids Surf., B*, 2013. **102**: p. 331-340.
24. Vuillard, L., T. RabilloudM.E. Goldberg, *Interactions of non-detergent sulfobetaines with early folding intermediates facilitate in vitro protein renaturation*. *Eur. J. Biochem.*, 1998. **256**(1): p. 128-135.
25. Wangkanont, K., K.T. ForestL.L. Kiessling, *The non-detergent sulfobetaine-201 acts as a pharmacological chaperone to promote folding and crystallization of the type II TGF- β receptor extracellular domain*. *Protein Expression Purif.*, 2015. **115**: p. 19-25.
26. Wu, J., Z. Xiao, A. Chen, H. He, C. He, X. Shuai, X. Li, S. Chen, Y. Zhang, B. Ren, J. ZhengJ. Xiao, *Sulfated zwitterionic poly(sulfobetaine methacrylate) hydrogels promote complete skin regeneration*. *Acta Biomater.*, 2018. **71**: p. 293-305.
27. Zhang, Z., S. Chen, Y. ChangS. Jiang, *Surface grafted sulfobetaine polymers via atom transfer radical polymerization as superlow fouling coatings*. *J. Phys. Chem. B*, 2006. **110**(22): p. 10799.
28. Chołuj, D., R. Karwowska, A. CiszewskaM. Jasińska, *Influence of long-term drought stress on osmolyte accumulation in sugar beet (Beta vulgaris L.) plants*. *Acta Physiologiae Plantarum*, 2008. **30**(5): p. 679.
29. Carr, L.R., H. XueS. Jiang, *Functionalizable and nonfouling zwitterionic carboxybetaine hydrogels with a carboxybetaine dimethacrylate crosslinker*. *Biomaterials*, 2011. **32**(4): p. 961-968.
30. Vasantha, V.A., C. Junhui, Z. Wenguang, A.M. van HerkA. Parthiban, *Reversible Photo- and Thermoresponsive, Self-Assembling Azobenzene Containing Zwitterionic Polymers*. *Langmuir*, 2019. **35**(5): p. 1465-1474.
31. Chien, H.W., W.B. TsaiS. Jiang, *Direct cell encapsulation in biodegradable and functionalizable carboxybetaine hydrogels*. *Biomaterials*, 2012. **33**(23): p. 5706-5712.
32. Huynh, V., A.H. Jesmer, M.M. ShoaibR.G. Wylie, *Influence of Hydrophobic Cross-Linkers on Carboxybetaine Copolymer Stimuli Response and Hydrogel Biological Properties*. *Langmuir*, 2019. **35**(5): p. 1631-1641.
33. Tsvetkov, N.V., A.A. Lezov, P.S. Vlasov, A.S. Gubarev, A.A. Lezova, E.V. Lebedeva, G.E. PolushinaN.S. Domnina, *Macromolecules of polycarboxybetaine poly(4-N,N-diallyl-N-methylammonio) butanoate: Synthesis and molecular characteristics*. *Polymer*, 2017. **122**: p. 34-44.
34. Yang, W., L. Zhang, S. Wang, A.D. WhiteS. Jiang, *Functionalizable and ultra stable nanoparticles coated with zwitterionic poly(carboxybetaine) in undiluted blood serum*. *Biomaterials*, 2009. **30**(29): p. 5617-5621.

35. Zhang, Z., S. ChenS. Jiang, *Dual-functional biomimetic materials: Nonfouling poly(carboxybetaine) with active functional groups for protein immobilization*. *Biomacromolecules*, 2006. **7**(12): p. 3311-3315.
36. Zhang, Z., H. Vaisocherová, G. Cheng, W. Yang, H. XueS. Jiang, *Nonfouling behavior of polycarboxybetaine-grafted surfaces: Structural and environmental effects*. *Biomacromolecules*, 2008. **9**(10): p. 2686-2692.
37. Zhao, G., X. DongY. Sun, *Self-Assembled Curcumin–Poly(carboxybetaine methacrylate) Conjugates: Potent Nano-Inhibitors against Amyloid β -Protein Fibrillogenesis and Cytotoxicity*. *Langmuir*, 2019. **35**(5): p. 1846-1857.
38. Chołuj, D., R. Karwowska, A. CiszewskaM. Jasińska, *Influence of long-term drought stress on osmolyte accumulation in sugar beet (*Beta vulgaris* L.) plants*. *Acta Physiol. Plant.*, 2008. **30**(5): p. 679-687.
39. Izumrudov, V.A., A.N. Zelikin, M.V. Zhiryakova, W. JaegerJ. Bohrisch, *Interpolyelectrolyte reactions in solutions of polycarboxybetaines*. *J. Phys. Chem.*, 2003. **107**(32): p. 7982-7986.
40. Kyomoto, M., T. Moro, S. Yamane, K. Watanabe, M. Hashimoto, S. TanakaK. Ishihara, *Hydrated Phospholipid Polymer Gel-Like Layer for Increased Durability of Orthopedic Bearing Surfaces*. *Langmuir*, 2019. **35**(5): p. 1954-1963.
41. Ishihara, K., H. Nomura, T. Mihara, K. Kurita, Y. IwasakiN. Nakabayashi, *Why do phospholipid polymers reduce protein adsorption?* *J. Biomed. Mater. Res.*, 1998. **39**(2): p. 323-330.
42. Ishihara, K., M. Mu, T. Konno, Y. InoueK. Fukazawa, *The unique hydration state of poly(2-methacryloyloxyethyl phosphorylcholine)*. *J. Biomater. Sci., Polym. Ed.*, 2017. **28**(10-12): p. 884-899.
43. Ishihara, K.Y. Iwasaki, *Reduced protein adsorption on novel phospholipid polymers*. *J. Biomater. Appl.*, 1998. **13**(2): p. 111-127.
44. Ishihara, K., T. UedaN. Nakabayashi, *Preparation of phospholipid polymers and their properties as polymer hydrogel membranes*. *Polym. J.*, 1990. **22**(5): p. 355-360.
45. Nakaya, T.Y.J. Li, *Phospholipid polymers*. *Prog. Polym. Sci.*, 1999. **24**(1): p. 143-181.
46. Tanaka, M.Y. Iwasaki, *Photo-assisted generation of phospholipid polymer substrates for regiospecific protein conjugation and control of cell adhesion*. *Acta Biomater.*, 2016. **40**: p. 54-61.
47. Wang, L., C. Shi, X. Wang, D. Guo, T.M. DuncanJ. Luo, *Zwitterionic Janus Dendrimer with distinct functional disparity for enhanced protein delivery*. *Biomaterials*, 2019. **215**: p. 119233.
48. Liao, Y.-T., A.C. Manson, M.R. DeLyser, W.G. NoidP.S. Cremer, *Trimethylamine N-oxide stabilizes proteins via a distinct mechanism compared with betaine and glycine*. *Proc. Natl. Acad. Sci. U. S. A.*, 2017. **114**(10): p. 2479-2484.
49. Feng, L., L. Xu, S. DongJ. Hao, *Thermo-reversible capture and release of DNA by zwitterionic surfactants*. *Soft matter*, 2016. **12**(36): p. 7495-7504.
50. Broy, S., C. Chen, T. Hoffmann, N.L. Brock, G. Nau-Wagner, M. Jebbar, S.H. Smits, J.S. DickschatE. Bremer, *Abiotic stress protection by ecologically abundant dimethylsulfonylpropionate and its natural and synthetic derivatives: insights from *B. subtilis**. *Environ. Microbiol.*, 2015. **17**(7): p. 2362-2378.
51. Stefels, J., *Physiological aspects of the production and conversion of DMSP in marine algae and higher plants*. *J. Sea Res.*, 2000. **43**(3-4): p. 183-197.
52. Imamura, R.H. Mori, *Synthesis of Zwitterionic Polymers Containing a Tertiary Sulfonium Group for Protein Stabilization*. *Biomacromolecules*, 2019. **20**(2): p. 904-915.
53. Danko, M., Z. Kroneková, M. Mrlik, J. Osicka, A. bin Yousaf, A. Mihálová, J. TkacP. Kasak, *Sulfobetaines Meet Carboxybetaines: Modulation of Thermo- and Ion-Responsivity, Water Structure, Mechanical Properties, and Cell Adhesion*. *Langmuir*, 2019. **35**(5): p. 1391-1403.
54. Iwasaki, Y.K. Ishihara, *Phosphorylcholine-containing polymers for biomedical applications*. *Anal. Bioanal. Chem.*, 2005. **381**(3): p. 534-546.

55. Ivanov, I., I. Tsacheva, V. Stoyanova, M. Nikolov, M.I. Tchorbadjieva, S. Petrova, L. Christov, V. GeorgievaG. Georgiev, *Chaperone-like effect of polyzwitterions on the interaction of C1q with IgG*. Z. Naturforsch., C: J. Biosci., 2009. **64**(1-2): p. 149-154.
56. Liu, S.S. Jiang, *Zwitterionic polymer-protein conjugates reduce polymer-specific antibody response*. Nano Today, 2016. **11**(3): p. 285-291.
57. Schlenoff, J.B., *Zwitteration: coating surfaces with zwitterionic functionality to reduce nonspecific adsorption*. Langmuir, 2014. **30**(32): p. 9625-9636.
58. Chen, S., J. Zheng, L. LiS. Jiang, *Strong resistance of phosphorylcholine self-assembled monolayers to protein adsorption: Insights into nonfouling properties of zwitterionic materials*. J. Am. Chem. Soc., 2005. **127**(41): p. 14473-14478.
59. Estephan, Z.G., J.A. JaberJ.B. Schlenoff, *Zwitterion-stabilized silica nanoparticles: Toward nonstick nano*. Langmuir, 2010. **26**(22): p. 16884-16889.
60. Chen, Y., Y. Wang, H. Wang, F. Jia, T. Cai, J. JiQ. Jin, *Zwitterionic supramolecular prodrug nanoparticles based on host-guest interactions for intracellular drug delivery*. Polymer, 2016. **97**: p. 449-455.
61. Huang, P., J. Liu, W. Wang, Y. Zhang, F. Zhao, D. Kong, J. LiuA. Dong, *Zwitterionic nanoparticles constructed from bioreducible RAFT-ROP double head agent for shell shedding triggered intracellular drug delivery*. Acta Biomater., 2016. **40**: p. 263-272.
62. Cao, Z., L. ZhangS. Jiang, *Superhydrophilic zwitterionic polymers stabilize liposomes*. Langmuir, 2012. **28**(31): p. 11625-11632.
63. Juan, E.C.M., M.T. Hossain, M.M. Hoque, K. Suzuki, T. SekiguchiA. Takenaka, *Crystal structure of uricase from Arthrobacter globiformis in complex with 8-azaxanthin (inhibitor)*. TO BE PUBLISHED, 2008.
64. Pettersen, E.F., T.D. Goddard, C.C. Huang, G.S. Couch, D.M. Greenblatt, E.C. MengT.E. Ferrin, *UCSF Chimera--a visualization system for exploratory research and analysis*. J. Comput. Chem., 2004. **25**(13): p. 1605-12.
65. Majorek, K.A., P.J. Porebski, A. Dayal, M.D. Zimmerman, K. Jablonska, A.J. Stewart, M. ChruszczW. Minor, *Structural and immunologic characterization of bovine, horse, and rabbit serum albumins*. Mol. Immunol., 2012. **52**(3): p. 174-182.
66. Rajan, R.K. Matsumura, *Inhibition of protein aggregation by zwitterionic polymer-based core-shell nanogels*. Sci. Rep., 2017. **7**: p. 45777.
67. Sakaki, S., N. NakabayashiK. Ishihara, *Stabilization of an antibody conjugated with enzyme by 2-methacryloyloxyethyl phosphorylcholine copolymer in enzyme-linked immunosorbent assay*. J. Biomed. Mater. Res., 1999. **47**(4): p. 523-528.
68. Wallis, A.K.R.B. Freedman, *Assisting Oxidative Protein Folding: How Do Protein Disulphide-Isomerases Couple Conformational and Chemical Processes in Protein Folding?*, in *Molecular Chaperones*, S. Jackson, Editor. 2013, Springer Berlin Heidelberg: Berlin, Heidelberg. p. 1-34.
69. Goldberg, M.E., N. Expert-Bezançon, L. VuillardT. Rabilloud, *Non-detergent sulphobetaines: A new class of molecules that facilitate in vitro protein renaturation*. Folding Des., 1996. **1**(1): p. 21-27.
70. Zhang, P., F. Sun, C. Tsao, S. Liu, P. Jain, A. Sinclair, H.-C. Hung, T. Bai, K. WuS. Jiang, *Zwitterionic gel encapsulation promotes protein stability, enhances pharmacokinetics, and reduces immunogenicity*. Proc. Natl. Acad. Sci. U. S. A., 2015. **112**(39): p. 12046-12051.
71. Yesilyurt, V., O. Veiseh, J.C. Doloff, J. Li, S. Bose, X. Xie, A.R. Bader, M. Chen, M.J. WebberA.J. Vegas, *A Facile and Versatile Method to Endow Biomaterial Devices with Zwitterionic Surface Coatings*. Adv. Healthcare Mater., 2017. **6**(4): p. 1601091.
72. Chen, S.-H., K. Fukazawa, Y. InoueK. Ishihara, *Photoinduced Surface Zwitterionization for Antifouling of Porous Polymer Substrates*. Langmuir, 2019. **35**(5): p. 1312-1319.
73. Liang, B., G. Zhang, Z. Zhong, Y. HuangZ. Su, *Superhydrophilic Anti-Icing Coatings Based on Polyzwitterion Brushes*. Langmuir, 2019. **35**(5): p. 1294-1301.

74. Lv, Y., Z. LinF. Svec, *Hypercrosslinked large surface area porous polymer monoliths for hydrophilic interaction liquid chromatography of small molecules featuring zwitterionic functionalities attached to gold nanoparticles held in layered structure*. *Anal. Chem.*, 2012. **84**(20): p. 8457-8460.
75. Raeeszadeh-Sarmazdeh, M., E. Hartzell, J.V. PriceW. Chen, *Protein nanoparticles as multifunctional biocatalysts and health assessment sensors*. *Curr. Opin. Chem. Eng.*, 2016. **13**: p. 109-118.
76. Song, J., Y. Zhu, J. Zhang, J. Yang, Y. Du, W. Zheng, C. Wen, Y. ZhangL. Zhang, *Encapsulation of AgNPs within Zwitterionic Hydrogels for Highly Efficient and Antifouling Catalysis in Biological Environments*. *Langmuir*, 2019. **35**(5): p. 1563-1570.
77. Ajmal, M., S. Demirci, M. Siddiq, N. AktasN. Sahiner, *Betaine microgel preparation from 2-(methacryloyloxy) ethyl] dimethyl (3-sulfopropyl) ammonium hydroxide and its use as a catalyst system*. *Colloids Surf., A*, 2015. **486**: p. 29-37.
78. Estephan, Z.G., P.S. SchlenoffJ.B. Schlenoff, *Zwitteration as an alternative to PEGylation*. *Langmuir*, 2011. **27**(11): p. 6794-6800.
79. Wu, J., Z. Xiao, C. He, J. Zhu, G. Ma, G. Wang, H. Zhang, J. XiaoS. Chen, *Protein diffusion characteristics in the hydrogels of poly(ethylene glycol) and zwitterionic poly(sulfobetaine methacrylate) (pSBMA)*. *Acta Biomater.*, 2016. **40**: p. 172-181.
80. Georgiev, G.S., E.B. Kamenska, E.D. Vassileva, I.P. Kamenova, V.T. Georgieva, S.B. IlievI.A. Ivanov, *Self-Assembly, Antipolyelectrolyte Effect, and Nonbiofouling Properties of Polyzwitterions*. *Biomacromolecules*, 2006. **7**(4): p. 1329-1334.
81. Yang, S., Y. Zhu, H. QianZ. Lü, *Molecular dynamics simulation of antipolyelectrolyte effect and solubility of polyzwitterions*. *Chem. Res. Chin. Univ.*, 2017. **33**(2): p. 261-267.
82. Bohrisch, J., T. Schimmel, H. EngelhardtW. Jaeger, *Charge interaction of synthetic polycarboxybetaines in bulk and solution*. *Macromolecules*, 2002. **35**(10): p. 4143-4149.
83. Bredas, J., R. ChanceR. Silbey, *Head-head interactions in zwitterionic associating polymers*. *Macromolecules*, 1988. **21**(6): p. 1633-1639.
84. Arotçaréna, M., B. Heise, S. IshayaA. Laschewsky, *Switching the Inside and the Outside of Aggregates of Water-Soluble Block Copolymers with Double Thermoresponsivity*. *J. Am. Chem. Soc.*, 2002. **124**(14): p. 3787-3793.
85. Bag, M.A.L.M. Valenzuela, *Impact of the hydration states of polymers on their hemocompatibility for medical applications: A review*. *Int. J. Mol. Sci.*, 2017. **18**(8): p. 1422.
86. Chen, S., L. Li, C. ZhaoJ. Zheng, *Surface hydration: Principles and applications toward low-fouling/nonfouling biomaterials*. *Polymer*, 2010. **51**(23): p. 5283-5293.
87. Sakamaki, T., Y. Inutsuka, K. Igata, K. Higaki, N.L. Yamada, Y. HigakiA. Takahara, *Ion-Specific Hydration States of Zwitterionic Poly(sulfobetaine methacrylate) Brushes in Aqueous Solutions*. *Langmuir*, 2019. **35**(5): p. 1583-1589.
88. Morozova, S., G. Hu, T. EmrickM. Muthukumar, *Influence of Dipole Orientation on Solution Properties of Polyzwitterions*. *ACS Macro Lett.*, 2016. **5**(1): p. 118-122.
89. Niu, A., D.J. Liaw, H.C. SangC. Wu, *Light-scattering study of a zwitterionic polycarboxybetaine in aqueous solution*. *Macromolecules*, 2000. **33**(9): p. 3492-3494.
90. Gong, L., L. Xiang, J. Zhang, L. Han, J. Wang, X. Wang, J. Liu, B. YanH. Zeng, *Interaction Mechanisms of Zwitterions with Opposite Dipoles in Aqueous Solutions*. *Langmuir*, 2019. **35**(7): p. 2842-2853.
91. Han, X., C. Leng, Q. Shao, S. JiangZ. Chen, *Absolute Orientations of Water Molecules at Zwitterionic Polymer Interfaces and Interfacial Dynamics after Salt Exposure*. *Langmuir*, 2018. **35**(5): p. 1327-1334.
92. Chen, L., Y. Honma, T. Mizutani, D.J. Liaw, J.P. GongY. Osada, *Effects of polyelectrolyte complexation on the UCST of zwitterionic polymer*. *Polymer*, 2000. **41**(1): p. 141-147.
93. Lezov, A.A., P.S. Vlasov, G.E. PolushinaA.V. Lezov, *Effect of chemical structure and charge distribution on behavior of polyzwitterions in solution*. *Macromol. Symp.*, 2012. **316**(1): p. 17-24.

94. Petroff, M.G., E.A. Garcia, M. Herrera-Alonso M.A. Bevan, *Ionic Strength-Dependent Interactions and Dimensions of Adsorbed Zwitterionic Copolymers*. Langmuir, 2019. **35**(14): p. 4976-4985.
95. Wang, F., J. Yang J. Zhao, *Understanding anti-polyelectrolyte behavior of a well-defined polyzwitterion at the single-chain level*. Polym. Int., 2015. **64**(8): p. 999-1005.
96. Collins, K.D., *Ions from the Hofmeister series and osmolytes: effects on proteins in solution and in the crystallization process*. Methods, 2004. **34**(3): p. 300-311.
97. Shao, Q., Y. He S. Jiang, *Molecular dynamics simulation study of ion interactions with zwitterions*. J. Phys. Chem. B, 2011. **115**(25): p. 8358-8363.
98. Shao, Q.S. Jiang, *Molecular Understanding and Design of Zwitterionic Materials*. Adv. Mater., 2015. **27**(1): p. 15-26.
99. Lezov, A.V., P.S. Vlasov, A.A. Lezov, N.S. Domnina G.E. Polushina, *Molecular properties of poly(carboxybetaine) in solutions with different ionic strengths and pH values*. Polym. Sci. - Series A, 2011. **53**(11): p. 1012-1018.
100. Delgado, J.D.J.B. Schlenoff, *Static and Dynamic Solution Behavior of a Polyzwitterion Using a Hofmeister Salt Series*. Macromolecules, 2017. **50**(11): p. 4454-4464.
101. Shimizu, S., W.M. McLaren N. Matubayasi, *The Hofmeister series and protein-salt interactions*. J. Chem. Phys., 2006. **124**(23): p. 234905.
102. Cacace, M.G., E.M. Landau J.J. Ramsden, *The Hofmeister series: Salt and solvent effects on interfacial phenomena*. Q. Rev. Biophys., 1997. **30**(3): p. 241-277.
103. Zhang, Y.P.S. Cremer, *Interactions between macromolecules and ions: the Hofmeister series*. Curr. Opin. Chem. Biol., 2006. **10**(6): p. 658-663.
104. Andreev, M., J.J. de Pablo, A. Chremos J.F. Douglas, *Influence of Ion Solvation on the Properties of Electrolyte Solutions*. J. Phys. Chem. B, 2018. **122**(14): p. 4029-4034.
105. Thormann, E., *On understanding of the Hofmeister effect: how addition of salt alters the stability of temperature responsive polymers in aqueous solutions*. RSC Adv., 2012. **2**(22): p. 8297-8305.
106. Estell, D., T. Graycar, J. Miller, D. Powers, J. Wells, J. Burnier P. Ng, *Probing steric and hydrophobic effects on enzyme-substrate interactions by protein engineering*. Science, 1986. **233**(4764): p. 659-663.
107. Quan, H., H. Tian, Z. Huang Y. Long, *Salt stimulus response of a carboxyl betaine amphoteric hydrophobic associative polyacrylamide*. Russ. J. Appl. Chem., 2017. **90**(7): p. 1193-1201.
108. Xiang, T., T. Lu, W.-F. Zhao C.-S. Zhao, *Ionic-Strength Responsive Zwitterionic Copolymer Hydrogels with Tunable Swelling and Adsorption Behaviors*. Langmuir, 2019. **35**(5): p. 1146-1155.
109. De Groot, J., W. Ogieglo, W.M. De Vos, M. Gironès, K. Nijmeijer N.E. Benes, *Swelling dynamics of zwitterionic copolymers: The effects of concentration and type of anion and cation*. Eur. Polym. J., 2014. **55**(1): p. 57-65.
110. Haraguchi, K., J. Ning G. Li, *Swelling/deswelling behavior of zwitterionic nanocomposite gels consisting of sulfobetaine polymer-clay networks*. Eur. Polym. J., 2015. **68**: p. 630-640.
111. Xiao, S., Y. Zhang, M. Shen, F. Chen, P. Fan, M. Zhong, B. Ren, J. Yang J. Zheng, *Structural Dependence of Salt-Responsive Polyzwitterionic Brushes with an Anti-Polyelectrolyte Effect*. Langmuir, 2018. **34**(1): p. 97-105.
112. Zhang, H., S. Guo, W. Fan Y. Zhao, *Ultrasensitive pH-Induced Water Solubility Switch Using UCST Polymers*. Macromolecules, 2016. **49**(4): p. 1424-1433.
113. Ning, J., K. Kubota, G. Li K. Haraguchi, *Characteristics of zwitterionic sulfobetaine acrylamide polymer and the hydrogels prepared by free-radical polymerization and effects of physical and chemical crosslinks on the UCST*. React. Funct. Polym., 2013. **73**(7): p. 969-978.
114. Zhang, Y., S. Furryk, L.B. Sagle, Y. Cho, D.E. Bergbreiter P.S. Cremer, *Effects of Hofmeister Anions on the LCST of PNIPAM as a Function of Molecular Weight*. J. Phys. Chem. C, 2007. **111**(25): p. 8916-8924.

115. Li, W., L. Huang, X. Ying, Y. Jian, Y. Hong, F. HuY. Du, *Antitumor Drug Delivery Modulated by A Polymeric Micelle with an Upper Critical Solution Temperature*. *Angew. Chem. Int. Ed.*, 2015. **54**(10): p. 3126-3131.
116. Rosen, M.J., *Synergism in mixtures containing zwitterionic surfactants*. *Langmuir*, 1991. **7**(5): p. 885-888.
117. Erfani, A., N.H. Flynn, J.D. RamseyC.P. Aichele, *Increasing protein stability by association with zwitterionic amphiphile cocamidopropyl betaine*. *J. Mol. Liq.*, 2019. **295**: p. 111631.
118. Nakaura, H., A. KawamuraT. Miyata, *Reductively Responsive Gel Capsules Prepared Using a Water-Soluble Zwitterionic Block Copolymer Emulsifier*. *Langmuir*, 2019. **35**(5): p. 1413-1420.
119. Cao, J., A. Lu, C. Li, M. Cai, Y. Chen, S. LiX. Luo, *Effect of architecture on the micellar properties of poly (ε-caprolactone) containing sulfobetaines*. *Colloids Surf., B*, 2013. **112**: p. 35-41.
120. Zhao, X., M. Abutalip, K. AfrozN. Nuraje, *Hydrophobically Modified Polycarboxybetaine: From Living Radical Polymerization to Self-Assembly*. *Langmuir*, 2019. **35**(5): p. 1606-1612.
121. Tsonchev, S., A. Troisi, G.C. SchatzM.A. Ratner, *All-atom numerical studies of self-assembly of zwitterionic peptide amphiphiles*. *J. Phys. Chem. B*, 2004. **108**(39): p. 15278-15284.
122. Chen, H., L. Yuan, W. Song, Z. WuD. Li, *Biocompatible polymer materials: Role of protein-surface interactions*. *Prog. Polym. Sci.*, 2008. **33**(11): p. 1059-1087.
123. Chou, Y.-N., F. Sun, H.-C. Hung, P. Jain, A. Sinclair, P. Zhang, T. Bai, Y. Chang, T.-C. Wen, Q. YuS. Jiang, *Ultra-low fouling and high antibody loading zwitterionic hydrogel coatings for sensing and detection in complex media*. *Acta Biomater.*, 2016. **40**: p. 31-37.
124. Zhang, L., Z. Cao, T. Bai, L. Carr, J.R. Ella-Menye, C. Irvin, B.D. RatnerS. Jiang, *Zwitterionic hydrogels implanted in mice resist the foreign-body reaction*. *Nat. Biotechnol.*, 2013. **31**(6): p. 553-556.
125. Lundqvist, M., J. Stigler, T. Cedervall, T. Berggård, M.B. Flanagan, I. Lynch, G. EliaK. Dawson, *The evolution of the protein corona around nanoparticles: A test study*. *ACS Nano*, 2011. **5**(9): p. 7503-7509.
126. Elechalawar, C.K., M.N. Hossen, L. McNally, R. BhattacharyaP. Mukherjee, *Analysing the nanoparticle-protein corona for potential molecular target identification*. *J Control Release*, 2020. **322**: p. 122-136.
127. Schöttler, S., G. Becker, S. Winzen, T. Steinbach, K. Mohr, K. Landfester, V. MailänderF. Wurm, *Protein adsorption is required for stealth effect of poly(ethylene glycol)- and poly(phosphoester)-coated nanocarriers*. *Nat. Nanotechnol.*, 2016. **11**(4): p. 372-377.
128. Debayle, M., E. Balloul, F. Dembele, X. Xu, M. Hanafi, F. Ribot, C. Monzel, M. Coppey, A. Fragola, M. Dahan, T. PonsN. Lequeux, *Zwitterionic polymer ligands: an ideal surface coating to totally suppress protein-nanoparticle corona formation?* *Biomaterials*, 2019. **219**: p. 118357, 1-8.
129. Walker, J.A., K.J. Robinson, C. Munro, T. Gengenbach, D.A. Muller, P.R. Young, L.H.L. LuaS.R. Corrie, *Antibody-Binding, Antifouling Surface Coatings Based on Recombinant Expression of Zwitterionic EK Peptides*. *Langmuir*, 2019. **35**(5): p. 1266-1272.
130. Zheng, G., S. Liu, J. Zha, P. Zhang, X. Xu, Y. ChenS. Jiang, *Protecting Enzymatic Activity via Zwitterionic Nanocapsulation for the Removal of Phenol Compound from Wastewater*. *Langmuir*, 2019. **35**(5): p. 1858-1863.
131. Armstrong, J.K., G. Hempel, S. Koling, L.S. Chan, T. Fisher, H.J. MeiselmanG. Garratty, *Antibody against poly(ethylene glycol) adversely affects PEG-asparaginase therapy in acute lymphoblastic leukemia patients*. *Cancer*, 2007. **110**(1): p. 103.
132. Grenier, P., I.M.r.d.O. Viana, E.M. LimaN. Bertrand, *Anti-polyethylene glycol antibodies alter the protein corona deposited on nanoparticles and the physiological pathways regulating their fate in vivo*. *J. Controlled Release*, 2018. **287**: p. 121-131.
133. Wittrup, A.J. Lieberman, *Knocking down disease: a progress report on siRNA therapeutics*. *Nat. Rev. Genet.*, 2015. **16**(9): p. 543.

134. Banskota, S., P. Yousefpour, N. Kirmani, X. Li, A. Chilkoti, *Long circulating genetically encoded intrinsically disordered zwitterionic polypeptides for drug delivery*. *Biomaterials*, 2019. **192**: p. 475-485.
135. Li, B., Z. Yuan, P. Zhang, A. Sinclair, P. Jain, K. Wu, C. Tsao, J. Xie, H.C. Hung, X. Lin, *Zwitterionic Nanocages Overcome the Efficacy Loss of Biologic Drugs*. *Adv. Mater.*, 2018. **30**(14): p. 1705728.
136. Xie, J., Y. Lu, W. Wang, H. Zhu, Z. Wang, Z. Cao, *Simple Protein Modification Using Zwitterionic Polymer to Mitigate the Bioactivity Loss of Conjugated Insulin*. *Adv. Healthcare Mater.*, 2017. **6**(11): p. 1601428.
137. Cavazzana-Calvo, M., S. Hacein-Bey, G. de Saint Basile, F. Gross, E. Yvon, P. Nusbaum, F. Selz, C. Hue, S. Certain, J.L. Casanova, P. Bousso, F.L. Deist, A. Fischer, *Gene therapy of human severe combined immunodeficiency (SCID)-X1 disease*. *Science (New York, N.Y.)*, 2000. **288**(5466): p. 669.
138. Pack, D.W., A.S. Hoffman, S. Pun, P.S. Stayton, *Design and development of polymers for gene delivery*. *Nat. Rev. Drug Discovery*, 2005. **4**(7): p. 581-593.
139. Sinclair, A., T. Bai, L.R. Carr, J.R. Ella-Menye, L. Zhang, S. Jiang, *Engineering buffering and hydrolytic or photolabile charge shifting in a polycarboxybetaine ester gene delivery platform*. *Biomacromolecules*, 2013. **14**(5): p. 1587-1593.
140. Li, S., B. Chen, Y. Qu, X. Yan, W. Wang, X. Ma, B. Wang, S. Liu, X. Yu, *ROS-Response-Induced Zwitterionic Dendrimer for Gene Delivery*. *Langmuir*, 2019. **35**(5): p. 1613-1620.
141. Xiu, K.M., N.N. Zhao, W.T. Yang, F.J. Xu, *Versatile functionalization of gene vectors via different types of zwitterionic betaine species for serum-tolerant transfection*. *Acta Biomater.*, 2013. **9**(7): p. 7439-7448.
142. Sun, J., F. Zeng, H. Jian, S. Wu, *Grafting zwitterionic polymer chains onto PEI as a convenient strategy to enhance gene delivery performance*. *Polym. Chem.*, 2013. **4**(24): p. 5810-5818.
143. Tian, H., Z. Guo, L. Lin, Z. Jiao, J. Chen, S. Gao, X. Zhu, X. Chen, *pH-responsive zwitterionic copolypeptides as charge conversional shielding system for gene carriers*. *J. Controlled Release*, 2014. **174**: p. 117-125.
144. Sun, J., F. Zeng, H. Jian, S. Wu, *Conjugation with betaine: a facile and effective approach to significant improvement of gene delivery properties of PEI*. *Biomacromolecules*, 2013. **14**(3): p. 728-736.
145. Wen, Y., Z. Zhang, J. Li, *Highly Efficient Multifunctional Supramolecular Gene Carrier System Self-Assembled from Redox-Sensitive and Zwitterionic Polymer Blocks*. *Adv. Funct. Mater.*, 2014. **24**(25): p. 3874-3884.
146. Stapleton, S., M. Milosevic, C. Allen, J. Zheng, M. Dunne, I. Yeung, D.A. Jaffray, *A mathematical model of the enhanced permeability and retention effect for liposome transport in solid tumors*. *PLoS One*, 2013. **8**(12): p. e81157.
147. Nakamura, Y., A. Mochida, P.L. Choyke, H. Kobayashi, *Nanodrug Delivery: Is the Enhanced Permeability and Retention Effect Sufficient for Curing Cancer?* *Bioconjugate Chem.*, 2016. **27**(10): p. 2225-2238.
148. Qin, Z., T. Chen, W. Teng, Q. Jin, J. Ji, *Mixed-Charged Zwitterionic Polymeric Micelles for Tumor Acidic Environment Responsive Intracellular Drug Delivery*. *Langmuir*, 2019. **35**(5): p. 1242-1248.
149. Aston, W.J., D.E. Hope, A.K. Nowak, B.W. Robinson, R.A. Lake, W.J. Lesterhuis, *A systematic investigation of the maximum tolerated dose of cytotoxic chemotherapy with and without supportive care in mice*. *BMC Cancer*, 2017. **17**(1): p. 684-684.
150. Ou, H., T. Cheng, Y. Zhang, J. Liu, Y. Ding, J. Zhen, W. Shen, Y. Xu, W. Yang, P. Niu, J. Liu, Y. An, Y. Liu, L. Shi, *Surface-adaptive zwitterionic nanoparticles for prolonged blood circulation time and enhanced cellular uptake in tumor cells*. *Acta Biomater.*, 2018. **65**: p. 339-348.
151. Chen, X., S.S. Parelkar, E. Henchey, S. Schneider, T. Emrick, *PolyMPC-doxorubicin prodrugs*. *Bioconjugate Chem.*, 2012. **23**(9): p. 1753-1763.

152. Lin, W., G. Ma, Z. Yuan, H. Qian, L. Xu, E. Sidransky, S. Chen, *Development of Zwitterionic Polypeptide Nanof ormulation with High Doxorubicin Loading Content for Targeted Drug Delivery*. *Langmuir*, 2019. **35**(5): p. 1273-1283.
153. Zhao, Y., Y. Deng, Z. Tang, Q. Jin, J. Ji, *Zwitterionic Reduction-Activated Supramolecular Prodrug Nanocarriers for Photodynamic Ablation of Cancer Cells*. *Langmuir*, 2019. **35**(5): p. 1919-1926.
154. Cai, M., J. Cao, Z. Wu, F. Cheng, Y. Chen, X. Luo, *In vitro and in vivo anti-tumor efficiency comparison of phosphorylcholine micelles with PEG micelles*. *Colloids Surf., B*, 2017. **157**: p. 268-279.
155. Di Santo, R., E. Quagliarini, S. Palchetti, D. Pozzi, V. Palmieri, G. Perini, M. Papi, A.L. Capriotti, A. Laganà, G. Caracciolo, *Microfluidic-generated lipid-graphene oxide nanoparticles for gene delivery*. *Appl. Phys. Lett.*, 2019. **114**(23).
156. Ma, J., K. Kang, Y. Zhang, Q. Yi, Z. Gu, *Detachable Polyzwitterion-Coated Ternary Nanoparticles Based on Peptide Dendritic Carbon Dots for Efficient Drug Delivery in Cancer Therapy*. *ACS Appl. Mater. Interfaces*, 2018. **10**(50): p. 43923.
157. Lin, W., G. Ma, N. Kampf, Z. Yuan, S. Chen, *Development of Long-Circulating Zwitterionic Cross-Linked Micelles for Active-Targeted Drug Delivery*. *Biomacromolecules*, 2016. **17**(6): p. 2010.
158. Ma, J., K. Kang, Q. Yi, Z. Zhang, Z. Gu, *Multiple pH responsive zwitterionic micelles for stealth delivery of anticancer drugs*. *RSC Adv.*, 2016. **6**(69): p. 64778-64790.
159. Wang, Y., L. Li, J. Li, B. Yang, C. Wang, W. Fang, F. Ji, Y. Wen, F. Yao, *Stable and pH-responsive polyamidoamine based unimolecular micelles capped with a zwitterionic polymer shell for anticancer drug delivery*. *RSC Adv.*, 2016. **6**(21): p. 17728-17739.
160. Cao, J., X. Xie, A. Lu, B. He, Y. Chen, Z. Gu, X. Luo, *Cellular internalization of doxorubicin loaded star-shaped micelles with hydrophilic zwitterionic sulfobetaine segments*. *Biomaterials*, 2014. **35**(15): p. 4517-4524.
161. Fan, L., X. Wang, Q. Cao, Y. Yang, D. Wu, *POSS-based supramolecular amphiphilic zwitterionic complexes for drug delivery*. *Biomater. Sci.*, 2019. **7**(5): p. 1984-1994.
162. Men, Y., S. Peng, P. Yang, Q. Jiang, Y. Zhang, B. Shen, P. Dong, Z. Pang, W. Yang, *Biodegradable Zwitterionic Nanogels with Long Circulation for Antitumor Drug Delivery*. *ACS Appl. Mater. Interfaces*, 2018. **10**(28): p. 23509-23521.
163. Shih, Y., A. Venault, L.L. Tayo, S.-H. Chen, A. Higuchi, A. Deratani, A. Chinnathambi, S.A. Alharbi, D. Quemener, Y. Chang, *A Zwitterionic-Shielded Carrier with pH-Modulated Reversible Self-Assembly for Gene Transfection*. *Langmuir*, 2017. **33**(8): p. 1914.
164. Kanto, R., Y. Qiao, K. Masuko, H. Furusawa, S. Yano, K. Nakabayashi, H. Mori, *Synthesis, Assembled Structures, and DNA Complexation of Thermoresponsive Lysine-Based Zwitterionic and Cationic Block Copolymers*. *Langmuir*, 2019. **35**(13): p. 4646-4659.
165. Di Santo, R., E. Quagliarini, S. Palchetti, D. Pozzi, V. Palmieri, G. Perini, M. Papi, A.L. Capriotti, A. Laganà, G. Caracciolo, *Microfluidic-generated lipid-graphene oxide nanoparticles for gene delivery*. *Appl. Phys. Lett.*, 2019. **114**(23): p. 233701, 1-5.
166. Miller, J.B., S. Zhang, P. Kos, H. Xiong, K. Zhou, S.S. Perelman, H. Zhu, D.J. Siegwart, *Non-Viral CRISPR/Cas Gene Editing In Vitro and In Vivo Enabled by Synthetic Nanoparticle Co-Delivery of Cas9 mRNA and sgRNA*. *Angew. Chem. Int. Ed.*, 2017. **56**(4): p. 1059-1063.
167. Xiong, Z., C.S. Alves, J. Wang, A. Li, J. Liu, M. Shen, J. Rodrigues, H. Tomás, X. Shi, *Zwitterion-functionalized dendrimer-entrapped gold nanoparticles for serum-enhanced gene delivery to inhibit cancer cell metastasis*. *Acta Biomater.*, 2019. **99**: p. 320-329.
168. Sanchez-Salcedo, S., M. Vallet-Regí, S.A. Shahin, C.A. Glackin, J.I. Zink, *Mesoporous core-shell silica nanoparticles with anti-fouling properties for ovarian cancer therapy*. *Chem. Eng. J.*, 2018. **340**: p. 114-124.

169. Shan, W., X. Zhu, W. Tao, Y. Cui, M. Liu, L. Wu, L. Li, Y. Zheng, Y. Huang, *Enhanced oral delivery of protein drugs using zwitterion-functionalized nanoparticles to overcome both the diffusion and absorption barriers*. ACS Appl. Mater. Interfaces, 2016. **8**(38): p. 25444-25453.
170. Expert-Bezançon, N., T. Rabilloud, L. Vuillard, M.E. Goldberg, *Physical-chemical features of non-detergent sulfobetaines active as protein-folding helpers*. Biophys. Chem., 2003. **100**(1-3): p. 469-479.
171. Tastet, C., S. Charmont, M. Chevallet, S. Luche, T. Rabilloud, *Structure-efficiency relationships of zwitterionic detergents as protein solubilizers in two-dimensional electrophoresis*. Proteomics, 2003. **3**(2): p. 111-121.
172. Seo, J.H., R. Matsuno, Y. Lee, M. Takai, K. Ishihara, *Conformational recovery and preservation of protein nature from heat-induced denaturation by water-soluble phospholipid polymer conjugation*. Biomaterials, 2009. **30**(28): p. 4859-4867.
173. Michanek, A., M. Yanez, H. Wacklin, A. Hughes, T. Nylander, E. Sparr, *RNA and DNA association to zwitterionic and charged monolayers at the air-liquid interface*. Langmuir, 2012. **28**(25): p. 9621-9633.
174. Mengistu, D.H., K. Bohinc, S. May, *Binding of DNA to Zwitterionic Lipid Layers Mediated by Divalent Cations*. J. Phys. Chem. B, 2009. **113**(36): p. 12277-12282.
175. Teplova, M., S.T. Wallace, V. Tereshko, G. Minasov, A.M. Symons, P.D. Cook, M. Manoharan, M. Egli, *Structural origins of the exonuclease resistance of a zwitterionic RNA*. Proc. Natl. Acad. Sci. U. S. A., 1999. **96**(25): p. 14240-14245.
176. Lin, X., K. Fukazawa, K. Ishihara, *Photoinduced inhibition of DNA unwinding in vitro with water-soluble polymers containing both phosphorylcholine and photoreactive groups*. Acta Biomater., 2016. **40**: p. 226-234.
177. Kano, T., C. Kakinuma, S. Wada, K. Morimoto, T. Ogihara, *Enhancement of drug solubility and absorption by copolymers of 2-methacryloyloxyethyl phosphorylcholine and n-butyl methacrylate*. Drug Metab. Pharmacokinet., 2011. **26**(1): p. 79-86.
178. Chatterjee, S.T. Ooya, *Hydrophobic Nature of Methacrylate-POSS in Combination with 2-(Methacryloyloxy)ethyl Phosphorylcholine for Enhanced Solubility and Controlled Release of Paclitaxel*. Langmuir, 2019. **35**(5): p. 1404-1412.
179. Zhang, P., F. Sun, C. Tsao, S. Liu, P. Jain, A. Sinclair, H.-C. Hung, T. Bai, K. Wu, S. Jiang, *Zwitterionic gel encapsulation promotes protein stability, enhances pharmacokinetics, and reduces immunogenicity*. Proceedings of the National Academy of Sciences, 2015. **112**(39): p. 12046-12051.
180. Keefe, A.J., S. Jiang, *Poly (zwitterionic) protein conjugates offer increased stability without sacrificing binding affinity or bioactivity*. Nature chemistry, 2012. **4**(1): p. 59.
181. Pu, Y., Z. Hou, M.M. Khin, R. Zamudio-Vázquez, K.L. Poon, H. Duan, M.B. Chan-Park, *Synthesis and Antibacterial Study of Sulfobetaine/Quaternary Ammonium-Modified Star-Shaped Poly[2-(dimethylamino)ethyl methacrylate]-Based Copolymers with an Inorganic Core*. Biomacromolecules, 2017. **18**(1): p. 44-55.
182. Chang, Y., W. Yandi, W.-Y. Chen, Y.-J. Shih, C.-C. Yang, Y. Chang, Q.-D. Ling, A. Higuchi, *Tunable Bioadhesive Copolymer Hydrogels of Thermoresponsive Poly(N-isopropyl acrylamide) Containing Zwitterionic Polysulfobetaine*. Biomacromolecules, 2010. **11**(4): p. 1101-1110.
183. Jansen, L.E., L.D. Amer, E.Y.T. Chen, T.V. Nguyen, L.S. Saleh, T. Emrick, W.F. Liu, S.J. Bryant, S.R. Peyton, *Zwitterionic PEG-PC Hydrogels Modulate the Foreign Body Response in a Modulus-Dependent Manner*. Biomacromolecules, 2018. **19**(7): p. 2880-2888.
184. Kostina, N.Y., C. Rodriguez-Emmenegger, M. Houska, E. Brynda, J. Michálek, *Non-fouling Hydrogels of 2-Hydroxyethyl Methacrylate and Zwitterionic Carboxybetaine (Meth)acrylamides*. Biomacromolecules, 2012. **13**(12): p. 4164-4170.
185. Zhang, Z., S. Chen, S. Jiang, *Dual-Functional Biomimetic Materials: Nonfouling Poly(carboxybetaine) with Active Functional Groups for Protein Immobilization*. Biomacromolecules, 2006. **7**(12): p. 3311-3315.

186. Liu, Q., A. Chiu, L. Wang, D. An, W. Li, E.Y. Chen, Y. Zhang, Y. Pardo, S.P. McDonough, L. Liu, W.F. Liu, J. ChenM. Ma, *Developing mechanically robust, triazole-zwitterionic hydrogels to mitigate foreign body response (FBR) for islet encapsulation*. *Biomaterials*, 2020. **230**: p. 119640.
187. Caló, E.V.V. Khutoryanskiy, *Biomedical applications of hydrogels: A review of patents and commercial products*. *European Polymer Journal*, 2015. **65**: p. 252-267.
188. Guo, J.L., Y.S. KimA.G. Mikos, *Biomacromolecules for Tissue Engineering: Emerging Biomimetic Strategies*. *Biomacromolecules*, 2019. **20**(8): p. 2904-2912.
189. Dera, R., H. Diliën, B. Billen, M. Gagliardi, N. Rahimi, N.M.S. Van Den Akker, D.G.M. Molin, C. Grandfils, P. Adriaensens, W. GuedensT.J. Cleij, *Phosphodiester Hydrogels for Cell Scaffolding and Drug Release Applications*. *Macromolecular Bioscience*, 2019. **19**(7): p. 1900090.
190. Guilherme, M.R., F.A. Aouada, A.R. Fajardo, A.F. Martins, A.T. Paulino, M.F. Davi, A.F. RubiraE.C. Muniz, *Superabsorbent hydrogels based on polysaccharides for application in agriculture as soil conditioner and nutrient carrier: A review*. *European Polymer Journal*, 2015. **72**: p. 365-385.
191. McClements, D.J., *Recent progress in hydrogel delivery systems for improving nutraceutical bioavailability*. *Food hydrocolloids*, 2017. **68**: p. 238-245.
192. Dzhonova, D., R. Olariu, J. Leckenby, A. Dhayani, P.K. Vemula, J.-C. Prost, Y. Banz, A. TaddeoR. Rieben, *Local release of tacrolimus from hydrogel-based drug delivery system is controlled by inflammatory enzymes in vivo and can be monitored non-invasively using in vivo imaging*. *PloS one*, 2018. **13**(8): p. e0203409.
193. Frokjaer, S.D.E. Otzen, *Protein drug stability: A formulation challenge*. *Nature Reviews Drug Discovery*, 2005. **4**(4): p. 298-306.
194. Jiskoot, W., T.W. Randolph, D.B. Volkin, C.R. Middaugh, C. Schöneich, G. Winter, W. Friess, D.J. CrommelinJ.F. Carpenter, *Protein instability and immunogenicity: roadblocks to clinical application of injectable protein delivery systems for sustained release*. *Journal of pharmaceutical sciences*, 2012. **101**(3): p. 946-954.
195. Fu, K., K. Griebenow, L. Hsieh, A.M. KlibanovR. Langer, *FTIR characterization of the secondary structure of proteins encapsulated within PLGA microspheres*. *Journal of Controlled Release*, 1999. **58**(3): p. 357-366.
196. Fujimoto, K., Y. Mizuhara, N. TamuraH. Kawaguchi, *Interactions between thermosensitive hydrogel microspheres and proteins*. *Journal of intelligent material systems and structures*, 1993. **4**(2): p. 184-189.
197. Martin, N., D. Ma, A. Herbet, D. Boquet, F.M. WinnikC. Tribet, *Prevention of Thermally Induced Aggregation of IgG Antibodies by Noncovalent Interaction with Poly(acrylate) Derivatives*. *Biomacromolecules*, 2014. **15**(8): p. 2952-2962.
198. Manning, M.C., D.K. Chou, B.M. Murphy, R.W. PayneD.S. Katayama, *Stability of protein pharmaceuticals: an update*. *Pharmaceutical research*, 2010. **27**(4): p. 544-575.
199. van de Weert, M., W.E. HenninkW. Jiskoot, *Protein instability in poly (lactic-co-glycolic acid) microparticles*. *Pharmaceutical research*, 2000. **17**(10): p. 1159-1167.
200. Hermeling, S., D.J. Crommelin, H. SchellekensW. Jiskoot, *Structure-immunogenicity relationships of therapeutic proteins*. *Pharmaceutical research*, 2004. **21**(6): p. 897-903.
201. Feng, Y., Q. Wang, M. He, X. Zhang, X. LiuC. Zhao, *Antibiofouling Zwitterionic Gradational Membranes with Moisture Retention Capability and Sustained Antimicrobial Property for Chronic Wound Infection and Skin Regeneration*. *Biomacromolecules*, 2019. **20**(8): p. 3057-3069.
202. Peng, S., B. Ouyang, Y. Men, Y. Du, Y. Cao, R. Xie, Z. Pang, S. ShenW. Yang, *Biodegradable zwitterionic polymer membrane coating endowing nanoparticles with ultra-long circulation and enhanced tumor photothermal therapy*. *Biomaterials*, 2020. **231**: p. 119680.
203. Stejskal, E.O.J.E. Tanner, *Spin diffusion measurements: spin echoes in the presence of a time-dependent field gradient*. *The journal of chemical physics*, 1965. **42**(1): p. 288-292.

204. Sinnaeve, D., *The Stejskal–Tanner equation generalized for any gradient shape—an overview of most pulse sequences measuring free diffusion*. Concepts in Magnetic Resonance Part A, 2012. **40**(2): p. 39-65.
205. Price, W.S., *NMR studies of translational motion: principles and applications*. 2009: Cambridge University Press.
206. Seland, J.G., G.H. Sørland, K. ZickB. Hafskjold, *Diffusion measurements at long observation times in the presence of spatially variable internal magnetic field gradients*. Journal of Magnetic Resonance, 2000. **146**(1): p. 14-19.
207. Córdova, J., J.D. Ryan, B.B. BoonyaratanakornkitD.S. Clark, *Esterase activity of bovine serum albumin up to 160 C: a new benchmark for biocatalysis*. Enzyme and Microbial Technology, 2008. **42**(3): p. 278-283.
208. Flynn, N., Ç.Ö. Topal, R.S.H. Koralege, S. Hartson, A. Ranjan, J. Liu, C. PopeJ.D. Ramsey, *Effect of cationic grafted copolymer structure on the encapsulation of bovine serum albumin*. Materials Science and Engineering: C, 2016. **62**: p. 524-531.
209. Shimada, N., S. KidoakiA. Maruyama, *Smart hydrogels exhibiting UCST-type volume changes under physiologically relevant conditions*. RSC Advances, 2014. **4**(94): p. 52346-52348.
210. Cao, Z.G. Zhang, *Dynamics of polyzwitterions in salt-free and salt solutions*. Physical Chemistry Chemical Physics, 2015. **17**(40): p. 27045-27051.
211. Gun'ko, V.M., I.N. SavinaS.V. Mikhalovsky, *Properties of water bound in hydrogels*. Gels, 2017. **3**(4): p. 37.
212. McConville, P.J.M. Pope, *A comparison of water binding and mobility in contact lens hydrogels from NMR measurements of the water self-diffusion coefficient*. Polymer, 2000. **41**(26): p. 9081-9088.
213. Fergg, F., F. KeilH. Quader, *Investigations of the microscopic structure of poly (vinyl alcohol) hydrogels by confocal laser scanning microscopy*. Colloid and Polymer Science, 2001. **279**(1): p. 61-67.
214. Schillemans, J.P., E. Verheyen, A. Barendregt, W.E. HenninkC.F. Van Nostrum, *Anionic and cationic dextran hydrogels for post-loading and release of proteins*. Journal of controlled release, 2011. **150**(3): p. 266-271.
215. Appel, E.A., X.J. Loh, S.T. Jones, C.A. DreissO.A. Scherman, *Sustained release of proteins from high water content supramolecular polymer hydrogels*. Biomaterials, 2012. **33**(18): p. 4646-4652.
216. Hester, K., J. Liu, N. Flynn, L.G. Sultatos, L. Geng, S. Brimijoin, J.D. Ramsey, S. Hartson, A. RanjanC. Pope, *Polyionic complexes of butyrylcholinesterase and poly-L-lysine-g-poly(ethylene glycol): Comparative kinetics of catalysis and inhibition and in vitro inactivation by proteases and heat*. Chemico-Biological Interactions, 2017. **275**: p. 86-94.
217. Pope, C., C. Uchea, N. Flynn, K. Poindexter, L. Geng, W.S. Brimijoin, S. Hartson, A. Ranjan, J.D. RamseyJ. Liu, *In vitro characterization of cationic copolymer-complexed recombinant human butyrylcholinesterase*. Biochemical Pharmacology, 2015. **98**(3): p. 531-539.
218. Crotts, G.T.G. Park, *Stability and release of bovine serum albumin encapsulated within poly(d,l-lactide-co-glycolide) microparticles*. Journal of Controlled Release, 1997. **44**(2): p. 123-134.
219. Goldberg, M.E., N. Expert-Bezançon, L. VuillardT. Rabilloud, *Non-detergent sulphobetaines: A new class of molecules that facilitate in vitro protein renaturation*. Folding and Design, 1996. **1**(1): p. 21-27.
220. Tsumoto, K., Y. Isozaki, H. YagamiM. Tomita, *Future perspectives of therapeutic monoclonal antibodies*. Immunotherapy, 2019. **11**(2): p. 119-127.
221. Candel, F.J., M. Peñuelas, C. Tabares, C. Garcia-Vidal, M. Matesanz, M. Salavert, P. RivasJ. Pemán, *Fungal infections following treatment with monoclonal antibodies and other immunomodulatory therapies*. Revista Iberoamericana de Micología, 2020. **37**(1): p. 5-16.
222. Walsh, G., *Biopharmaceutical benchmarks 2010*. Nature biotechnology, 2010. **28**(9): p. 917.
223. Marovich, M., J.R. MascolaM.S. Cohen, *Monoclonal antibodies for prevention and treatment of COVID-19*. Jama, 2020. **324**(2): p. 131-132.

224. Shanmugaraj, B., K. Siri wattananon, K. Wangkanont W. Phoolcharoen, *Perspectives on monoclonal antibody therapy as potential therapeutic intervention for Coronavirus disease-19 (COVID-19)*. Asian Pac J Allergy Immunol, 2020. **38**(1): p. 10-18.
225. Levine, M.M., *Monoclonal antibody therapy for Ebola virus disease*. 2019, Mass Medical Soc.
226. Bilati, U., E. Allémann E. Doelker, *Strategic approaches for overcoming peptide and protein instability within biodegradable nano- and microparticles*. European Journal of Pharmaceutics and Biopharmaceutics, 2005. **59**(3): p. 375-388.
227. Madani, F., H. Hsein, V. Busignies P. Tchoreloff, *An overview on dosage forms and formulation strategies for vaccines and antibodies oral delivery*. Pharmaceutical Development and Technology, 2020. **25**(2): p. 133-148.
228. Kesten, S., J. Balarashti, C. Besch-Williford H. Nelson-Keherly, *Pulmonary Delivery of Human IgG Antibody Using a Novel Digital Inhaler in a Rodent Animal Model*, in *B68. ONCOGENIC MUTATIONS, METASTASIS, AND NOVEL THERAPEUTICS*. 2019, American Thoracic Society. p. A3945-A3945.
229. Viola, M., J. Sequeira, R. Seíça, F. Veiga, J. Serra, A.C. Santos A.J. Ribeiro, *Subcutaneous delivery of monoclonal antibodies: how do we get there?* Journal of controlled release, 2018. **286**: p. 301-314.
230. Koleba, T.M.H. Ensom, *Pharmacokinetics of intravenous immunoglobulin: a systematic review*. Pharmacotherapy: The Journal of Human Pharmacology and Drug Therapy, 2006. **26**(6): p. 813-827.
231. Wang, Y., L. Guo, S. Dong, J. Cui J. Hao, *Microgels in biomaterials and nanomedicines*. Advances in Colloid and Interface Science, 2019. **266**: p. 1-20.
232. Guziewicz, N., A. Best, B. Perez-Ramirez D.L. Kaplan, *Lyophilized silk fibroin hydrogels for the sustained local delivery of therapeutic monoclonal antibodies*. Biomaterials, 2011. **32**(10): p. 2642-2650.
233. Giteau, A., M.-C. Venier-Julienne, A. Aubert-Pouëssel J.-P. Benoit, *How to achieve sustained and complete protein release from PLGA-based microparticles?* International journal of pharmaceutics, 2008. **350**(1-2): p. 14-26.
234. Sinha, V.A. Trehan, *Biodegradable microspheres for protein delivery*. Journal of controlled release, 2003. **90**(3): p. 261-280.
235. Oh, K.S., S.K. Han, H.S. Lee, H.M. Koo, R.S. Kim, K.E. Lee, S.S. Han, S.H. Cho S.H. Yuk, *Core/shell nanoparticles with lecithin lipid cores for protein delivery*. Biomacromolecules, 2006. **7**(8): p. 2362-2367.
236. Zhu, G., S.R. Mallery S.P. Schwendeman, *Stabilization of proteins encapsulated in injectable poly (lactide-co-glycolide)*. Nature biotechnology, 2000. **18**(1): p. 52-57.
237. van de Weert, M., W.E. Hennink W. Jiskoot, *Protein Instability in Poly(Lactic-co-Glycolic Acid) Microparticles*. Pharmaceutical Research, 2000. **17**(10): p. 1159-1167.
238. Sharma, P.K.Y. Singh, *Glyoxylic hydrazone linkage-based PEG hydrogels for covalent entrapment and controlled delivery of doxorubicin*. Biomacromolecules, 2019. **20**(6): p. 2174-2184.
239. Schöttler, S., G. Becker, S. Winzen, T. Steinbach, K. Mohr, K. Landfester, V. Mailänder F.R. Wurm, *Protein adsorption is required for stealth effect of poly (ethylene glycol)-and poly (phosphoester)-coated nanocarriers*. Nature nanotechnology, 2016. **11**(4): p. 372-377.
240. Anderson, J.M.K.M. Miller, *Biomaterial biocompatibility and the macrophage*. Biomaterials, 1984. **5**(1): p. 5-10.
241. Mosqueira, V.C.F., P. Legrand, A. Gulik, O. Bourdon, R. Gref, D. Labarre G. Barratt, *Relationship between complement activation, cellular uptake and surface physicochemical aspects of novel PEG-modified nanocapsules*. Biomaterials, 2001. **22**(22): p. 2967-2979.
242. Lynn, A.D., T.R. Kyriakides S.J. Bryant, *Characterization of the in vitro macrophage response and in vivo host response to poly(ethylene glycol)-based hydrogels*. Journal of Biomedical Materials Research Part A, 2010. **93A**(3): p. 941-953.

243. Lee, L.L.Y.J.C. Lee, *Thermal stability of proteins in the presence of poly(ethylene glycols)*. *Biochemistry*, 1987. **26**(24): p. 7813-7819.
244. Erfani, A., N.H. Flynn, C.P. AicheleJ.D. Ramsey, *Encapsulation and delivery of protein from within poly (sulfobetaine) hydrogel beads*. *Journal of Applied Polymer Science*, 2020: p. 49550.
245. Kim, P.-H., H.-G. Yim, Y.-J. Choi, B.-J. Kang, J. Kim, S.-M. Kwon, B.-S. Kim, N.S. HwangJ.-Y. Cho, *Injectable multifunctional microgel encapsulating outgrowth endothelial cells and growth factors for enhanced neovascularization*. *Journal of Controlled Release*, 2014. **187**: p. 1-13.
246. Wang, Q., Z. Zuo, C.K.C. CheungS.S.Y. Leung, *Updates on thermosensitive hydrogel for nasal, ocular and cutaneous delivery*. *International Journal of Pharmaceutics*, 2019. **559**: p. 86-101.
247. Mejías, J.C.K. Roy, *In-vitro and in-vivo characterization of a multi-stage enzyme-responsive nanoparticle-in-microgel pulmonary drug delivery system*. *Journal of Controlled Release*, 2019. **316**: p. 393-403.
248. Kline, S.R., *Reduction and analysis of SANS and USANS data using IGOR Pro*. *Journal of applied crystallography*, 2006. **39**(6): p. 895-900.
249. Doucet, M., J.H. Cho, G. Alina, J. Bakker, W. Bouwman, P. Butler, K. Campbell, M. Gonzales, R. HeenanA. Jackson, *SasView version 4.1*. Zenodo and <http://www.sasview.org>, 2017.
250. Saffer, E.M., M.A. Lackey, D.M. Griffin, S. Kishore, G.N. TewS.R. Bhatia, *SANS study of highly resilient poly (ethylene glycol) hydrogels*. *Soft Matter*, 2014. **10**(12): p. 1905-1916.
251. Chien, H.-W., J. Yu, S.T. Li, H.-Y. ChenW.-B. Tsai, *An in situ poly (carboxybetaine) hydrogel for tissue engineering applications*. *Biomaterials science*, 2017. **5**(2): p. 322-330.
252. Yang, W., T. Bai, L.R. Carr, A.J. Keefe, J. Xu, H. Xue, C.A. Irvin, S. Chen, J. WangS. Jiang, *The effect of lightly crosslinked poly(carboxybetaine) hydrogel coating on the performance of sensors in whole blood*. *Biomaterials*, 2012. **33**(32): p. 7945-7951.
253. Ghadimi, A., M. Amirilargani, T. Mohammadi, N. KasiriB. Sadatnia, *Preparation of alloyed poly(ether block amide)/poly(ethylene glycol diacrylate) membranes for separation of CO₂/H₂ (syngas application)*. *Journal of Membrane Science*, 2014. **458**: p. 14-26.
254. Hammouda, B., D.L. HoS. Kline, *Insight into clustering in poly (ethylene oxide) solutions*. *Macromolecules*, 2004. **37**(18): p. 6932-6937.
255. Evmenenko, G.T. Budtova, *Structural changes in hydrogels immersed in a linear polymer solution, studied by SANS*. *Polymer*, 2000. **41**(13): p. 4943-4947.
256. Shibayama, M., T. TanakaC.C. Han, *Small angle neutron scattering study on poly (N-isopropyl acrylamide) gels near their volume-phase transition temperature*. *The Journal of chemical physics*, 1992. **97**(9): p. 6829-6841.
257. Popko, K., E. Gorska, A. Stelmaszczyk-Emmel, R. Plywaczewski, A. Stoklosa, D. Gorecka, B. PyrzakU. Demkow, *Proinflammatory cytokines Il-6 and TNF- α and the development of inflammation in obese subjects*. *European journal of medical research*, 2010. **15**(2): p. 120.
258. Agbanoma, G., C. Li, D. Ennis, A.C. Palfreeman, L.M. WilliamsF.M. Brennan, *Production of TNF- α in Macrophages Activated by T Cells, Compared with Lipopolysaccharide, Uses Distinct IL-10-Dependent Regulatory Mechanism*. *The Journal of Immunology*, 2012. **188**(3): p. 1307-1317.
259. Jiang, P., K.M. Jacobs, M.P. OhrK.E. Swindle-Reilly, *Chitosan-Polycaprolactone Core-Shell Microparticles for Sustained Delivery of Bevacizumab*. *Molecular Pharmaceutics*, 2020. **17**(7): p. 2570-2584.
260. Choi, J.-M., S.-S. HanH.-S. Kim, *Industrial applications of enzyme biocatalysis: Current status and future aspects*. *Biotechnology advances*, 2015. **33**(7): p. 1443-1454.
261. Adhikary, T., A. Nanda, K. Thangapandi, S. RoyS. Kumar, *Trends in Biosensors and Role of Enzymes as Their Sensing Element for Healthcare Applications*. *Microbial Fermentation and Enzyme Technology*, 2020.
262. Pastor, M., A. EsquisabelJ.L. Pedraz, *Biomedical Applications of immobilized enzymes: An update*, in *Immobilization of Enzymes and Cells*. 2013, Springer. p. 285-299.

263. Brandenberg, O.F., K. ChenF.H. Arnold, *Directed Evolution of a Cytochrome P450 Carbene Transferase for Selective Functionalization of Cyclic Compounds*. Journal of the American Chemical Society, 2019.
264. Wu, Z., S.J. Kan, R.D. Lewis, B.J. WittmannF.H. Arnold, *Machine learning-assisted directed protein evolution with combinatorial libraries*. Proceedings of the National Academy of Sciences, 2019. **116**(18): p. 8852-8858.
265. Research, G.V., *Enzymes Market Size, Share & Trends Analysis Report By Application (Industrial Enzymes, Specialty Enzymes), By Product (Carbohydrase, Proteases, Lipases), By Source, By Region, And Segment Forecasts, 2020 - 2027*. 2020, grand view research.
266. Wang, Y., S. Zhang, E. Haque, B.Y. Zhang, J.Z. Ou, J. Liu, Z. Liu, Y. Li, W. Gao, F. Haque, K. Xu, H. Wang, D. Cahill, L.X. KongW. Yang, *Immobilisation of microperoxidase-11 into layered MoO₃ for applications of enzymatic conversion*. Applied Materials Today, 2019. **16**: p. 185-192.
267. Zhang, Y., J. Gao, X. Xin, L. Wang, H. Li, X. ZhengY. Jiang, *Immobilization laccase on heterophase TiO₂ microsphere as a photo-enzyme integrated catalyst for emerging contaminants degradation under visible light*. Applied Materials Today, 2020. **21**: p. 100810.
268. Silva, C., M. Martins, S. Jing, J. FuA. Cavaco-Paulo, *Practical insights on enzyme stabilization*. Critical reviews in biotechnology, 2018. **38**(3): p. 335-350.
269. Unsworth, L.D., J. van der OostS. Koutsopoulos, *Hyperthermophilic enzymes— stability, activity and implementation strategies for high temperature applications*. The FEBS journal, 2007. **274**(16): p. 4044-4056.
270. Löhr, M., F. Hummel, G. Faulmann, J. Ringel, R. Saller, J. Hain, W.H. GünzburgB. Salmons, *Microencapsulated, CYP2B1-transfected cells activating ifosfamide at the site of the tumor: the magic bullets of the 21st century*. Cancer chemotherapy and pharmacology, 2002. **49**(1): p. 21-24.
271. Storm, G., M.H. Vingerhoeds, D.J. CrommelinH.J. Haisma, *Immunoliposomes bearing enzymes (immuno-enzymosomes) for site-specific activation of anticancer prodrugs*. Advanced drug delivery reviews, 1997. **24**(2-3): p. 225-231.
272. Osman, R., P.L. Kan, G. Awad, N. Mortada, E.-S. Abd-ElhameedO. Alpar, *Enhanced properties of discrete pulmonary deoxyribonuclease I (DNaseI) loaded PLGA nanoparticles during encapsulation and activity determination*. International journal of pharmaceutics, 2011. **408**(1-2): p. 257-265.
273. Kapoor, M.R. Rajagopal, *Enzymatic bioremediation of organophosphorus insecticides by recombinant organophosphorous hydrolase*. International biodeterioration & biodegradation, 2011. **65**(6): p. 896-901.
274. Rakshit, S., S.K. HalderK.C. Mondal, *Appraisal of Chitosan-Based Nanomaterials in Enzyme Immobilization and Probiotics Encapsulation*, in *Nanomaterials and Environmental Biotechnology*. 2020, Springer. p. 163-188.
275. Mizutani, T., *Estimation of Protein and Drug Adsorption onto Silicone-Coated Glass Surfaces*. Journal of Pharmaceutical Sciences, 1981. **70**(5): p. 493-496.
276. Nayef, L.M., M.F. KhanM.A. Brook, *Low molecular weight silicones particularly facilitate human serum albumin denaturation*. Colloids and Surfaces B: Biointerfaces, 2015. **128**: p. 586-593.
277. Vaisocherová, H., E. BryndaJ. Homola, *Functionalizable low-fouling coatings for label-free biosensing in complex biological media: advances and applications*. Analytical and bioanalytical chemistry, 2015. **407**(14): p. 3927-3953.
278. Li, B., P. Jain, J. Ma, J.K. Smith, Z. Yuan, H.-C. Hung, Y. He, X. Lin, K. WuJ. Pfaendtner, *Trimethylamine N-oxide-derived zwitterionic polymers: A new class of ultralow fouling bioinspired materials*. Science Advances, 2019. **5**(6): p. eaaw9562.
279. Lozano, P., T. De DiegoJ.L. Iborra, *Dynamic structure/function relationships in the α -chymotrypsin deactivation process by heat and pH*. European journal of biochemistry, 1997. **248**(1): p. 80-85.

280. Williams, A., *Chymotrypsin-catalyzed phenyl ester hydrolysis. Evidence for electrophilic assistance on carbonyl oxygen*. *Biochemistry*, 1970. **9**(17): p. 3383-3390.
281. Kézdy, F.J., S.P. JindalM.L. Bender, *The α -chymotrypsin-catalyzed hydrolysis of esters of α -amino acids*. *Journal of Biological Chemistry*, 1972. **247**(18): p. 5746-5752.
282. Knierbein, M., C. HeldG. Sadowski, *The role of molecular interactions on Michaelis constants of α -chymotrypsin catalyzed peptide hydrolyses*. *The Journal of Chemical Thermodynamics*, 2020. **148**: p. 106142.
283. Munasinghe, A., S.L. Baker, P. Lin, A.J. RussellC.M. Colina, *Structure–function–dynamics of α -chymotrypsin based conjugates as a function of polymer charge*. *Soft Matter*, 2020. **16**(2): p. 456-465.
284. Terra, W.R.C. Ferreira, *Biochemistry and molecular biology of digestion*, in *Insect molecular biology and biochemistry*. 2012, Elsevier. p. 365-418.
285. Lan, J., G. Jiang, J. Yang, H. Zhu, Z. LeZ. Xie, *α -Chymotrypsin-Induced Acetalization of Aldehydes and Ketones with Alcohols*. *Synthesis*, 2020.
286. Roy, I.M.N. Gupta, *Preparation of highly active α -chymotrypsin for catalysis in organic media*. *Bioorganic & medicinal chemistry letters*, 2004. **14**(9): p. 2191-2193.
287. Kisee, H., K. FujimotoH. Noritomi, *Enzymatic reactions in aqueous-organic media. VI. Peptide synthesis by α -chymotrypsin in hydrophilic organic solvents*. *Journal of Biotechnology*, 1988. **8**(4): p. 279-290.
288. Tavano, O.L., A. Berenguer-Murcia, F. SecundoR. Fernandez-Lafuente, *Biotechnological applications of proteases in food technology*. *Comprehensive reviews in food science and food safety*, 2018. **17**(2): p. 412-436.
289. Pettersen, E.F., T.D. Goddard, C.C. Huang, G.S. Couch, D.M. Greenblatt, E.C. MengT.E.J.J.o.c.c. Ferrin, *UCSF Chimera—a visualization system for exploratory research and analysis*. 2004. **25**(13): p. 1605-1612.
290. Rusmini, F., Z. ZhongJ. Feijen, *Protein immobilization strategies for protein biochips*. *Biomacromolecules*, 2007. **8**(6): p. 1775-1789.
291. Wong, L.S., F. KhanJ. Micklefield, *Selective covalent protein immobilization: strategies and applications*. *Chemical reviews*, 2009. **109**(9): p. 4025-4053.
292. Erfani, A., N.H. Flynn, J.D. RamseyC.P. Aichele, *Increasing protein stability by association with zwitterionic amphiphile cocamidopropyl betaine*. *Journal of Molecular Liquids*, 2019. **295**: p. 111631.
293. Erfani, A., J. Seaberg, C.P. AicheleJ.D. Ramsey, *Interactions between biomolecules and zwitterionic moieties: a review*. *Biomacromolecules*, 2020.
294. Wang, T.S. Gunasekaran, *State of water in chitosan–PVA hydrogel*. *Journal of Applied Polymer Science*, 2006. **101**(5): p. 3227-3232.
295. Fersht, A.R.M. Renard, *pH Dependence of chymotrypsin catalysis. Appendix. Substrate binding to dimeric α -chymotrypsin studied by X-ray diffraction and the equilibrium method*. *Biochemistry*, 1974. **13**(7): p. 1416-1426.
296. Rezaei-Ghaleh, N., H. Ramshini, A. Ebrahim-Habibi, A.A. Moosavi-MovahediM. Nemat-Gorgani, *Thermal aggregation of α -chymotrypsin: role of hydrophobic and electrostatic interactions*. *Biophysical chemistry*, 2008. **132**(1): p. 23-32.
297. Ikeda, K., S. KunugiH. Hirohara, *Catalytic Activity of Dimeric α -Chymotrypsin: Acylation Kinetics at Low pH's*. *The Journal of Biochemistry*, 1980. **87**(3): p. 871-880.
298. Kumar, A.P. Venkatesu, *Overview of the stability of α -chymotrypsin in different solvent media*. *Chemical Reviews*, 2012. **112**(7): p. 4283-4307.
299. Weers, J.G., J.F. Rathman, F.U. Axe, C.A. Crichlow, L.D. Foland, D.R. Scheuing, R.J. WiersemaA.G. Zielske, *Effect of the intramolecular charge separation distance on the solution properties of betaines and sulfobetaines*. *Langmuir*, 1991. **7**(5): p. 854-867.

300. Kamerzell, T.J., R. Esfandiary, S.B. Joshi, C.R. Middaugh, D.B. Volkin, *Protein–excipient interactions: Mechanisms and biophysical characterization applied to protein formulation development*. *Advanced drug delivery reviews*, 2011. **63**(13): p. 1118-1159.
301. Arca-Ramos, A., G. Eibes, M. Moreira, G. Feijoo, J. Lema, *Surfactant-assisted two phase partitioning bioreactors for laccase-catalyzed degradation of anthracene*. *Process biochemistry*, 2012. **47**(7): p. 1115-1121.
302. Khan, T.A., H.-C. Mahler, R.S.K. Kishore, *Key interactions of surfactants in therapeutic protein formulations: A review*. *European Journal of Pharmaceutics and Biopharmaceutics*, 2015. **97**: p. 60-67.
303. Whitehead, K., N. Karr, S. Mitragotri, *Safe and effective permeation enhancers for oral drug delivery*. *Pharmaceutical research*, 2008. **25**(8): p. 1782-1788.
304. Wang, F., X. Chen, Y. Xu, S. Hu, Z. Gao, *Enhanced electron transfer for hemoglobin entrapped in a cationic gemini surfactant films on electrode and the fabrication of nitric oxide biosensor*. *Biosensors and Bioelectronics*, 2007. **23**(2): p. 176-182.
305. Roy, J.K.A.K. Mukherjee, *Applications of a high maltose forming, thermo-stable α -amylase from an extremely alkalophilic *Bacillus licheniformis* strain AS08E in food and laundry detergent industries*. *Biochemical Engineering Journal*, 2013. **77**: p. 220-230.
306. Han, X., Y. Lu, J. Xie, E. Zhang, H. Zhu, H. Du, K. Wang, B. Song, C. Yang, Y. Shi, *Zwitterionic micelles efficiently deliver oral insulin without opening tight junctions*. *Nature Nanotechnology*, 2020: p. 1-10.
307. Tripp, B.C., J.J. Magda, J.D. Andrade, *Adsorption of globular proteins at the air/water interface as measured via dynamic surface tension: concentration dependence, mass-transfer considerations, and adsorption kinetics*. *Journal of colloid and interface science*, 1995. **173**(1): p. 16-27.
308. Chen, P., R. Prokop, S. Susnar, A. Neumann, *Interfacial tensions of protein solutions using axisymmetric drop shape analysis*, in *Studies in Interface Science*. 1998, Elsevier. p. 303-339.
309. Hjelmeland, L.M., D.W. Nebert, J.C. Osborne Jr, *Sulfobetaine derivatives of bile acids: Nondenaturing surfactants for membrane biochemistry*. *Analytical biochemistry*, 1983. **130**(1): p. 72-82.
310. Gerola, A.P., P.F.A. Costa, F.H. Quina, H.D. Fiedler, F. Nome, *Zwitterionic surfactants in ion binding and catalysis*. *Current Opinion in Colloid & Interface Science*, 2017. **32**: p. 39-47.
311. Karande, P., A. Jain, K. Ergun, V. Kispersky, S. Mitragotri, *Design principles of chemical penetration enhancers for transdermal drug delivery*. *Proceedings of the National Academy of Sciences*, 2005. **102**(13): p. 4688-4693.
312. Doussin, S., N. Birlirakis, D. Georjgin, F. Taran, P. Berthault, *Novel zwitterionic reverse micelles for encapsulation of proteins in low-viscosity media*. *Chemistry–A European Journal*, 2006. **12**(15): p. 4170-4175.
313. Alonso, L., É.J.S. Cardoso, S.A. Mendanha, A. Alonso, *Interactions of miltefosine with erythrocyte membrane proteins compared to those of ionic surfactants*. *Colloids and Surfaces B: Biointerfaces*, 2019. **180**: p. 23-30.
314. Whitehead, K.S. Mitragotri, *Mechanistic analysis of chemical permeation enhancers for oral drug delivery*. *Pharmaceutical research*, 2008. **25**(6): p. 1412-1419.
315. Belton, G., *Langmuir adsorption, the Gibbs adsorption isotherm, and interfacial kinetics in liquid metal systems*. *Metallurgical and Materials Transactions B*, 1976. **7**(1): p. 35-42.
316. Butt, H.-J., K. Graf, M. Kappl, *Physics and chemistry of interfaces*. 2006: John Wiley & Sons.
317. Khosharay, S., S. Tourang, F. Tajfar, *Modeling surface tension and interface of (water+methanol), (water+ethanol), (water+1-propanol), and (water+MEG) mixtures*. *Fluid Phase Equilibria*, 2017. **454**: p. 99-110.
318. Tahery, R.S. Khosharay, *Surface tension of binary mixtures of dimethylsulfoxide+ methanol, ethanol and, propanol between 293.15 and 308.15 K*. *Journal of Molecular Liquids*, 2017. **247**: p. 354-365.

319. Erfani, A., S. Khosharay C.P. Aichele, *Surface tension and interfacial compositions of binary glycerol/alcohol mixtures*. The Journal of Chemical Thermodynamics, 2019. **135**: p. 241-251.
320. Fainerman, V., R. Miller, E. Aksenenko, A. Makievski, J. Krägel, G. Loglio L. Liggieri, *Effect of surfactant interfacial orientation/aggregation on adsorption dynamics*. Advances in colloid and interface science, 2000. **86**(1-2): p. 83-101.
321. Mousavi, N.S.S.J.F.P.E. Khosharay, *Investigation on the interfacial behavior of aqueous solutions of cetyltrimethyl ammonium bromide in the presence of polyethylene glycols*. 2016. **465**: p. 58-64.
322. Kopac, T., K. Bozgeyik J. Yener, *Effect of pH and temperature on the adsorption of bovine serum albumin onto titanium dioxide*. Colloids and Surfaces A: Physicochemical and Engineering Aspects, 2008. **322**(1-3): p. 19-28.
323. Kim, S.S., Y. Lee, H.S. Shin J.H. Lee, *Highly sensitive chemiluminescence enzyme immunoassay for the quantification of carcinoembryonic antigen in the presence of an enhancer and a stabilizer*. Journal of immunological methods, 2019. **471**: p. 18-26.
324. Herrwerth, S., H. Leidreiter, H. Wenk, M. Farwick, I. Ulrich-Brehm B. Grüning, *Highly Concentrated Cocamidopropyl Betaine—The Latest Developments for Improved Sustainability and Enhanced Skin Care*. Tenside Surfactants Detergents, 2008. **45**(6): p. 304-308.
325. Erfani, A.F. Varaminian, *Kinetic promotion of non-ionic surfactants on cyclopentane hydrate formation*. Journal of Molecular Liquids, 2016. **221**: p. 963-971.
326. Erfani, A.F. Varaminian, *Experimental investigation on structure H hydrates formation kinetics: Effects of surfactants on interfacial tension*. Journal of Molecular Liquids, 2017. **225**: p. 636-644.
327. Berry, J.D., M.J. Neeson, R.R. Dagastine, D.Y. Chan R.F. Tabor, *Measurement of surface and interfacial tension using pendant drop tensiometry*. Journal of colloid and interface science, 2015. **454**: p. 226-237.
328. Fainerman, V.B.R. Miller, *Chemical potentials and equation of state of surface layers for a model assuming two-dimensional compressibility of adsorbed molecules*. Colloids and Surfaces A: Physicochemical and Engineering Aspects, 2008. **319**(1): p. 8-12.
329. Fainerman, V.B., R. Miller E.V. Aksenenko, *Simple model for prediction of surface tension of mixed surfactant solutions*. Advances in Colloid and Interface Science, 2002. **96**(1): p. 339-359.
330. Rodriguez-Abreu, C.H. Kunieda, *Equilibrium and dynamic surface tension properties of aqueous solutions of sulfonated cationic-nonionic fluorocarbon surfactants*. Journal of dispersion science and technology, 2005. **26**(4): p. 435-440.
331. McClellan, S.J.E.I. Franses, *Effect of concentration and denaturation on adsorption and surface tension of bovine serum albumin*. Colloids and Surfaces B: Biointerfaces, 2003. **28**(1): p. 63-75.
332. Erickson, J.S., S. Sundaram K.J. Stebe, *Evidence that the Induction Time in the Surface Pressure Evolution of Lysozyme Solutions Is Caused by a Surface Phase Transition*. Langmuir, 2000. **16**(11): p. 5072-5078.
333. Danov, K., S. Kralchevska, P. Kralchevsky, K. Ananthapadmanabhan A. Lips, *Mixed solutions of anionic and zwitterionic surfactant (betaine): surface-tension isotherms, adsorption, and relaxation kinetics*. Langmuir, 2004. **20**(13): p. 5445-5453.
334. Niño, M.R.R.J.R. Patino, *Surface tension of bovine serum albumin and tween 20 at the air-aqueous interface*. Journal of the American Oil Chemists' Society, 1998. **75**(10): p. 1241.
335. Göbel, J.G. Joppien, *Dynamic Interfacial Tensions of Aqueous Triton X-100 Solutions in Contact with Air, Cyclohexane, n-Heptane, and n-Hexadecane*. Journal of colloid and interface science, 1997. **191**(1): p. 30-37.
336. Noskov, B.A.M.M. Krycki, *Formation of protein/surfactant adsorption layer as studied by dilational surface rheology*. Advances in colloid and interface science, 2017. **247**: p. 81-99.
337. Pettersson, E., D. Topgaard, P. Stilbs O. Söderman, *Surfactant/nonionic polymer interaction. a NMR diffusometry and NMR electrophoretic investigation*. Langmuir, 2004. **20**(4): p. 1138-1143.

338. Santos, S.F., D. Zanette, H. FischerR. Itri, *A systematic study of bovine serum albumin (BSA) and sodium dodecyl sulfate (SDS) interactions by surface tension and small angle X-ray scattering*. Journal of colloid and interface science, 2003. **262**(2): p. 400-408.
339. Schott, H.S.K. Han, *Effect of inorganic additives on solutions of nonionic surfactants III: CMC's and surface properties*. Journal of pharmaceutical sciences, 1976. **65**(7): p. 975-978.
340. Webbook, N.C.
341. Li, W., M. Zhang, J. ZhangY. Han, *Self-assembly of cetyl trimethylammonium bromide in ethanol-water mixtures*. Frontiers of Chemistry in China, 2006. **1**(4): p. 438-442.

APPENDICES

APPENIX A

**Effect of Zwitterionic Betaine Surfactant on Interfacial Behavior of
Bovine Serum Albumin (BSA)**

Overview

In Appendix A, I present an experimental investigation on interfacial properties of a protein-surfactant mixture. Although the studied mixture includes a zwitterionic moiety, I have decided not to include this as a chapter in the main body of thesis. This decision was carried out to ensure the thesis is more focused on zwitterionic hydrogels. The interfacial adsorption and denaturation of proteins is a significant concern for the loss of protein structure and function during protein processing or storage and is an important concern for formulation of biopharmaceuticals. Surfactants can be used to prevent interfacial damage to proteins. Zwitterionic surfactants have shown intriguing effects on stability and activity of proteins. The aim of this research was to study the effect of cocamidopropyl betaine (CAPB), a non-denaturing zwitterionic carboxy betaine containing surfactant, on the air/water interfacial adsorption of a model protein bovine serum albumin (BSA). Dynamic and equilibrium surface tensions were measured using the pendant drop method. The results of surface tension measurements were coupled with a thermodynamic analysis, based on the interface and bulk chemical potentials, to estimate the surface coverage of the components and to calculate surface adsorption. Our results indicated that CAPB can effectively associate with the protein at different concentrations, even at concentrations lower than the critical micelle concentration (CMC). Furthermore, the addition of the protein significantly increased the CMC of the CAPB from 45 ppm to 407 ppm. Most importantly, CAPB prevented the adsorption of the protein at the interface. The interface of aqueous solution of CAPB+BSA was also compared with the Triton X-100+BSA.

A1. Introduction

Proteins and surfactants co-exist in different environments such as therapeutic protein formulations [300] and bioreactors [301]. Proteins as amphiphilic (containing both hydrophilic and hydrophobic moieties) molecules also demonstrate surface activity [302]. Furthermore, protein adsorption at interfaces is a key step in many applications such as drug delivery [303], biosensors [304], and food [305]. For instance, in the case of formulation of protein therapeutics, protein aggregation can be prevented by the addition of surfactants [300]. Surfactant can also help with transdermal and oral delivery of proteins by increasing protein penetration through the mucus and epithelial cell layers [303, 306].

Surface activity of proteins has been a topic of interest especially with regard to protein stability. When proteins adsorb onto interfaces, they can undergo conformational changes that lead to aggregation and possibly gelation. Trip et al. extensively studied the adsorption of globular proteins at an air/water interface (i.e. a hydrophobic/hydrophilic interface) using the pendant drop method and explained the results based on concepts such as surface hydrophobicity and conformational stability [307]. Chen et al. utilized drop shape analysis to study the interfacial behavior of proteins [308]. They discussed the criteria and method to estimate the equilibrium value of surface tension by extrapolating the dynamic surface tension (DST) results.

Surfactants contain both hydrophilic and hydrophobic groups. The super-hydrophilicity of betaine containing molecules such as sulfobetaine or carboxybetaine makes them useful as building blocks for surfactant molecule head groups [293]. Such zwitterionic (containing both anionic and cationic moieties) surfactants have been reported to interact synergistically with ionic surfactants to reduce the solution surface tension below the sum of the individual

surfactants [116].

Zwitterionic surfactants are often non-denaturing and have weak interactions with proteins compared to ionic surfactants [117, 309], opening the possibility of using zwitterionic surfactants in combination with proteins for a range of purposes [310]. For example, sulfobetaine and carboxybetaine are zwitterionic head groups that are natural osmolytes and can increase the conformational stability of proteins by increasing hydrophobic effects [28]. In fact, zwitterionic surfactants have been used to improve stability of proteins, to facilitate oral [306] and transdermal drug delivery [311], to encapsulate proteins [312], and to improve solubility of hydrophobic proteins [313]. Because of their generally low toxicity and ability to transport proteins across membranes, zwitterions have also been explored as permeation enhancers for drug delivery [314]. For example, through the screening of a library of potential permeation enhancers, palmityldimethyl ammoniopropane sulfonate (a sulfobetaine-based zwitterionic surfactant) was identified as the best choice to enhance permeation of a macromolecular drug [303, 314]. Doussin et al. investigated the encapsulation of a model protein using a zwitterionic surfactant [312]. They found that it is possible to encapsulate cytochrome C by using a zwitterionic compound (2-ammonioethyl 2,3-bis(3-ethylheptanoyloxy)propyl phosphate) in its native state. Their results indicate that this encapsulation can benefit the structural studies of proteins during protein NMR spectroscopy. Lastly, a study of systems containing surfactants and proteins was carried out to find suitable detergents to increase solubility of membrane proteins and found zwitterionic surfactants as effective detergents for membrane protein solubility [171].

Surface coverage is one of the most important interfacial properties that can be used to explain the adsorption process. The most straightforward theoretical approach that relates changes in surface tension to surface coverage and adsorption is the Gibbs adsorption isotherm

[315]. Unfortunately, this simple approach is not valid for systems that undergo surface compression, reorientation, or show elastic behavior (e.g. solid-like behavior) at the interface [316]. Systems containing polymers or proteins can potentially undergo most of these changes, thereby complicating the determination of their interfacial behavior. We previously used thermodynamic models to estimate surface coverage, where the chemical potential in the solution was set equal to the chemical potential at the interface [317-319].

A theoretical description of interfacial adsorption behavior of complex fluids including surfactants and macromolecules was introduced by Fainerman et al. [320]. They derived a theoretical approach to describe the interfacial behavior of surfactant containing solutions that undergo agglomeration, reorientation, and similar changes at the interface. Their approach has been successfully applied to systems containing surfactants [317] and surfactant+polymer (PEG + CTAB) solutions [321].

In this study bovine serum albumin (BSA) was used as a model protein. BSA is an abundant globular protein with very known physicochemical properties [322]. BSA is widely used as an enzyme stabilizer [323] and in cell culture [322]. Studies containing both experimental and theoretical interfacial behavior of systems containing both amphiphiles and proteins are not prevalent in the literature. Therefore, this research was aimed at investigating the surface behavior of BSA in the presence of a zwitterionic betaine containing surfactant. The zwitterionic betaine containing surfactant was selected for two main reasons. Firstly, there are fewer studies that have investigated the interactions between zwitterionic surfactants and proteins compared to anionic, cations and non-ionic surfactants. Secondly for the interesting effects of betaines on the protein conformational stability. The experimental results were coupled with theoretical thermodynamic models to give us more information about what happens

at the interface. We also compared the surfactant+protein interactions and possible associations between a system of (zwitterionic CAPB+ protein) and (non-ionic surfactant Triton X-100+protein). The surface to solution distributions and protein surface coverage for each of the studied aqueous solutions were utilized to explain the surface properties of protein-surfactant systems within the concentration limits of this study.

A.2 Experimental

A.2.1 Chemicals

Table 1 summarizes the specifications of the materials utilized in this research. All chemicals were used without any further purification. Bovine serum albumin (BSA) and Triton X-100 were purchased from Sigma Aldrich. A concentrated form of CAPB with commercial name Tego-betaine C60 (Evonik) was used as the zwitterionic surfactant [324].

Table A1. Specifications of materials utilized in this research.

Chemical	CAS registry number	Supplier	Purity as stated by the supplier (mass fraction)	Details
Bovine Serum Albumin (BSA)	9048-46-8	Sigma Aldrich	0.98 \geq	lyophilized powder
Triton X-100	9002-93-1	Sigma Aldrich	1.0	Octylphenol Ethoxylate, molecular biology grade
Cocamidopropyl betaine (CAPB)	61789-40-0	Evonik	0.46 \geq (aqueous solution)	{(3-(Dodecanoylamino)propyl) (dimethyl)ammonio} acetate, aqueous solution

A.2.2. Pendant Drop Method

Due to the complexity of protein solutions, the present investigation requires a suitable selection of the tensiometry method. While methods such as ring tensiometry are desired for

generating large amounts of data [319], the slow adsorption of the protein might hinder the validity of the result. On the contrary, the pendant drop method (used in this work) has been used widely for systems with surface adsorption of the components [325-327]. After solutions were carefully made, a pendant drop was formed by using a 0.8 mm flat needle. The air was saturated with water to avoid evaporation and concentration changes during the test. The drop was formed approximately 2-3 mm from the water surface. The tests were carried out at 293 K and atmospheric pressure (97.8 kPa, not controlled). The drop images were recorded using a digital microscope every 30 seconds. Drop shapes were analyzed using Raméhart *DROPimage* software.

A.3. Modeling: Equality of the Chemical Potentials

The basis for modeling surface tension is the equality of chemical potentials in the bulk liquid and at the surface layer. Eq. (1) describes the chemical potential of each component in the bulk phase:

$$\mu_i^\alpha = \mu_i^{0\alpha} + RT \ln f_i^\alpha x_i^\alpha \quad (1)$$

In which μ_i is the chemical potential of component i , μ_i^0 is the standard chemical potential, f is the activity coefficient, x_i indicates the mole fraction of component i in the liquid, R is the universal gas constant, and T is the absolute temperature. The superscript α refers to the bulk phase.

At the surface phase, the surface tension exists in the chemical potential of each component as follows:

$$\mu_i^\sigma = \mu_i^{0\sigma} + RT \ln f_i^\sigma x_i^\sigma - \gamma \omega_i \quad (2)$$

In Eq. (2), γ is the surface tension of the solution and ω is the partial molar surface area. The superscript σ refers to the surface (interface) phase. Based on the thermodynamic equilibrium criteria, μ_i^α and μ_i^σ are equal. Furthermore, the standard state of the solvent ($i=0$) is the pure solvent. This means $x_0^\sigma = x_0^\alpha = 1$, $f_0^\sigma = f_0^\alpha = 1$, and $\gamma = \gamma_0$. Using these assumptions and some rearrangements leads to the following equation:

$$\mu_0^{0\sigma} - \gamma_0 \omega_0 = \mu_0^{0\alpha} \quad (3)$$

The infinite dilute solution ($x_1^\alpha \rightarrow 0$) is considered for the standard state of the solute ($i=1$). Therefore, $f_1^\sigma = f_1^\alpha = 1$ and $\gamma = \gamma_0$. The following relations are derived from Eqs. (1)-(3) [328, 329]. And can be rewritten as follows:

$$\pi = - \frac{RT}{\omega_0} (\ln f_0^\sigma + \ln x_0^\sigma) \quad (4)$$

$$\ln \frac{f_1^\sigma x_1^\sigma / f_{10}^\sigma}{K_1 f_1^\alpha x_1^\alpha} = \frac{\omega_1}{\omega_0} (\ln f_0^\sigma + \ln x_0^\sigma) \quad (5)$$

In which $K_1 = \frac{x_1^\sigma}{x_1^\alpha} |_{x_1^\alpha \rightarrow 0}$ describes the distribution constant at infinite dilution of solute. $\pi = \gamma_0 - \gamma$ represents the surface pressure, and f_{10} is used to describe infinite dilution. Eq. (6) describes how the interfacial mole fraction of the solution and the surface coverage are related.

$$x_i^\sigma = \frac{\theta_i}{n_i \sum_{i \geq 0} \frac{\theta_i}{n_i}} ; \quad n_i = \frac{\omega_i}{\omega_0} ; \quad \theta_i = \Gamma_i \omega_i \quad (6)$$

In Eq. (6), θ is the surface coverage and Γ is the surface excess concentration. ω_i and ω_0 indicate the molar surface area of surfactant and solvent, respectively.

For the solution of a single surface-active component, the following expressions for the activity coefficients are used [328].

$$\ln f_0^\sigma = \ln\left(1 - \left(1 - \frac{1}{n_1}\right)\theta_1\right) + \left(1 - \frac{1}{n_1}\right)\theta_1 + a\theta_1^2 \quad (7)$$

$$\ln f_1^\sigma = \ln(n_1 - (1 - n_1)\theta_1) + (1 - n_1)(1 - \theta_1) + an_1\theta_1^2 \quad (8)$$

$$\ln f_{10}^\sigma = \ln(n_1) + (1 - n_1) + an_1 \quad (9)$$

Here, a is the interaction parameter. By replacing Eqs. (7)-(9) into Eqs. (4) and (5) with $f_1^a=1$, the equation of state and adsorption isotherm are obtained as follows:

$$\pi = \frac{RT}{\omega_0} \left(\ln(1 - \theta_1) + \left(1 - \frac{1}{n_1}\right)\theta_1 + a\theta_1^2 \right) \quad (10)$$

$$b^*c = \frac{\theta_1}{n_1(1 - \theta_1)^{n_1}} \exp(-2an_1\theta_1) \quad (11)$$

In Eqs. (10) and (11), c is the bulk concentration and b is surface-to-solution distribution constant ($b^*c = K_1X_1^a$). ω_0 is the molar surface area of the water.

a , b and ω_1 are adjustable parameters that are determined by minimizing mean absolute deviations. For surface tensions, average absolute deviations (AAD) are given by:

$$AAD = \frac{100}{N} \sum_{i=1}^N \left| \frac{\gamma^{\text{exp}} - \gamma^{\text{cal}}}{\gamma^{\text{exp}}} \right| \quad (12)$$

In Eq. (12), N represents the number of experimental points. π and θ are unknown variables that are obtained by simultaneous solution of Eqs. (10) and (11).

A.4. Results and Discussion

A.4.1 Dynamic and equilibrium surface tensions

Figure A1 shows a typical protein dynamic surface tension (DST) trend. One can see that the DST consists of three different kinetic regimes that need to be analyzed and discussed separately. The first region is the induction time. This is an initial period of constant DST. Induction time for surface-active systems have been previously reported for surfactants [330] and also for low concentrations of proteins in the solutions [331]. Previously observed lysozyme surface behavior indicated that the induction time can be caused by transition of the surface phase [332]. In this transition, the surface phase changes from a gaseous like phase (with no surfactant or protein) to a liquid-expanded phase (with ability to dissolve the surface-active molecules) [332]. For systems studied in this work, we observed the induction time for BSA solutions lower than 1000 ppm. The 100 ppm BSA concentration was illustrated in Figure A1 as the “induction time” region is more visible for experiments with low protein concentration such as 100 ppm.

The second region is the diffusion/adsorption regime in which the surface-active molecules diffuse through the solution and simultaneously adsorb on the surface layer. The surface tension reached by the end of this stage is considered the final or equilibrium surface tension of the system. The third region contains the conformational changes, aggregation, and gelation. In this stage, protein molecules which are in contact with air can go through conformational changes due to unfolding of the hydrophobic groups.

For identifying the equilibrium surface tension, DST values were plotted as a function of $1/(t^{0.5})$. The DST was then extrapolated linearly to infinite time (y-intercept). The y-intercept was reported as the surface tension of the system. The same strategy was used for similar investigations [307, 333]. Figure A2 shows an example of this procedure. In Figure A2, BSA

concentration of 1000 ppm was chosen as most of the results in following sections are at 1000 ppm. Table 2 compares the experimental results with literature values.

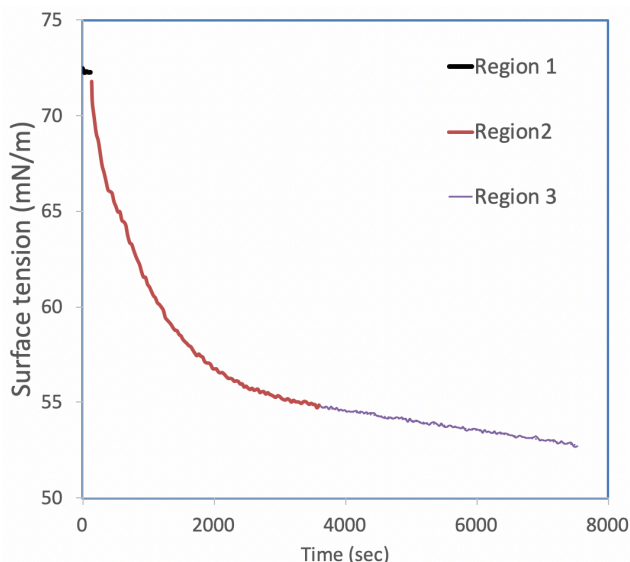


Figure A1. Dynamic surface tension of 100 ppm BSA in deionized water indicating different regimes for dynamic surface tension. Region1: Induction; Region 2: Diffusion/adsorption; Region 3: Conformational changes and denaturation of protein at the interface.

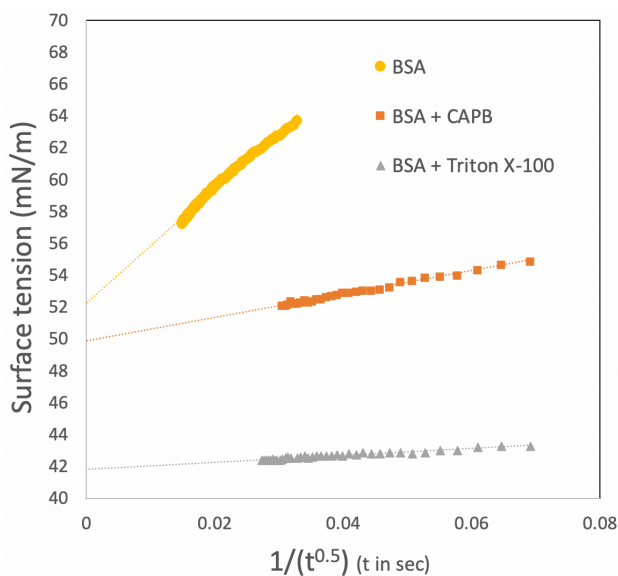


Figure A2. Dynamic surface tension vs. $1/(t^{0.5})$. This method was applied for all the surface tension experiments (three are shown as examples). For the data shown here, the BSA concentration was set to 1000 ppm for the presented data while the surfactant (CAPB or Triton X-100) concentration was set to 50 ppm.

Table A2. Comparison of measured surface tension with literature values [307, 331, 334, 335].

Sample	Experimental (mN/m)	Literature (mN/m)	Method	Relative standard deviation
BSA	53.0 (at 100 ppm)	53.8 (at 100 ppm) [307]	Pendant drop	1.1 %
	51.5 (at 1000 ppm)	52.0 (at 100 ppm) [331]	Pulsating bubble	1.2 % 0.6 %
		51.1 (at 1000 ppm) [334]	Wilhelmy plate	1.6 %
		52.7 (at 1000 ppm) [307]	Pendant drop	
Triton X-100	52.7 (at 10 ppm)	52.4 (at 10 ppm) [335]	Wilhelmy plate	0.4 % 0.4 %
	40.2 (at 50 ppm)	40.4 (at 50 ppm) [335]	Wilhelmy plate	1.4 %
	30.5 (at 300 ppm)	31.1 [335]	Wilhelmy plate	

4.2. Surface Tension of CAPB+BSA and Triton X-100+BSA

As indicated in Figure A3 A, BSA concentrations as low as 5 ppm reduced the surface tension of aqueous mixture to 54 mN/m (Table 2). This behavior resembles high affinity Langmuir-type adsorption [316] and shows that BSA molecules strongly and almost irreversibly adsorb on the air/water interface. Figure A3 B and C shows the surface tension measured at different concentrations of surfactants at a constant BSA concentration. For aqueous solutions of surfactants, increasing the concentration of surfactant ultimately produces micelles. The concentration where this occurs is known as the critical micelle concentration (CMC). After aqueous solutions of surfactants reach the CMC, there are no significant changes in surface tension with increasing concentration of surfactant. Interestingly, as can be seen in Figure A3 B, the CMC of CAPB has been affected by the presence of the BSA protein. While the CAPB CMC

without protein is 45 ppm (0.13 mM), the CMC of CAPB increased to 186 ppm (0.53 mM) in the presence of BSA.

Our results indicated that a mixture of CAPB and BSA is not as surface-active as pure CAPB. Based on this, CAPB molecules appear to prefer to adsorb on the protein molecules rather than adsorb on the surface layer. Moreover, the change of surface tension was not monotonic in terms of concentration. For the CAPB+BSA system, increasing CAPB concentration resulted in an increase in surface tension over CAPB concentrations in the range (10-50 ppm). This indicates that CAPB molecules associate with BSA molecules such that BSA molecules leave the surface. At CAPB concentrations greater than 50 ppm, the air-water surface is preferentially covered by CAPB molecules as evidenced by the decrease in surface tension (Figure A3 B).

The interfacial behavior of this system was also studied as a function of protein concentration (Figure A4). By increasing the concentration of the protein, the CMC of the zwitterionic surfactant increased. For surfactant+protein systems, one can postulate the formation of micelle-like aggregates. The concentration at which these aggregates are formed is the critical aggregate concentration (CAC). The CAC can be followed by formation of micelles at the CMC [336]. In such conditions, in a multi-component mixture, the free micelles can co-exist with protein-surfactant complex. The CAC indicates the onset of the interaction of the protein and the surfactant [337]. CAC has been reported for systems such as SDS+BSA mixture [338]. Yet our results indicated that the interactions between CAPB and BSA lead to the onset of CAC at very low concentrations (lower than 5 ppm). This very low concentration meant that the association between CAPB and BSA was spontaneous. Figure A5 shows a schematic representation of BSA surface behavior with and without the studied zwitterionic surfactant. The zwitterionic

surfactants studied here is no-denaturing. This means that a mechanism such as necklace-bead model can not be applied to it.

In order to compare the results with a non-ionic surfactant, the interfacial behavior of Triton X-100 with BSA (Fig.3C) at different concentrations was studied. When compared to the CAPB system, the interfacial behavior of Triton X-100 is much simpler to explain. The surface tension of the Triton X-100+BSA system is not significantly different from the aqueous Triton X-100 system (i.e., no BSA), which indicated that Triton X-100 molecules adsorb to the air/water interface regardless of the presence of the protein molecules. Similar to the aqueous solutions of CAPB and Triton X-100, the CMCs of these aqueous solutions were evaluated and are reported in Table 3. The CMC values were identified as the intersection between the linear regression of the high and low concentration surface tensions (logarithmic scale) [339]. The influence of protein molecules on micelle formation is much more significant in the case of the zwitterionic surfactant.

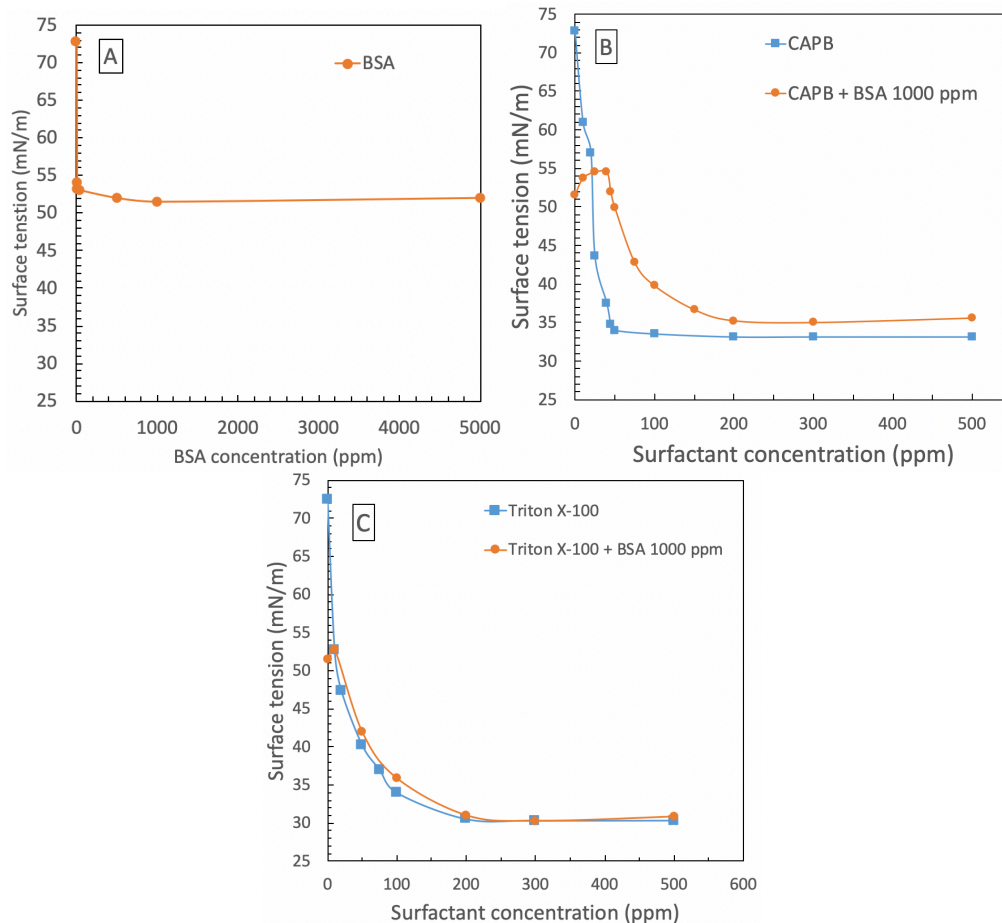


Figure A3. **(A)**: Surface tension of bovine serum albumin (BSA) aqueous solutions at different concentrations. **(B)** Surface tension of CAPB and CAPB+BSA systems at 1000 ppm BSA and different concentrations of CAPB. Surfactant+protein interactions change the CMC. **(C)** Surface tension of Triton X-100 and Triton X-100+BSA system at 1000 ppm BSA and different concentrations of non-ionic surfactant Triton X-100 (ethoxylated octyl phenol). The non-ionic surfactant CMC is not affected by the protein.

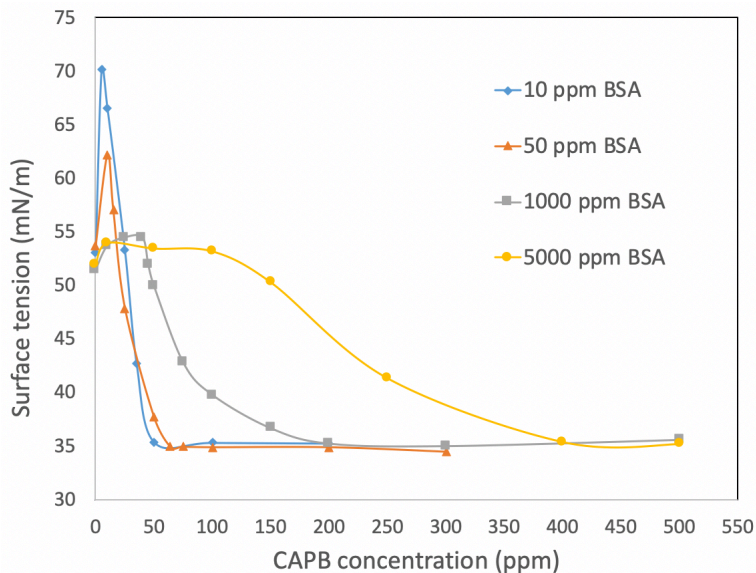


Figure A4. Surface tension of the CAPB+BSA system at different BSA and CAPB concentrations. Increases in the protein concentration result in increasing the CMC.

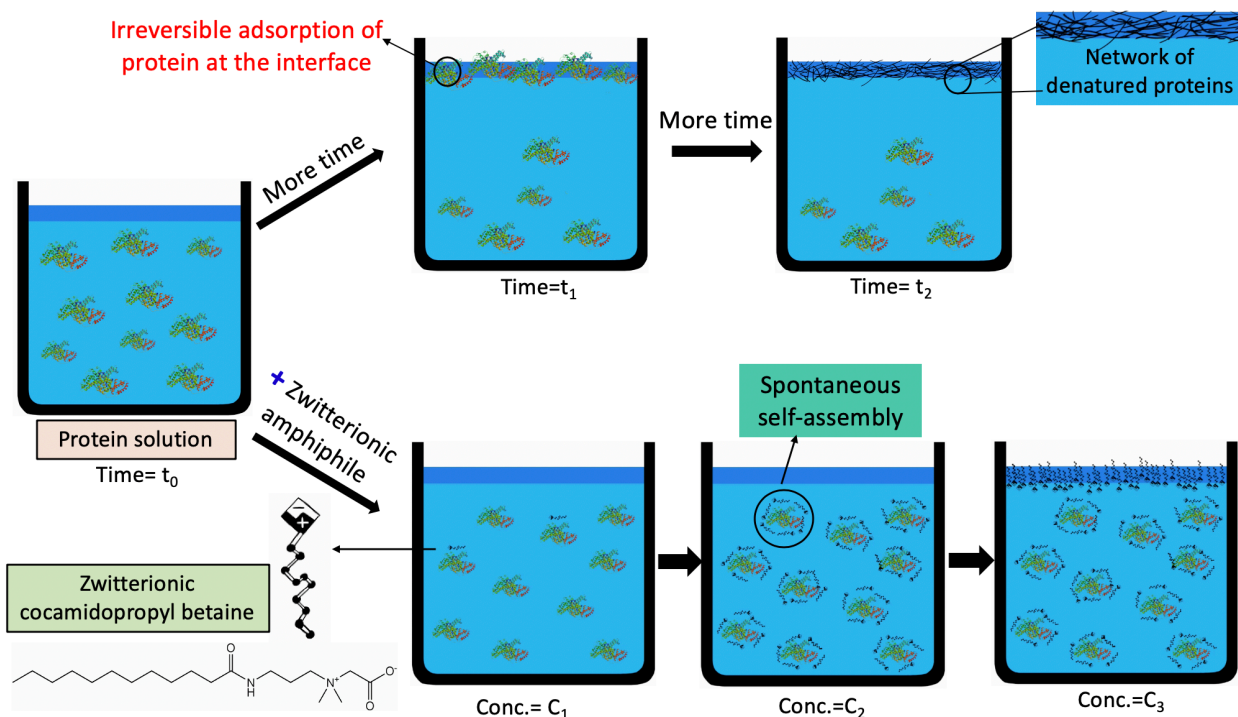


Figure A5. Schematic of the surface behavior of BSA with and without the non-denaturing zwitterionic surfactant cocamidopropyl betaine (CAPB). The protein solution (top) undergoes surface adsorption which is followed by surface aggregation and denaturing of the protein. The

mixture of protein and zwitterionic surfactant (bottom) is less surface-active as the surfactant interacts with the protein.

Table A3. The experimental values for critical micelle concentration (CMC) for surfactant solutions and surfactant+protein mixtures at 293 K.

System	CMC (ppm)
Triton X-100	167
Triton X-100 + 1000 ppm BSA	185
CAPB	45
CAPB + 10 ppm BSA	51
CAPB + 50 ppm BSA	76
CAPB + 1000 ppm BSA	186
CAPB + 5000 ppm BSA	407

A.4.3 Thermodynamic Analysis: Protein and Surfactant Surface Coverages

Based on the experimental results, the surface tensions of aqueous solutions of CAPB and Triton X-100 decreased by increasing the concentrations of these two surfactants. The main purpose of the thermodynamic analysis is to interpret the surface tension results and evaluate the protein and surfactant surface coverages.

The adjustable coefficients of the models are a (interaction parameter), b (surface-to-solution distribution) and ω_1 (partial molar surface area of the surface-active component). These parameters were fitted based on the separately measured surface tensions for each component. Table 4 presents these regressed parameters. For the calculation of ω_0 , Eq. (16) was used. Moreover, to apply Eq. (16), V_b and V_c were set equal to $18.069 \text{ cm}^3 \text{ mol}^{-1}$ and $57.1 \text{ cm}^3 \text{ mol}^{-1}$, respectively [340]. It should be noted that this model is applicable only for the concentrations lower than the CMC. Interestingly, BSA has the highest surface-to-solution distribution constant

(see figure A3 A). Also as one would expect, BSA has a larger surface area than CAPB and Triton X-100.

Table A4. Adjustable parameters of the theoretical models for aqueous solutions of pure BSA, CAPB, and Triton X-100. Parameter ω is the partial molar surface area, while a is the interaction parameter and b is surface-to-solution distribution.

Component	Model		
	ω ($10^5 \text{ m}^2/\text{mol}$)	a	b (m^3/mol)
BSA	8.243	0.714	971.93
CAPB	0.865	0.418	165.05
Triton X-100	2.141	-0.4244	458.83

The model was applied to the aqueous solutions of CAPB+BSA and Triton X-100+BSA. The surface coverages of the surfactants and protein were calculated for aqueous solutions of Triton X-100+BSA and CAPB+BSA. The results of the surfactant surface coverage calculations are presented in Figure A6 and indicated that the surface coverage of CAPB and Triton X-100 decreased in the presence of BSA. The decrease in the surface coverage of CAPB, however, is much more significant than the Triton X-100. This can be attributed to the weaker interaction of Triton X-100, as a non-ionic surfactant, with the protein. Interestingly Triton X-100 surface coverage was higher than of CAPB at all concentrations. This can be attributed to the higher calculated molar surface area of Triton-X100 (refer to Table 4).

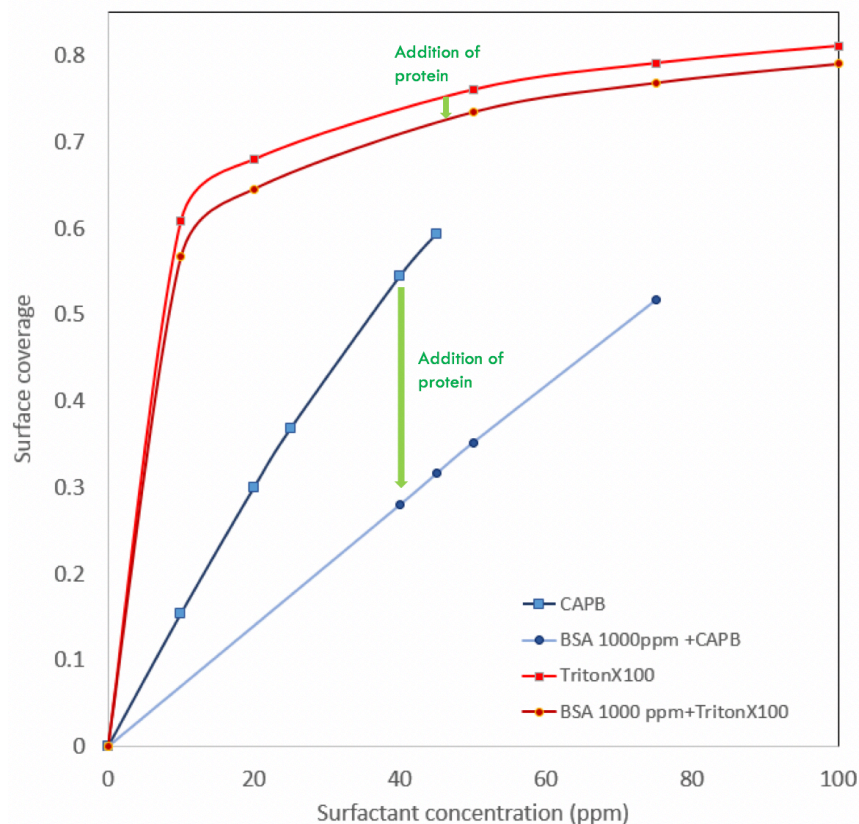


Figure A6. Surfactant surface coverage (area/area) calculated for aqueous solutions of Triton X-100, Triton X-100+BSA, CAPB, and CAPB+BSA as a function of surfactant concentration at T=293 K.

In aqueous solution (without protein), the applied surfactants adsorb at the air–water surface due to their hydrophobic tails. The interactions between the tail group of surfactants and the water molecules control such behavior. In the presence of BSA, interactions between the tail group and the protein and head betaine group with water also exist. Effects of these interactions can be quantified using the model. Therefore, the solubility of the hydrophobic tail group increases in the aqueous solution of BSA, and the surface coverage of the applied surfactants decreases. This indicates how association between the CAPB and BSA leads to complexes that are less surface-active. Additionally, the hydrophobic effects due to the hydrophobic tail of surfactants can be recognized as a main driving force of micelle formation [341]. Our results

indicated that the interaction between the zwitterionic surfactants and BSA is stronger than the one that exists between the air/water interface and the hydrophobic tails. Therefore, in the presence of BSA, micelles of CAPB form at higher concentrations than in the pure water.

A.4.4 Implications of CAPB+BSA Association

The competition of CAPB surface adsorption with the protein molecules was investigated by studying the surface coverage for each component. Figure A7 shows the substantial effect of surfactant on the protein surface coverage. For the BSA aqueous system, up to 29% of the surface can be covered by protein molecules. On the contrary, for the system containing 50 ppm CAPB, the protein surface coverage dropped to nearly zero. Figure A8 compares the dynamic surface tension (DST) of BSA and CAPB+BSA systems to illustrate this difference in protein surface coverage. The DST of BSA did not reach a constant value during the time of the experiment (more than 2 hours). This can be attributed to the slow conformational changes of the protein at the interface followed by the aggregation of protein molecules and eventually gelation. On the contrary, the CAPB+BSA system reached the equilibrium surface tension quickly and did not undergo any further changes. This tendency of CAPB to prevent protein adsorption at the interface can have applications in protein formulation. Further, osmolytes are commonly added to formulations to increase protein stability, and CAPB, having the natural osmolyte betaine [1], may serve the dual purpose of acting as an osmolyte and preventing protein adsorption at the interface.

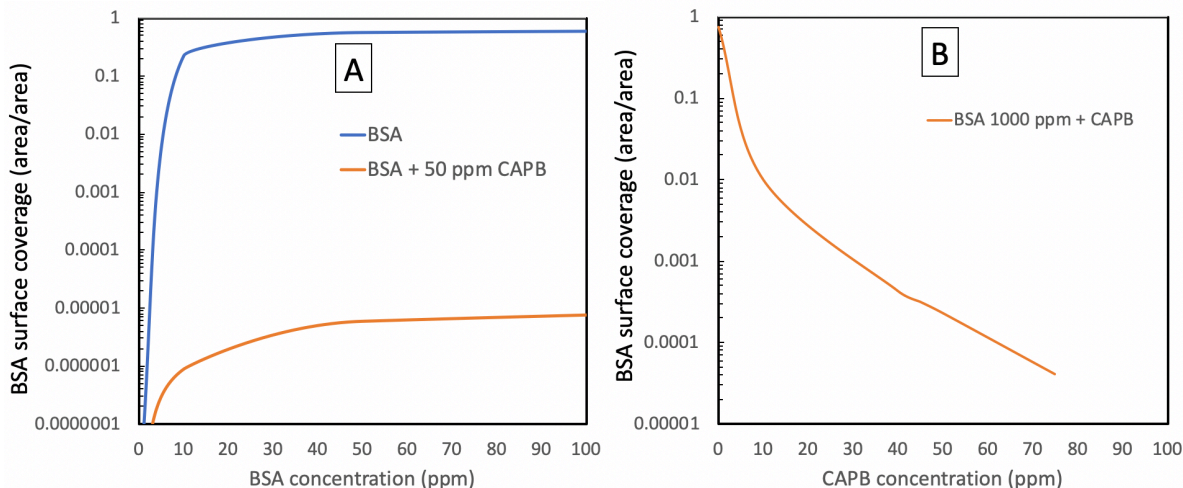


Figure A7. Effect of surfactant CAPB on the protein (BSA) surface coverage. **A:** At fixed CAPB concentration of 50 ppm and variable BSA concentration. **B:** At fixed BSA concentration of 1000 ppm BSA and variable CAPB concentration.

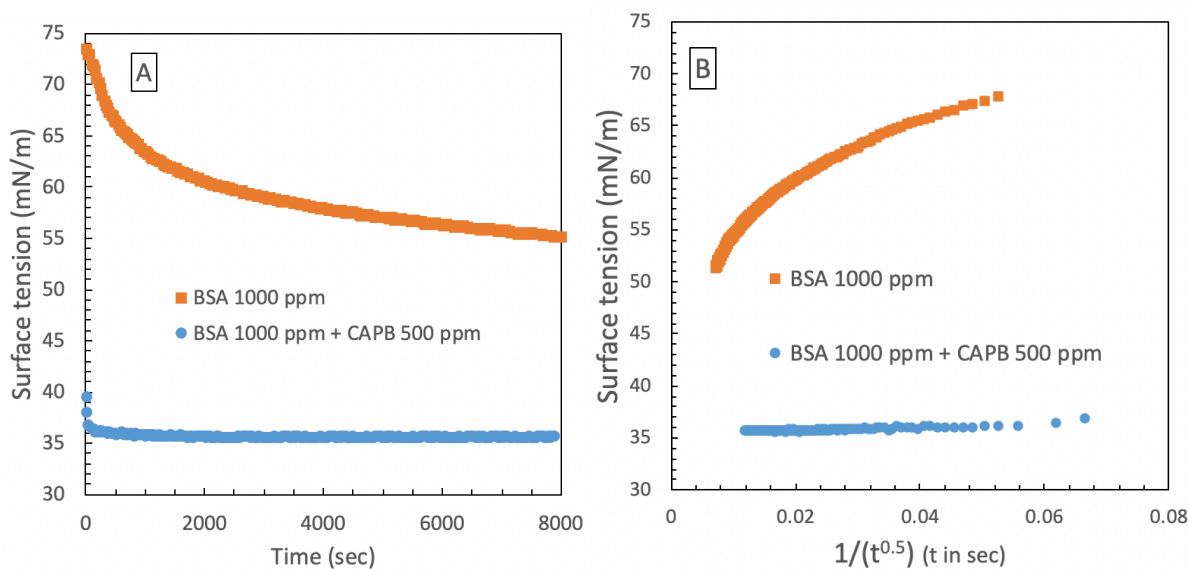


Figure A8. Dynamic Surface tension of system of BSA (1000 ppm) and CAPB (500 ppm)+BSA (1000 ppm) versus time (A) or versus $1/t^{0.5}$ (B). The reduction in surface coverage of BSA by using zwitterionic CAPB results in preventing protein denaturing and conformational changes due to surface adsorption.

A.5. Conclusions

The interfacial behavior of bovine serum albumin (BSA) was studied in the presence of a zwitterionic surfactant cocamidopropyl betaine (CAPB) and non-ionic surfactant Triton X-100. The experimental surface tensions were coupled with a thermodynamic analysis to evaluate the surface coverage of the components. Our results indicated that CAPB dramatically decreased the surface activity of protein in the CAPB+BSA system. The presence of the protein increased the CMC of the zwitterionic CAPB by up to ten times. BSA did not affect the CMC of the non-ionic surfactant Triton X-100. Furthermore, the association of CAPB and the protein affected the surface coverage of CAPB molecules. Results of this study may aid in the rational design of formulations for increasing protein stability during storage or processes.

List of Symbols

a: Interaction parameter	AAD: average absolute deviation
b: surface-to-solution distribution constant.	C: concentration
cal: calculated	exp: experimental
f: activity coefficient	K: infinite dilution distribution constant
n: ratio of the molar area	N: number of experimental data
N_a : Avogadro number	R: ideal gas constant
S: shape factor	T: temperature
V: molar volume	x: mole fraction
α : bulk phase	γ : surface tension
Γ : surface excess	θ : surface coverage
μ_i : chemical potential of component I	Π : surface pressure
ρ : density	σ : interface
Δ : difference	ω : molar area
b: bulk	c: critical
i,j: components i and j	S: surface

Acknowledgements

This chapter was previously published as:

Erfani, Amir, Shahin Khosharay, Nicholas H. Flynn, Joshua D. Ramsey, and Clint P. Aichele. "Effect of zwitterionic betaine surfactant on interfacial behavior of bovine serum albumin (BSA)." *Journal of Molecular Liquids* 318 (2020): 114067.

and,

Erfani, Amir, Nicholas H. Flynn, Joshua D. Ramsey, and Clint P. Aichele. "Increasing protein stability by association with zwitterionic amphiphile cocamidopropyl betaine." *Journal of Molecular Liquids* 295 (2019): 111631.

VITA

Amir Erfani

Candidate for the Degree of

Doctor of Philosophy

Thesis: Zwitterionic Microscale Hydrogels for Protein Delivery, Stabilization, and Immobilization

Major Field: Chemical Engineering

Biographical:

Education:

Completed the requirements for the Doctor of Philosophy in Chemical Engineering at Oklahoma State University, Stillwater, Oklahoma in May 2021.

Master of Science in Chemical Engineering at Semnan University, Semnan, Iran in Aug 2015.

Bachelor of Science in Chemical Engineering at Semnan University, Semnan, Iran, Aug 2013.

Experience:

Graduate Teaching and Research Assistant at the School of Chemical Engineering, Oklahoma State University, Stillwater, Oklahoma